Computational Design of Vaccines Against *Plasmodium falciparum* Malaria

Mark Langowski

A dissertation
submitted in partial fulfillment of the
requirements for the degree of

Doctor of Philosophy

University of Washington
2024

Reading Committee:
Neil P. King, Chair
Marion Pepper
Sean C. Murphy

Program Authorized to Offer Degree:
Molecular and Cellular Biology

University of Washington

Abstract

Computational Design of Vaccines Against *Plasmodium falciparum* Malaria

Mark Langowski

Chair of the supervisory committee:

Neil P. King

Department of Biochemistry

Malaria caused by *P. falciparum* resulted in over 600,000 deaths per year in 2022, with the majority of deaths occurring in children under five years of age. Recently, two vaccines have been recommended by the WHO for use in children in areas of moderate-to-high malaria transmission activity in Africa. These vaccines, RTS,S/AS01 and R21/Matrix-M, offer vaccine efficacies of 50-70% at 1 year but there are concerns about antibody quality and durability. Here, in my dissertation, I describe multiple approaches to address issues with antibody quality elicited by CSP vaccination. First, I explore the use of a computationally designed self-assembling nanoparticle displaying a series of different CSP repeat epitopes to elicit antibodies towards novel epitopes not found in RTS,S or R21. Building on this, the next project utilizes CSP nanoparticles where the nanoparticle surface is coated in N-linked oligomannose glycans to take advantage of mannose-binding lectin complement pathways so that they traffic efficiently to the germinal center. These CSP glycosylated nanoparticles enhance early B cell responses and improve protection in mouse models of infection. Finally, I investigate the use of deep-learning based protein design methods for the display of protective epitopes from CSP such as CIS43 and L9, two monoclonal antibodies that have shown promise in the field as

passive immunizations. These *de novo* immunogens exhibit specific binding to their target antibodies with little cross-reactivity to known non-protective antibodies and are able to activate and recruit inferred-germline CIS43 and L9 B cells to the germinal centers of recipient mice. These immunogens offer a new way to try and improve anti-CSP repeat B cell responses.

Acknowledgments

Joining the Molecular and Cellular Biology Program at the University of Washington has been one of the best decisions I have made in my life, and the most important of my career. The community here is collaborative and welcoming, and it inspires me to push forward everyday with the best effort I can provide to pass that same spirit back on.

I rotated in Neil's lab just before the pandemic started in 2020 (I think it actually ended right when the lockdowns began), and worked on a purely computational rotation project with little experience in this area. It was difficult, but I received enough support to understand *just enough* to feel comfortable that maybe I really could be a computational protein designer. I thought that I would maybe work on something else besides malaria, but in the end Neil offered me an opportunity to use computational tools to address this disease that I believed I could not pass up. Neil's mentorship has been invaluable; he always had his door open when he could spare the time to listen to me ramble on about new ideas, provided the autonomy to go after those ideas, and had timely recommendations on the newest methods that I could use to tackle my problems. Neil's support and his willingness to collaborate with so many people to tackle a problem this big has made all of the work in this dissertation possible.

Since I joined the King lab, every single day of work has been an absolute joy. To all of my colleagues, being able to spend time talking science or laughing about something else entirely made it so that I never dreaded going in (except for the occasional hard and physically taxing experiment to run). Having lab lunch with all of you every Wednesday has been one of the highlights of my time here, and I'm glad I have made so many connections with all of you.

To my first mentor when I joined the lab, Quinton Dowling, a big thank you for showing me how to be a computational biologist. Whether you knew it at the time or not, you set a standard for me that I've always tried to follow. To Annie Dosey, you've been a fantastic mentor (and bench partner) that has made me better in so many ways from vaccinology, soundboarding ideas off one another, and to appreciating the utility of so many lab techniques (nsEM, BLI, and ELISAs too I guess). Thanks to Chloe Adams for always helping me submit tickets about the AKTAs. Also a massive thank you to the mentorship (and friendship) of Sebastian Ols and Chelsea Fries– you both have offered so much advice that has made me a better scientist and my time here wouldn't have been as great without you two. And a huge thank you to the mentorship of the RPXDock team who shaped the early part of my PhD back when I made nanoparticles (Erin Yang, Yang Hsia, Alena Khmelinskaia, and Will Sheffler), and to the people that helped me learn many of the brand new deep learning methods developed at the Institute for Protein Design (David Juergens, Joe Watson, Sidney Lisanza, and Jue Wang).

Naveen Jasti– my partner in crime in antigen design– it's been an absolute pleasure to work with you over the years. We've brainstormed a lot about vaccines (which has led us to have far too many projects), and have shared more laughs than I can count. I also wanted to give a shout out to the people in my dry lab row; Sam, Zac, Marti, Cara, Richmond, and Dan H– thanks for putting up with me. To our visiting scientists Rob, Yoann, Joel, Joan, Svea, and Ivan; it was a pleasure working with all of you.

To my mentors before I came to UW, I can never repay the fundamentals and hard work you've instilled in me. To Jason Switzer, my high school biology teacher, thank you for printing me out a paper on *Bacillus anthracis* lineage tracing that piqued my interest in biology. To Shiv Kale, you taught me how to use a pipette and that proteins are endlessly interesting. To Sheetij Dutta, I am forever grateful for the opportunity to work in your lab on malaria vaccines and for teaching me to be a vaccinologist, and your continued mentorship over the years.

To the many collaborators that I've worked with– Robert Seder, Azza Idris, Daria Nikolaeva, Marie Pancera, Nick Hurlburt, Marion Pepper, Courtney McDougal, Kelly Lee, Chengbo Chen, Facundo Batista, and Jahyun Koo– thanks for making all of this work a reality. And thank you to my committee members– Marion, Sean, Kelly, and Leo– your insight and support were never taken for granted.

To my family (Dad, Mom, and Thomas), thank you for endless support even through all the distance of the last five years. I love you and couldn't have done it without you.

To Miya, your sense of adventure inspires me to never be afraid to learn new things. You are the center of my heart.

Table of Contents

Chapter 0: Introduction

In the 20th century, it is estimated that 150 to 300 million people died from malaria, and may have caused between 2 and 5% of all deaths in this time[1]. Malaria is a disease caused by *Plasmodium* sporozoites deposited by the blood meal of a female *Anopheles* mosquito. Sporozoites must then traverse the skin and into the bloodstream, where they travel to the liver to infect hepatocytes. A single sporozoite is required for infection of a hepatocyte, where it then replicates tens of thousands of times into the merozoite stage and ruptures from hepatocytes to infect red blood cells (RBCs). These merozoites can then asexually replicate and rupture from and re-infect RBCs, causing the symptomatic stage of malaria. A small fraction of parasites become gametocytes which must then be taken back up by the blood meal of a mosquito, mate in the mosquito midgut, and then form oocysts which develop into sporozoites, beginning the cycle again. Five species of *Plasmodium* infect humans, but *P. falciparum* and *P. vivax* pose the most significant health burdens worldwide, accounting for over 200 million malaria cases per year[2]. *P. falciparum* malaria is the deadliest form, accounting for an estimated 95% of the 608,000 deaths that occurred in 2022, and a majority of these deaths from African children under 5 years of age[2]. In the last 20 years, this number has fallen significantly through the use of insecticide-treated bednets, rapid diagnostic testing, and readily available medicines for treatment and chemoprevention[2,3]. These reductions have plateaued, but newly available vaccines offer promise for further reducing malaria burden globally.

The development of vaccines against malaria has been ongoing since the 1960s and initially involved the use of attenuated sporozoites. Nussenzweig and colleagues immunized mice with irradiated *P. berghei* sporozoites and showed that they were protected against parasite challenge[4]. This same principle was used in humans in the 1970s, where radiation-attenuated *P. falciparum* sporozoites were delivered to individuals by hundreds of mosquito bites, and showed immunity against parasite challenge[5,6]. Fabs isolated from mice immunized with irradiated sporozoites bound the circumsporozoite protein (CSP), the major surface antigen of sporozoites, and could protect mice from infection[7]. In the 1980s, the gene for CSP was isolated[8], and its tetrapeptide NANP major repeats were used to immunize rodents and showed inhibitory activity in vitro against *P. falciparum*[9]. Since then, a number of vaccines have been tested that target *P. falciparum* CSP, with the two WHO recommended vaccines, RTS,S/AS01 (Mosquirix) and R21/Matrix-M, both having their antigens derived from this protein.

CSP is important for the development[10], motility[11], and infectivity of sporozoites[12]. *P. falciparum* CSP is composed of three domains: an intrinsically disordered N-terminal domain that contains a conserved KLKQP site known as Region I found in all mammalian *Plasmodia*[13]; a disordered tetrapeptide repeat domain that begins with a single NPDP junctional repeat and is followed by primarily NANP major repeats with minor NVDP repeats interspersed within this region depending on the strain[14]; and a C-terminal domain that adopts an α-Thrombospondin type-I repeat (αTSR) fold[15] and is attached to the sporozoite membrane at its carboxy-terminus by a glycosylphosphatidylinositol (GPI) anchor[16,17]. A cleavage event at the Region I N-terminus is known to occur[18], and this site interacts with heparan sulfate proteoglycans (HSPGs) on the surface of hepatocytes for invasion and masks the CSP C-terminal domain during migration

through the skin[19,20]. The C-terminal domain is known to be important for sporozoite egress from oocysts[21], and the αTSR contains homology to the TSR superfamily which are involved in cell adhesion and attachment[15], but its role during hepatocyte invasion is unclear. There is no structure of the full-length CSP molecule, owing to its status as a disordered protein[22], but structures do exist of the C-terminal αTSR domain with[23,24] and without antibodies[15], and small peptides of the N-terminal domain around Region I from antibody-antigen structures[25,26]. Early studies determined the repeats were flexible and primarily adopted type I β-turn conformations[27,28], and a plethora of recent antibody structures against small and large repeat domain peptides confirms this observation[29–43]. The importance of CSP function has made it a clear target for the development of anti-infective vaccines.

The world's first licensed vaccine, RTS,S/AS01 (Mosquirix), displays a truncated segment of CSP that corresponds to 18.5 major repeats (R) and the C-terminal domain for the inclusion of T cell epitopes (T), as a genetic fusion to the Hepatitis B surface antigen (S), and is co-assembled with free S antigen to form virus-like nanoparticles at 20% valency[44]. A second malaria vaccine was recently recommended by the WHO, R21, which contains 100% valency of this truncated RT segment on its surface[45]. RTS,S/AS01 and R21/Matrix-M are being distributed to children in areas of moderate-to-high malaria transmission intensity in Africa, and have shown efficacies in the field at 1 year of 55.8% and 68%, respectively[46,47]. RTS,S/AS01 was also shown to reduce deaths in children by 13% over 4 years[48]. These are extremely promising results and offer great hope at further reducing the burden of disease caused by *P. falciparum*. However, there are potential problems that need to be addressed in these vaccines. The antibody titers generated by these vaccines rapidly wane[47,49], and there is some evidence that RTS,S/AS01 vaccinated children were more susceptible to malaria five years after vaccination[50], meaning that both of these vaccines require yearly boosters to maintain their efficacy[46,47]. There is also data that shows possible vaccine escape towards the polymorphic C-terminus of CSP[51,52], though there are correlations with responses toward the C-terminus being beneficial for protection that would argue for its inclusion[53–55]. The general consensus is that antibodies against the repeats correlate with protection elicited by these vaccines and as such are the primary targets of next-generation vaccines[49,56].

Structure-based vaccine design has allowed for great gains in the development of potent vaccines for class I viral fusion proteins[57]. For example, the pre-fusion structure for Respiratory Syncytial Virus F protein (RSV F) was solved and antibodies that targeted this conformation were determined to be much more potently neutralizing than post-fusion RSV F targeting antibodies[58]. This prompted the development of structure-based design to stabilize RSV F in its pre-fusion conformation[59], and this vaccine elicited more potently neutralizing antibodies compared to post-fusion vaccines. This concept of using known antibodies to determine protective or neutralizing conformations, which then guide structure-based antigen design, is known as Reverse vaccinology 2.0[60]. These principles have prompted the stabilization of many different viral glycoproteins[61]. Though there is currently nothing akin to a pre- or post-fusion structure with the flexible CSP, in the late 2010s several antibodies were isolated from individuals living in endemic areas or after vaccination and structural determination found that they targeted the *P. falciparum* CSP repeats, and potently neutralized parasites *in vitro* or

protected mice from transgenic parasite challenge *in vivo*[29,31–35,43]. These antibodies bind the NANP major, NVDP minor, or NPDP junctional repeats with minimal epitopes that range from 2.5-3 repeats[29], primarily in type I β-turn or Asn pseudo3_{10} conformations, and there is evidence that antibodies that cross-react between these repeats with high affinity have higher protective capacity[35,38]. Isolated antibodies that bind the N-terminal or C-terminal domains have been weakly or non-protective in transgenic parasite challenge models[23,24,62], though it should be noted that there is one antibody that targets the N-terminus and is protective when delivered as an IgA[26].

With this information in hand, it was hypothesized that one way to improve upon the RTS,S and R21 vaccines, which only contain NANP major repeats[44,45], would be to include the NPDP junctional and NVDP minor repeats in next-generation vaccines[63,64]. Most isolates in the field contain these repeats at the junction between the CSP N-terminal domain and repeat region and are known as the “junctional region,” which corresponds to KQPADGNPDPNANPNVDPN in the CSP 3D7 reference strain[31,32,43]. Two antibodies that target this region, CIS43 and L9, have been tested as passive immunizations in controlled human malaria infections (CHMI) and in the field, and have been shown to be protective against malaria at serum concentrations of 50 μg/mL[65–67], which is far below the titer of 188 μg/mL of anti-repeat titer generated by RTS,S/AS01 in protected individuals in one CHMI trial[56]. Several groups have displayed CSP repeats that correspond to the junctional region and major repeat epitopes without the C-terminal domain on nanoparticles as a way to improve vaccines, though none of them have reported definitively increased protection when these additional epitopes are included[42,68–76]. One reason for this may be due to the flexibility of the repeats which can bind other antibodies that are weakly or non-neutralizing, but recognize these same sequences in different conformations (e.g., non-protective CIS42 binds the same sequence as CIS43)[32]. Thus it is necessary to find solutions that target the conformations of protective antibodies to preferentially elicit them while disallowing non-protective ones.

Computational protein design uses biophysical and deep learning based algorithms and models for a variety of tasks including the design of completely *de novo* proteins[77–81], creating entirely new symmetric assemblies[82–84], improving stability of existing enzymes through sequence design[85,86], scaffolding existing motifs into new proteins[87], stabilizing antigens of interest[88,89], and highly accurate deep learning based prediction algorithms to select designs[90–92]. Scaffolding motifs of antibody minimal epitopes has been explored using the biophysically-based Rosetta software developed here at the University of Washington[93], and there have been successes in designed proteins that elicit epitope-specific responses that either bind target inferred-germline lineages of antibodies[94,95], or can display epitopes on supporting proteins that elicit neutralizing titers of antibody in animal models[96–98]. There have been no reports at this time of computationally designed proteins that display stabilized conformations of *P. falciparum* CSP repeats for eliciting protective antibodies, which is a difficult task considering they comprise small and flexible repeat epitopes.

Here, I’ll describe three projects that involve the use of computationally designed nanoparticle assemblies for the display of *P. falciparum* CSP repeats, the same nanoparticle with N-linked

glycans engineered into its surface which display the CSP repeats, and the deep-learning based design of *de novo* epitope scaffolds that display stabilized CIS43 and L9 epitopes described earlier. My first project involves using I53-50[83], a computationally designed self-assembling nanoparticle platform that has been used to display SARS-CoV-2 RBD and is a licensed vaccine in South Korea (SKYCovione™, SK Biosciences). I53-50 was used here to display various constructs from CSP that correspond to the RT antigen found in RTS,S (named RT-I53-50), and was compared to a two dozen other constructs that included the junctional region targeted by CIS43 and L9. This was done in mouse models and these nanoparticles were immunogenic and were able to elicit immunity against the sporozoite stage of the parasite in a transgenic parasite challenge model. We also performed a head-to-head benchmarking study against R21, the second vaccine to be licensed against malaria, which no other group has reported in a pre-clinical vaccine paper.

My second project involves the display of N-linked glycans on the surface of RT-I53-50 nanoparticles to enhance the antibody response towards CSP and improve protection against parasite challenge. This project involved the use of a modified version of I53-50, I53-50-4gly, which had N-linked glycan sequons inserted into it by a Rosetta-based protocol[99]. Studies have shown that the presence of oligomannose at N-linked glycans on viral glycoproteins and nanoparticles allow them to be opsonized by the mannose-binding lectin pathway of complement and this traffics them more efficiently to the germinal center[99,100]. One group has already reported on something similar, with the display of CSP repeats on a glycosylated HpFerritin nanoparticle, but they did not perform a granular analysis on the specific contributions of these glycoforms[71]. I produced several variants of RT-I53-50-glycosylated nanoparticles that had different numbers of glycans and different glycoforms, and they were tested by my collaborators to determine if they elicited B cell phenotypes and if mice immunized with these nanoparticles were protected from challenge after two doses, a bar that we could not reach with the original RT-I53-50. These nanoparticles showed improvements in early anti-CSP B cell responses and could significantly reduce liver burden after parasite challenge after only two doses.

Finally, my third project involved the computational design of immunogens that display protective epitopes against the CSP repeats. I primarily focused on CIS43 and L9 epitopes as a proof-of-concept that we could generate highly specific immunogens that bind these antibodies while reducing the binding of off-target antibodies. Immunogen design for this project involved 1) utilizing RFdiffusion, a generative model that can produce backbones that stabilize and support CIS43 and L9 epitopes; 2) the design of these generated backbones with deep-learning based sequence design method ProteinMPNN to ascribe them with an optimal sequence that will likely fold; and 3) filtering designs with AlphaFold2 to ensure the highest possibility of wet lab success for designs ordered. I produced these designs and found multiple immunogens that were able to specifically bind CIS43 over off-target CIS42, and for L9 bind two Fabs at once which is a feature of this specific antibody[39,101]. These designs were tested by collaborators in knock-in mouse models that contained the inferred-germline precursors of these two antibodies, and they showed the ability to activate and recruit these cells to the germinal center with mutations found in the original CIS43 antibody, and we are currently awaiting sequence results for L9 antibodies.

A cryo-EM structure of one L9 immunogen was obtained at a high resolution and closely matched the design model, showing the precise atomic accuracy of the computational designs.

Beyond the projects that are described above, I also worked on a variety of projects that did not involve CSP. I computationally designed nanoparticles that display *Plasmodium* macrophage-migration inhibitory factor-like proteins (MIF) and showed the ability to protect against *P. yoelii* parasites in mice. I have also performed a significant amount of work on the stabilization and domain-based design of reticulocyte-binding protein homolog 5 (RH5), which is an advanced vaccine candidate against the *P. falciparum* blood-stage. I have also worked on the design of epitope-specific immunogens against *P. falciparum* erythrocyte membrane protein 1 (PfEMP1), a blood-stage antigen implicated in severe malaria. The work described herein is only possible because of the collaboration of many groups of scientists that are passionate about making vaccines to address problems in global health. This includes collaborators at Institute for Protein Design here at the University of Washington (UW), the Department of Immunology and the Department of Medicinal Chemistry at UW, the Fred Hutchinson Cancer Center, the National Institutes of Health Vaccine Research Center, the Ragon Institute of Mass General, the University of Antwerp, the University of Georgia, Yale University, the Scripps Research Institute, and the University of Oxford. Modern vaccine design is highly interdisciplinary and requires the expertise of many different fields to make advancements as quick and efficient as possible.

References

1. Carter, R. & Mendis, K. N. Evolutionary and historical aspects of the burden of malaria. *Clin. Microbiol. Rev.* **15**, 564–594 (2002).
2. *World Malaria Report 2023*. https://www.who.int/teams/global-malaria-programme/reports/world-malaria-report-2023 (2023).
3. Cibulskis, R. E. *et al.* Malaria: Global progress 2000 - 2015 and future challenges. *Infect. Dis. Poverty* **5**, 61 (2016).
4. Nussenzweig, R. S., Vanderberg, J., Most, H. & Orton, C. Protective immunity produced by the injection of x-irradiated sporozoites of plasmodium berghei. *Nature* **216**, 160–162 (1967).
5. Clyde, D. F., McCARTHY, V. C., Miller, R. M. & Hornick, R. B. Specificity of protection of man immunized against sporozoite-induced falciparum malaria. *Am. J. Med. Sci.* **266**, 398–404 (1973).
6. Clyde, D. F. Immunization of man against falciparum and vivax malaria by use of attenuated sporozoites. *Am. J. Trop. Med. Hyg.* **24**, 397–401 (1975).
7. Potocnjak, P., Yoshida, N., Nussenzweig, R. S. & Nussenzweig, V. Monovalent fragments

(Fab) of monoclonal antibodies to a sporozoite surface antigen (Pb44) protect mice against malarial infection. *J. Exp. Med.* **151**, 1504–1513 (1980).

8. Dame, J. B. *et al.* Structure of the gene encoding the immunodominant surface antigen on the sporozoite of the human malaria parasite Plasmodium falciparum. *Science* **225**, 593–599 (1984).
9. Zavala, F. *et al.* Rationale for development of a synthetic vaccine against plasmodium falciparum malaria. *Science* **228**, 1436–1441 (1985).
10. Ménard, R. *et al.* Circumsporozoite protein is required for development of malaria sporozoites in mosquitoes. *Nature* **385**, 336–340 (1997).
11. Stewart, M. J., Nawrot, R. J., Schulman, S. & Vanderberg, J. P. Plasmodium berghei sporozoite invasion is blocked in vitro by sporozoite-immobilizing antibodies. *Infect. Immun.* **51**, 859–864 (1986).
12. Cerami, C. *et al.* The basolateral domain of the hepatocyte plasma membrane bears receptors for the circumsporozoite protein of Plasmodium falciparum sporozoites. *Cell* **70**, 1021–1033 (1992).
13. Geens, R. *et al.* Biophysical characterization of the Plasmodium falciparum circumsporozoite protein's N-terminal domain. *Protein Sci.* **33**, e4852 (2024).
14. Bowman, N. M. *et al.* Comparative population structure of Plasmodium falciparum circumsporozoite protein NANP repeat lengths in Lilongwe, Malawi. *Sci. Rep.* **3**, 1990 (2013).
15. Doud, M. B. *et al.* Unexpected fold in the circumsporozoite protein target of malaria vaccines. *Proc. Natl. Acad. Sci. U. S. A.* **109**, 7817–7822 (2012).
16. Wang, Q., Fujioka, H. & Nussenzweig, V. Mutational analysis of the GPI-anchor addition sequence from the circumsporozoite protein of Plasmodium: Mutational analysis of Plasmodium CS protein. *Cell. Microbiol.* **7**, 1616–1626 (2005).
17. Nagar, R. *et al.* The major surface protein of malaria sporozoites is GPI-anchored to the plasma membrane. *J. Biol. Chem.* **300**, 107557 (2024).
18. Coppi, A., Pinzon-Ortiz, C., Hutter, C. & Sinnis, P. The Plasmodium circumsporozoite protein is proteolytically processed during cell invasion. *J. Exp. Med.* **201**, 27–33 (2005).
19. Coppi, A. *et al.* Heparan sulfate proteoglycans provide a signal to Plasmodium sporozoites to stop migrating and productively invade host cells. *Cell Host Microbe* **2**, 316–327 (2007).
20. Coppi, A. *et al.* The malaria circumsporozoite protein has two functional domains, each with distinct roles as sporozoites journey from mosquito to mammalian host. *J. Exp. Med.* **208**, 341–356 (2011).

21. Wang, Q., Fujioka, H. & Nussenzweig, V. Exit of Plasmodium sporozoites from oocysts is an active process that involves the circumsporozoite protein. *PLoS Pathog.* **1**, e9 (2005).
22. Plassmeyer, M. L. *et al.* Structure of the Plasmodium falciparum circumsporozoite protein, a leading malaria vaccine candidate. *J. Biol. Chem.* **284**, 26951–26963 (2009).
23. Scally, S. W. *et al.* Rare PfCSP C-terminal antibodies induced by live sporozoite vaccination are ineffective against malaria infection. *J. Exp. Med.* **215**, 63–75 (2018).
24. Beutler, N. *et al.* A novel CSP C-terminal epitope targeted by an antibody with protective activity against Plasmodium falciparum. *PLoS Pathog.* **18**, e1010409 (2022).
25. Thai, E. *et al.* A high-affinity antibody against the CSP N-terminal domain lacks Plasmodium falciparum inhibitory activity. *J. Exp. Med.* **217**, (2020).
26. Tan, J. *et al.* Functional human IgA targets a conserved site on malaria sporozoites. *Sci. Transl. Med.* **13**, eabg2344 (2021).
27. Dyson, H. J., Satterthwait, A. C., Lerner, R. A. & Wright, P. E. Conformational preferences of synthetic peptides derived from the immunodominant site of the circumsporozoite protein of Plasmodium falciparum by 1H NMR. *Biochemistry* **29**, 7828–7837 (1990).
28. Ghasparian, A., Moehle, K., Linden, A. & Robinson, J. A. Crystal structure of an NPNA-repeat motif from the circumsporozoite protein of the malaria parasite Plasmodium falciparum. *Chem. Commun.* 174–176 (2006) doi:10.1039/b510812h.
29. Oyen, D. *et al.* Structural basis for antibody recognition of the NANP repeats in Plasmodium falciparum circumsporozoite protein. *Proc. Natl. Acad. Sci. U. S. A.* **114**, E10438–E10445 (2017).
30. Oyen, D. *et al.* Cryo-EM structure of P. falciparum circumsporozoite protein with a vaccine-elicited antibody is stabilized by somatically mutated inter-Fab contacts. *Sci Adv* **4**, eaau8529 (10 2018).
31. Tan, J. *et al.* A public antibody lineage that potently inhibits malaria infection through dual binding to the circumsporozoite protein. *Nat. Med.* **24**, 401–407 (2018).
32. Kisalu, N. K. *et al.* A human monoclonal antibody prevents malaria infection by targeting a new site of vulnerability on the parasite. *Nat. Med.* **24**, 408–416 (2018).
33. Triller, G. *et al.* Natural Parasite Exposure Induces Protective Human Anti-Malarial Antibodies. *Immunity* **47**, 1197–1209.e10 (2017).
34. Imkeller, K. *et al.* Antihomotypic affinity maturation improves human B cell responses against a repetitive epitope. *Science* **360**, 1358–1362 (2018).
35. Murugan, R. *et al.* Evolution of protective human antibodies against Plasmodium falciparum circumsporozoite protein repeat motifs. *Nat. Med.* **26**, 1135–1145 (2020).

36. Pholcharee, T. *et al.* Structural and biophysical correlation of anti-NANP antibodies with in vivo protection against P. falciparum. *Nat. Commun.* **12**, 1063 (2021).
37. Pholcharee, T. *et al.* Diverse Antibody Responses to Conserved Structural Motifs in Plasmodium falciparum Circumsporozoite Protein. *J. Mol. Biol.* **432**, 1048–1063 (2020).
38. Thai, E. *et al.* Molecular determinants of cross-reactivity and potency by VH3-33 antibodies against the Plasmodium falciparum circumsporozoite protein. *Cell Rep.* **42**, (2023).
39. Martin, G. M. *et al.* Structural basis of epitope selectivity and potent protection from malaria by PfCSP antibody L9. *Nat. Commun.* **14**, 2815 (2023).
40. Martin, G. M. *et al.* Affinity-matured homotypic interactions induce spectrum of PfCSP structures that influence protection from malaria infection. *Nat. Commun.* **14**, 4546 (2023).
41. Wang, L. T. *et al.* The light chain of the L9 antibody is critical for binding circumsporozoite protein minor repeats and preventing malaria. *Cell Rep.* **38**, 110367 (2022).
42. Kucharska, I. *et al.* High-density binding to Plasmodium falciparum circumsporozoite protein repeats by inhibitory antibody elicited in mouse with human immunoglobulin repertoire. *PLoS Pathog.* **18**, e1010999 (2022).
43. Wang, L. T. *et al.* A Potent Anti-Malarial Human Monoclonal Antibody Targets Circumsporozoite Protein Minor Repeats and Neutralizes Sporozoites in the Liver. *Immunity* **53**, 733–744.e8 (2020).
44. Gordon, D. M. *et al.* Safety, immunogenicity, and efficacy of a recombinantly produced Plasmodium falciparum circumsporozoite protein-hepatitis B surface antigen subunit vaccine. *J. Infect. Dis.* **171**, 1576–1585 (1995).
45. Collins, K. A., Snaith, R., Cottingham, M. G., Gilbert, S. C. & Hill, A. V. S. Enhancing protective immunity to malaria with a highly immunogenic virus-like particle vaccine. *Sci. Rep.* **7**, 46621 (2017).
46. RTS,S Clinical Trials Partnership. Efficacy and safety of RTS,S/AS01 malaria vaccine with or without a booster dose in infants and children in Africa: final results of a phase 3, individually randomised, controlled trial. *Lancet* **386**, 31–45 (2015).
47. Datoo, M. S. *et al.* Safety and efficacy of malaria vaccine candidate R21/Matrix-M in African children: a multicentre, double-blind, randomised, phase 3 trial. *Lancet* **403**, 533–544 (2024).
48. Wadman, M. First malaria vaccine slashes early childhood mortality. *American Association for the Advancement of Science* https://www.science.org/content/article/first-malaria-vaccine-slashes-early-childhood-deaths (2023).

49. White, M. T. *et al.* Immunogenicity of the RTS,S/AS01 malaria vaccine and implications for duration of vaccine efficacy: secondary analysis of data from a phase 3 randomised controlled trial. *Lancet Infect. Dis.* **15**, 1450–1458 (2015).
50. Olotu, A. *et al.* Seven-Year Efficacy of RTS,S/AS01 Malaria Vaccine among Young African Children. *N. Engl. J. Med.* **374**, 2519–2529 (2016).
51. Neafsey, D. E. *et al.* Genetic Diversity and Protective Efficacy of the RTS,S/AS01 Malaria Vaccine. *N. Engl. J. Med.* **373**, 2025–2037 (2015).
52. Chaudhury, S. *et al.* Breadth of humoral immune responses to the C-terminus of the circumsporozoite protein is associated with protective efficacy induced by the RTS,S malaria vaccine. *Vaccine* **39**, 968–975 (2021).
53. Ubillos, I. *et al.* Baseline exposure, antibody subclass, and hepatitis B response differentially affect malaria protective immunity following RTS,S/AS01E vaccination in African children. *BMC Med.* **16**, 197 (2018).
54. Dobaño, C. *et al.* Concentration and avidity of antibodies to different circumsporozoite epitopes correlate with RTS,S/AS01E malaria vaccine efficacy. *Nat. Commun.* **10**, 2174 (2019).
55. Das, J. *et al.* Delayed fractional dosing with RTS,S/AS01 improves humoral immunity to malaria via a balance of polyfunctional NANP6- and Pf16-specific antibodies. *Med* **2**, 1269–1286.e9 (11/2021).
56. Kester, K. E. *et al.* Randomized, Double-Blind, Phase 2a Trial of Falciparum Malaria Vaccines RTS,S/AS01B and RTS,S/AS02A in Malaria-Naive Adults: Safety, Efficacy, and Immunologic Associates of Protection. *J. Infect. Dis.* **200**, 337–346 (2009).
57. Graham, B. S., Gilman, M. S. A. & McLellan, J. S. Structure-Based Vaccine Antigen Design. *Annu. Rev. Med.* **70**, 91–104 (2019).
58. McLellan, J. S. *et al.* Structure of RSV fusion glycoprotein trimer bound to a prefusion-specific neutralizing antibody. *Science* **340**, 1113–1117 (2013).
59. McLellan, J. S. *et al.* Structure-based design of a fusion glycoprotein vaccine for respiratory syncytial virus. *Science* **342**, 592–598 (2013).
60. Rappuoli, R., Bottomley, M. J., D'Oro, U., Finco, O. & De Gregorio, E. Reverse vaccinology 2.0: Human immunology instructs vaccine antigen design. *J. Exp. Med.* **213**, 469–481 (2016).
61. Byrne, P. O. & McLellan, J. S. Principles and practical applications of structure-based vaccine design. *Curr. Opin. Immunol.* **77**, 102209 (2022).
62. Wang, L. T. *et al.* Protective effects of combining monoclonal antibodies and vaccines

against the Plasmodium falciparum circumsporozoite protein. *PLoS Pathog.* **17**, e1010133 (2021).

63. Julien, J.-P. & Wardemann, H. Antibodies against Plasmodium falciparum malaria at the molecular level. *Nat. Rev. Immunol.* **19**, 761–775 (12 2019).
64. Cockburn, I. A. & Seder, R. A. Malaria prevention: from immunological concepts to effective vaccines and protective antibodies. *Nat. Immunol.* **19**, 1199–1211 (2018).
65. Gaudinski, M. R. *et al.* A Monoclonal Antibody for Malaria Prevention. *N. Engl. J. Med.* **385**, 803–814 (2021).
66. Wu, R. L. *et al.* Low-Dose Subcutaneous or Intravenous Monoclonal Antibody to Prevent Malaria. *N. Engl. J. Med.* **387**, 397–407 (2022).
67. Lyke, K. E. *et al.* Low-dose intravenous and subcutaneous CIS43LS monoclonal antibody for protection against malaria (VRC 612 Part C): a phase 1, adaptive trial. *Lancet Infect. Dis.* **23**, 578–588 (2023).
68. Francica, J. R. *et al.* Design of Alphavirus Virus-Like Particles Presenting Circumsporozoite Junctional Epitopes That Elicit Protection against Malaria. *Vaccines (Basel)* **9**, 272 (2021).
69. Jelínková, L. *et al.* An epitope-based malaria vaccine targeting the junctional region of circumsporozoite protein. *npj Vaccines* **6**, 1–10 (2021).
70. Whitacre, D. C. *et al.* P. falciparum and P. vivax Epitope-Focused VLPs Elicit Sterile Immunity to Blood Stage Infections. *PLoS One* **10**, (2015).
71. Ludwig, J. *et al.* Glycosylated nanoparticle-based PfCSP vaccine confers long-lasting antibody responses and sterile protection in mouse malaria model. *NPJ Vaccines* **8**, 52 (2023).
72. McCoy, M. E. *et al.* Mechanisms of protective immune responses induced by the Plasmodium falciparum circumsporozoite protein-based, self-assembling protein nanoparticle vaccine. *Malar. J.* **12**, 136 (2013).
73. Langowski, M. D. *et al.* Restricted valency (NPNA)n repeats and junctional epitope-based circumsporozoite protein vaccines against Plasmodium falciparum. *npj Vaccines* **7**, 1–11 (2022).
74. Langowski, M. D. *et al.* Optimization of a Plasmodium falciparum circumsporozoite protein repeat vaccine using the tobacco mosaic virus platform. *Proc. Natl. Acad. Sci. U. S. A.* **117**, 3114–3122 (2020).
75. Khan, F. *et al.* Head-to-Head Comparison of Soluble vs. Qβ VLP Circumsporozoite Protein Vaccines Reveals Selective Enhancement of NANP Repeat Responses. *PLoS One* **10**, (2015).

76. Kurtovic, L. *et al.* Novel Virus-Like Particle Vaccine Encoding the Circumsporozoite Protein of Plasmodium falciparum Is Immunogenic and Induces Functional Antibody Responses in Mice. *Front. Immunol.* **12**, 641421 (2021).
77. Huang, P.-S., Boyken, S. E. & Baker, D. The coming of age of de novo protein design. *Nature* **537**, 320–327 (2016).
78. Wang, J. *et al.* Scaffolding protein functional sites using deep learning. *Science* **377**, 387–394 (2022).
79. Anishchenko, I. *et al.* De novo protein design by deep network hallucination. *Nature* **600**, 547–552 (2021).
80. Watson, J. L. *et al.* De novo design of protein structure and function with RFdiffusion. *Nature* **620**, 1089–1100 (2023).
81. Ingraham, J. B. *et al.* Illuminating protein space with a programmable generative model. *Nature* **623**, 1070–1078 (2023).
82. King, N. P. *et al.* Accurate design of co-assembling multi-component protein nanomaterials. *Nature* **510**, 103–108 (2014).
83. Bale, J. B. *et al.* Accurate design of megadalton-scale two-component icosahedral protein complexes. *Science* **353**, 389–394 (2016).
84. Hsia, Y. *et al.* Design of a hyperstable 60-subunit protein dodecahedron. [corrected]. *Nature* **535**, 136–139 (2016).
85. Sumida, K. H. *et al.* Improving protein expression, stability, and function with ProteinMPNN. *J. Am. Chem. Soc.* **146**, 2054–2061 (2024).
86. Dauparas, J. *et al.* Robust deep learning–based protein sequence design using ProteinMPNN. *Science* **378**, 49–56 (2022).
87. Castro, K. M., Scheck, A., Xiao, S. & Correia, B. E. Computational design of vaccine immunogens. *Curr. Opin. Biotechnol.* **78**, 102821 (2022).
88. Campeotto, I. *et al.* One-step design of a stable variant of the malaria invasion protein RH5 for use as a vaccine immunogen. *Proceedings of the National Academy of Sciences* **114**, 998–1002 (2017).
89. Kudlacek, S. T. *et al.* Designed, highly expressing, thermostable dengue virus 2 envelope protein dimers elicit quaternary epitope antibodies. *Science Advances* **7**, eabg4084 (2021).
90. Jumper, J. *et al.* Highly accurate protein structure prediction with AlphaFold. *Nature* **596**, 583–589 (2021).
91. Baek, M. *et al.* Accurate prediction of protein structures and interactions using a three-track neural network. *Science* **373**, 871–876 (2021).

92. Bennett, N. R. *et al.* Improving de novo protein binder design with deep learning. *Nat. Commun.* **14**, 2625 (2023).
93. Leaver-Fay, A. *et al.* ROSETTA3: an object-oriented software suite for the simulation and design of macromolecules. *Methods Enzymol.* **487**, 545–574 (2011).
94. Jardine, J. *et al.* Rational HIV immunogen design to target specific germline B cell receptors. *Science* **340**, 711–716 (2013).
95. Schiffner, T. *et al.* Vaccination induces broadly neutralizing antibody precursors to HIV gp41. *Nat. Immunol.* **25**, 1073–1082 (2024).
96. Correia, B. E. *et al.* Proof of principle for epitope-focused vaccine design. *Nature* **507**, 201–206 (2014).
97. Sesterhenn, F. *et al.* Boosting subdominant neutralizing antibody responses with a computationally designed epitope-focused immunogen. *PLoS Biol.* **17**, e3000164 (2019).
98. Sesterhenn, F. *et al.* De novo protein design enables the precise induction of RSV-neutralizing antibodies. *Science* **368**, eaay5051 (2020).
99. Read, B. J. *et al.* Mannose-binding lectin and complement mediate follicular localization and enhanced immunogenicity of diverse protein nanoparticle immunogens. *Cell Rep.* **38**, 110217 (2022).
100. Tokatlian, T. *et al.* Innate immune recognition of glycans targets HIV nanoparticle immunogens to germinal centers. *Science* **363**, 649–654 (2019).
101. Tripathi, P. *et al.* Cryo-EM structures of anti-malarial antibody L9 with circumsporozoite protein reveal trimeric L9 association and complete 27-residue epitope. *Structure* **31**, 480–491.e4 (2023).

Chapter 1: Elicitation of liver-stage immunity by nanoparticle immunogens displaying *P. falciparum* CSP-derived antigens

This chapter is in review as:
Mark D. Langowski, Joseph R. Francica, Alex L. Roederer, Nicholas K. Hurlburt, Justas Rodarte, Lais Da Silva Pereira, Barbara J. Flynn, Brian Bonilla, Marlon Dillon, Patience Kiyuka, Rashmi Ravichandran, Connor Weidle, Lauren Carter, Mangala Rao, Gary R. Matyas, Marion Pepper, Azza H. Idris, Robert A. Seder, Marie Pancera*, Neil P. King*;
Elicitation of liver-stage immunity by nanoparticle immunogens displaying *P. falciparum* CSP-derived antigens.

Affiliations:
Institute for Protein Design, University of Washington, Seattle, WA, USA
Department of Biochemistry, University of Washington, Seattle, WA, USA
Graduate Program in Molecular and Cellular Biology, University of Washington, Seattle, WA, USA
Vaccine Research Center, National Institute of Allergy and Infectious Diseases, National Institutes of Health, Bethesda, MD, USA
Vaccine and Infectious Disease Division, Fred Hutchinson Cancer Center, Seattle, WA, USA
Henry M. Jackson Foundation for the Advancement of Military Medicine, Bethesda, MD, USA
U.S. Military HIV Research Program, Center for Infectious Diseases Research, Walter Reed Army Institute of Research, Silver Spring, MD, USA
Department of Immunology, University of Washington, Seattle, WA, USA

Abstract

A vaccine that provides robust, durable protection against malaria remains a global health priority. Although a breakthrough in the fight against malaria has recently been achieved by the licensure of two vaccines based on the circumsporozoite protein (CSP), the effectiveness and durability of protection can still be improved. Both vaccines contain a portion of CSP that does not include epitopes targeted by recently identified, potently protective monoclonal antibodies, suggesting that newer immunogens can expand the breadth of immunity and potentially increase protection. Here we explored more than 100 alternative CSP-based immunogens and evaluated immunogenicity and protection against a large number of candidates and compared them to the approved R21 vaccine. The data highlight several general features that improve the stability and immunogenicity of CSP-based vaccines, such as inclusion of the C-terminal domain and high-density display on protein nanoparticle scaffolds. We also identify antigen design strategies that do not warrant further exploration, such as synthetic repeat regions that include non-native repeat cadences. The benchmark R21 vaccine outperformed our best immunogen for immunogenicity and protection. Overall, our data provide valuable insights on the inclusion of junctional region epitopes that will guide the development of potent and durable vaccines against malaria.

Introduction

According to the WHO malaria report, malaria caused an estimated 249 million cases and 608,000 deaths in 2022[1]. The majority of these deaths were caused by *Plasmodium falciparum* (Pf), primarily in children under 5 years of age in Africa. Though control efforts have reduced these numbers over the past two decades, disruptions from the COVID-19 pandemic and growing artemisinin and insecticide resistance threaten advances in treatment and vector control[1]. The substantial morbidity, mortality, and economic impact of malaria motivate the development of immune interventions such as highly effective vaccines or protective antibodies to prevent and ultimately eliminate malaria worldwide.

Although malaria vaccine development is complicated by the complex, multi-stage life cycle of *Plasmodium*, the potential of preventing infection has led many vaccine efforts to focus on the pre-erythrocytic stage. These vaccines aim to prevent the relatively small number of sporozoites that enter the dermis or blood from reaching the liver, thereby providing sterile protection[2]. However, because sporozoites access the liver within 1-3 hours and a single parasite can initiate liver infection, an effective vaccine must elicit high and durable levels of protective antibodies[3]. The circumsporozoite protein (CSP) is the most abundantly expressed protein on the surface of sporozoites[4] and is the antigenic component of the RTS,S/AS01 and R21/Matrix-M vaccines, which showed 55.8% and 68% efficacy in standard sites at 1 year respectively in clinical trials[5,6] and are approved by European regulators and African countries, and recommended by the WHO[7,8]. Although there is no structure of full-length PfCSP and its function remains unclear, the protein comprises three distinct regions. The N-terminal domain (NTD) includes a signal peptide, a free cysteine, a pair of *Plasmodium* Export Element (PEXEL) sites and protease cleavage sites that are suspected to be necessary for hepatocyte invasion[9–11]. The central part of the protein consists of a series of tetrapeptide repeats, the exact number and sequence of which vary across *P. falciparum* strains[12]. In the prototypic strain 3D7, the central repeat region begins with a “junctional region” which consists of a single “junctional” NPDP motif, followed by three “major” NANP and “minor” NVDP tandem repeats. The rest of the repeat region consists of 35 copies of the NANP repeat with a single NVDP repeat at its center. Finally, the C-terminal domain (CTD), for which a crystal structure is available, adopts a thrombospondin-like fold followed by a GPI anchor sequence[13]. RTS,S and R21 both contain a truncated portion of PfCSP comprising 18.5 NANP repeats and the CTD, which may limit antibody responses to other epitopes that could contribute to protection[14,15]. Indeed, until recently, the majority of known anti-CSP protective antibodies targeted the central NANP repeat region. However, human antibodies against novel sites of vulnerability not present in RTS,S/R21—including the junctional and minor epitopes—have now been identified[14–17]. Passive immunization of adults with one such antibody targeting the junctional epitope, CIS43LS, led to a 75% (10 mg/kg dose) and 88% (40 mg/kg dose) reduction in infection over 6 months in a recent Phase II clinical trial[18], and passive immunization of children with minor repeat targeting L9LS showed up to 77% efficacy against clinical malaria in a Phase II clinical trial[19]. These results establish that junctional and minor repeat epitope sites on PfCSP are indeed neutralizing sites to be used for the design and evaluation of vaccines beyond those present in RTS,S and R21. Such vaccines may increase the breadth and potency of the immune

response to potentially overcome the waning immune responses observed with RTS,S/AS01 and R21/Matrix-M[3,20].

Structural biology is a powerful tool that informs vaccine development by visualizing antigen in complex with protective (and non-protective) antibodies[21]. The two most successful examples of structure-based vaccine design to date, both of which led to licensed vaccines, targeted RSV[22,23] and SARS-CoV-2[24–26]. In both cases, structures of the viral fusion glycoprotein (or those of other betacoronaviruses in the case of SARS-CoV-2[27,28]) in its native-like prefusion conformation enabled the design of prefusion-stabilized antigens that elicit potent neutralizing antibody responses[28,29]. By contrast, the lack of detailed information on the structure of the full-length PfCSP on the surface of the parasite has hindered structure-based vaccine design. However, over the last several years there have been major advances in the structural information on protective monoclonal antibodies (mAbs) targeting the major repeats, minor repeats, and junctional region of PfCSP[14–16,30–37]. These structures, which mainly comprise mAbs bound to PfCSP-derived peptides or truncated proteins, and other biophysical analyses, have revealed a structural heterogeneity in the antigens that suggests the repeat region of PfCSP is relatively disordered and can adopt various conformations[38]. Although designed antigens based on these structures have not yet been reported, they have led to the exploration of immunogens that include additional regions of CSP beyond the major repeats and CTD. Most of these have comprised peptide antigens based on the junctional region[39–44], although in one case a peptide antigen fused to a major repeat-targeting Fab was displayed on a self-assembling nanoparticle to favor the acquisition of homotypic Fab-Fab contacts during affinity maturation[45], a phenomenon observed in some major repeat-targeting antibodies and the minor repeat-targeting antibody L9[36,46].

Multivalent display of antigens on self-assembling or particulate scaffolds has been shown to improve vaccine-elicited antibody responses by enhancing vaccine trafficking, antigen presentation, and B cell activation[47–50]. Multivalent antigen display has been extensively explored as an approach to malaria vaccine design, and in fact RTS,S was until recently the only licensed vaccine in which an antigen is displayed on a heterologous self-assembling scaffold, in this case Hepatitis B virus surface antigen virus-like particles[51]. Beyond RTS,S and R21, numerous groups have used virus-like particles, ferritin, lumazine synthase, or self-assembling peptides to improve the potency of CSP-derived antigens in preclinical studies[39–41,45,52–57]. Computationally designed self-assembling protein nanoparticles have recently emerged as a robust and versatile platform for multivalent antigen display that enables many structural and antigenic characteristics of the immunogen to be precisely varied[58–63]. Furthermore, a computationally designed two-component nanoparticle vaccine for SARS-CoV-2, SKYCovione™, recently became the second licensed vaccine—after RTS,S—in which an antigen is displayed on a heterologous self-assembling protein scaffold, establishing the clinical and commercial viability of the platform[62,64].

Here we combined extensive exploration of different PfCSP-based antigens with multivalent display on self-assembling protein scaffolds, including computationally designed protein nanoparticles, and benchmark them against the state-of-the-art vaccine R21. We found that the

epitope specificity of vaccine-elicited antibodies could be tuned by displaying antigens comprising different target epitopes in PfCSP, and that the most potently protective responses were elicited by nanoparticle immunogens primarily displaying the major repeats.

Results

Design of stabilized PfCSP variants with increased expression

We began by expressing full-length PfCSP so that we could use it as a benchmark antigen in our studies (**Fig. 1a**). We noticed that the wild-type (WT) protein expressed poorly (50 µg/L after purification) in HEK293E cells and that its apparent molecular weight according to SDS-PAGE and size exclusion chromatography (SEC) was closer to ~70 kDa than the expected 41.5 kDa (**Fig. 1b**). This difference has been observed by others and is likely due to the protein being disordered[38]. We also noticed that recombinant PfCSP appeared sensitive to cleavage when left overnight at 4°C[65]. We performed N-terminal sequencing of this protein sample and found that the protein was cleaved between $_{66}$KKNSR$_{70}$ and $_{71}$SLGENDD$_{77}$, within the PEXEL II sequence ($_{70}$RSLGE$_{74}$; ref. [66]) (**Fig. 1c**). Since the KKNSR sequence preceding the cleavage site resembles a furin cleavage site, we used site-directed mutagenesis to mutate the positively charged residues (Lys and Arg) to serine and alanine to change $_{66}$KKNSR$_{70}$ to $_{66}$SSNSA$_{70}$, similar to what was done for the HIV-1 Env and SARS-CoV-2 Spike glycoproteins[67–69]. We transiently expressed this construct, named C25-SAmut, in HEK293E cells and observed a 400-fold increase in protein expression to 20 mg/L (**Fig. 1d**). However, a large portion of the protein eluted as what appeared to be a dimer on SEC. We noticed the presence of an unpaired cysteine residue at position 25 in the NTD and hypothesized it was likely responsible for mediating dimerization via an intermolecular disulfide bond. We therefore further mutated C25-SAmut to generate SAmut by mutating the cysteine to serine[70]. SAmut expressed well (20 mg/L), eluted during SEC as a single symmetric peak, and did not degrade upon storage at 4°C (**Fig. 1e**).

Although full-length PfCSP contains all possible protective epitopes in the protein and could therefore in principle elicit a variety of protective antibodies, we wanted to test the hypothesis that a high frequency of the major repeat epitope NANP may reduce the immunogenicity of other protective epitopes. We therefore designed additional SAmut variants with truncated numbers of NANP repeats. SAmut-19/3 and SAmut-5/3 contain 19 and 5 NANP major repeats, respectively, 3 NVDP minor repeats, and the NPDP tetrapeptide from the junctional epitope targeted by CIS43[14] (**Fig. 1a**). SAmut-19/3 has the same number of major repeats as the construct used in RTS,S and R21[51,71], while SAmut-5/3 is more balanced, with 3 CIS43 epitopes and 3 L9 epitopes as well as 2 epitopes for 317, as was determined by isothermal titration calorimetry[16], and thus could be a better immunogen for targeting these alternative epitopes. We characterized the antigenicity of the SAmut variants in comparison to full-length WT PfCSP by ELISA, using a panel of PfCSP-directed antibodies (**Fig. 1f**). NHP20 is an unpublished antibody isolated from a non-human primate immunized with WT PfCSP that binds to the NTD. CIS43 (junctional epitope), L9 (minor epitope), and mAb10 (major repeat) are all repeat-binding mAbs, and mAb15 is a CTD-directed mAb[16]. All mAbs bound the stabilized variant proteins similarly as the WT full-length PfCSP, indicating that the mutations we introduced did not impact their

recognition. Together, these data show that we generated a series of antigenically intact PfCSP variants with substantially improved expression and stability.

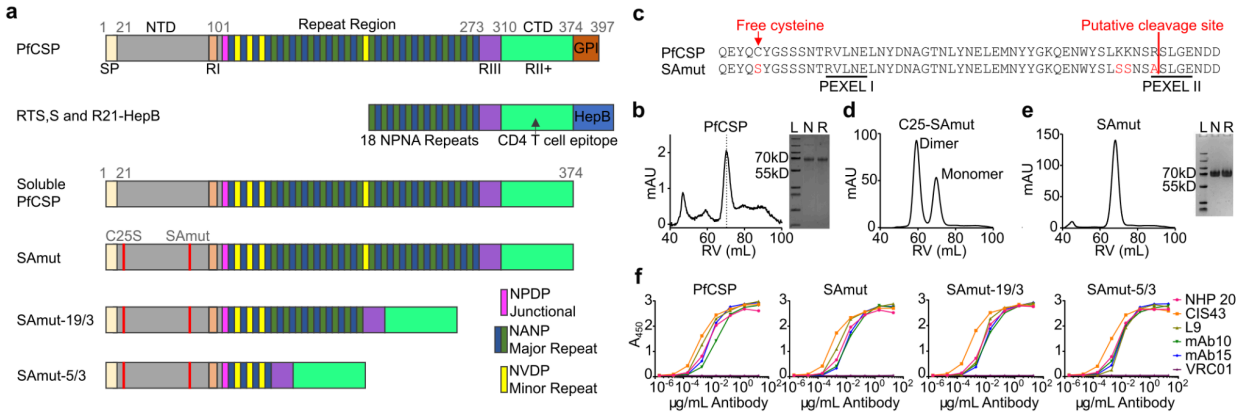

Figure 1. Biophysical characterization and antigenicity of stabilized PfCSP variants. a Primary structures of various PfCSP variants, including the R21 immunogen. SP, signal peptide; RI, Region I; RIII, Region III; RII+, Region II; GPI, glycosylphosphatidylinositol anchor sequence. **b** SEC and SDS-PAGE of WT PfCSP. L, ladder; N, non-reduced; R, reduced. **c** Sequences of the WT PfCSP and SAmut NTDs. SEC and SDS-PAGE of **d** C25-SAmut and **e** SAmut. **f** Binding of WT PfCSP and SAmut variants to PfCSP-directed mAbs measured by ELISA. NHP20 binds the NTD, CIS43 is a dual binder for the junctional epitope and NANP, L9 is a dual binder for the minor NVDP epitope and NANP, mAb10 is a NANP repeat-only directed antibody, and mAb15 binds the CTD. VRC01 is an anti-HIV-1 antibody used as a negative control.

Immunogenicity and protective efficacy of stabilized PfCSP variants displayed on nanoparticles

To evaluate the effect of multimerization on PfCSP immunogenicity, we used the SpyTag-SpyCatcher (ST-SC) "plug-and-display" technology[72] to display SpyTagged SAmut-5/3. We selected SAmut-5/3 as it contained the fewest immunodominant NANP repeats and consequently the most balanced complement of epitopes. We displayed this antigen on a variety of self-assembling protein nanoparticles—C4b[87], ferritin[88], and I53-50[58]—which present 7, 24, and 60 copies of SC, respectively. We expressed and purified SAmut-5/3-ST protein and the homomeric SC-nanoparticles (SC-C4b and SC-ferritin) separately and then conjugated the antigen to each SC-nanoparticle. For the two-component SC-I53-50 nanoparticle, we conjugated SAmut-5/3-ST to the trimeric SC-I53-50A component (**Supplementary Fig. 1**), assembled the nanoparticle by adding the I53-50B.4PT1 pentamer[58], and purified the assembled nanoparticle by SEC. SDS-PAGE revealed little unconjugated SC-bearing protein in each case, suggesting highly efficient conjugation (**Supplementary Fig. 1**), and SEC and negative stain electron microscopy (nsEM) indicated that each nanoparticle immunogen retained the expected size and morphology after conjugation (**Fig. 2a-c**). All of the mAbs in the panel described earlier bound each nanoparticle by ELISA, establishing that the SAmut-5/3 retained its antigenicity when multimerized (**Fig. 2d**).

To evaluate the effect of multimerization and antigen copy number on immunogenicity and protection, we immunized groups of 10 C57BL/6 (B6 albino) mice with a constant molar dose of

antigen at weeks 0 and 3 using ALFQ adjuvant[73] (**Fig. 2e**). ALFQ is a liposome based adjuvant with synthetic monophosphoryl lipid A analog, 3D-PHAD®, and QS-21 similar to the composition of AS01 used as an adjuvant for the RTS,S vaccine. As we could not access RTS,S for these studies, we included R21, also adjuvanted with ALFQ, as a benchmark immunogen. We intravenously challenged the mice at week 6 with 2,000 transgenic *P. berghei* parasites that express PfCSP in place of endogenous PbCSP and GFP/luciferase for measuring liver burden (Pb-PfCSP-GFP/LUC)[74]. Liver burden measurements two days after challenge indicated that increased antigen copy number resulted in significantly increased protection compared to the unvaccinated control mice: the I53-50 nanoparticles displaying ~60 copies of SAmut-5/3 conferred higher protection than the ferritin (~24 copies) or C4b (~7 copies) nanoparticles (**Fig. 2f**). In addition, only SAmut-5/3-I53-50 significantly reduced liver burden compared to an unimmunized control group ($p<0.01$). R21 more significantly reduced liver burden compared to the unvaccinated group (max burden; $p<0.0001$) than any of the other multimeric antigens. The superior performance of R21 may be due to the different antigen it displays (**Fig. 1a**) or other features of the HBsAg particle.

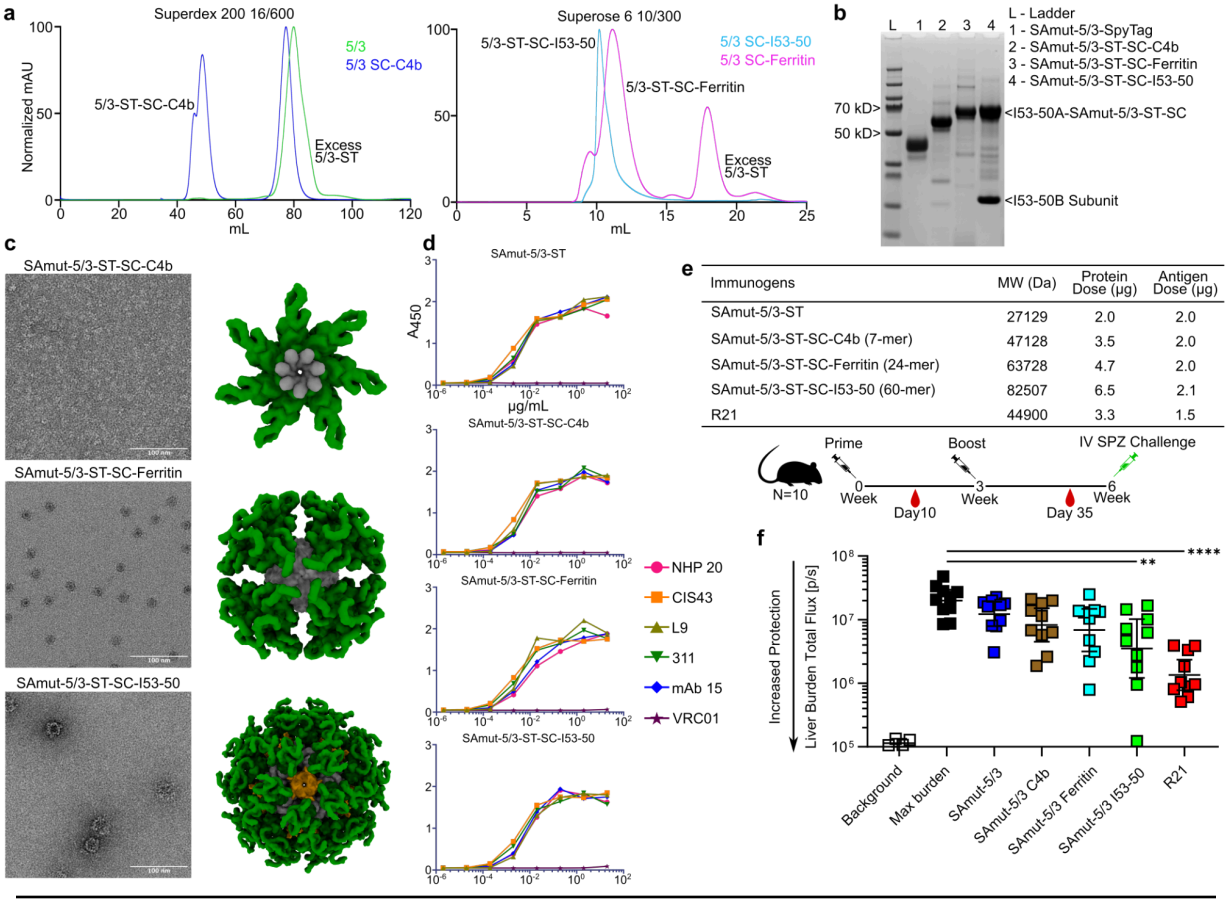

Immunogens	MW (Da)	Protein Dose (µg)	Antigen Dose (µg)
SAmut-5/3-ST	27129	2.0	2.0
SAmut-5/3-ST-SC-C4b (7-mer)	47128	3.5	2.0
SAmut-5/3-ST-SC-Ferritin (24-mer)	63728	4.7	2.0
SAmut-5/3-ST-SC-I53-50 (60-mer)	82507	6.5	2.1
R21	44900	3.3	1.5

Figure 2. Biophysical characterization, antigenicity, and immunogenicity of SAmut-5/3 multimers. a SEC profiles of each multimer. **b** Reducing SDS-PAGE of purified SAmut-5/3 immunogens. **c** nsEM of the SAmut-5/3 multimers. Micrographs and structural models of each multimer are shown. **d** Binding of multimers to PfCSP-directed mAbs measured by ELISA. 311 is a major repeat-targeting mAb. **e** Immunization regimen and details. IV, intravenous; SPZ, sporozoite. **f**

Parasite burden in the liver after challenge with transgenic sporozoites. R21 was used as a benchmark immunogen. *, $p < 0.1$; **, $p < 0.01$; ***, $p < 0.001$; **** $p < 0.0001$ as calculated by Kruskal-Wallis test with multiple comparisons.

Design and characterization of nanoparticle immunogens comprising the CSP junctional region

Given that the I53-50-based immunogen showed good protection in our initial study and this nanoparticle has proven capable of displaying a wide variety of antigens[60–62,75], we selected I53-50 as a platform for iterative CSP-based nanoparticle vaccine design. Our overall aims were to evaluate the contribution of each region of CSP to immunogenicity and protection, and to evaluate whether variants of the repeat region could increase the likelihood of eliciting protective antibodies that bind the junctional and minor epitopes that are not present in RTS,S and R21[14–16]. We used genetic fusion for these studies rather than SC-ST conjugation to generate well-defined immunogens and to simplify our workflow by eliminating the need for a conjugation step. We began by genetically fusing the truncated repeat region and CTD of CSP found in RTS,S and R21 (i.e., the "RT" antigen) to I53-50A, the trimeric component of I53-50 (**Fig. 3a,b**). *In vitro* assembly of RT-I53-50A with I53-50B.4PT1 followed by preparative SEC yielded monodisperse nanoparticles of the expected size and morphology (**Supplementary Fig. 2**). We then replaced RT with a series of antigens that included the full NTD or Region I (RI), comprised several different variations of the central repeat region, and lacked the CTD (CSP A-H, **Supplementary Table 1**). Though the CTD contains T cell helper epitopes[76,77], we explored whether it could be excluded because it has been shown that antibodies targeting it are weakly neutralizing or do not inhibit parasite traversal/development[78,79]. These designs all expressed but were prone to aggregation except for CSP F, the only design which contained a truncated N-terminal domain comprising only the RI (**Fig. 3b**). We were able to successfully assemble and characterize CSP F nanoparticles that closely resembled RT-I53-50 (**Supplementary Fig. 2**). We then tested whether similarly truncating the N-terminal domain in the other proteins would improve their solution properties, but the new constructs (CSP A2-H2; **Supplementary Table 1**) also aggregated and were not pursued further.

We then tested a new family of designs that included the CTD, as it appeared to be important for the solution properties of I53-50A fusion proteins displaying CSP-derived antigens. Four designs contained RI, the junctional region, and increasing numbers of major repeats (up to 17; CSP P, Q, R, and J), while a fifth was identical to CSP J except that it lacked the RI (CSP K; **Fig. 3b**). All of these constructs were successfully expressed in *E. coli*, purified, and assembled into nanoparticles by mixing with I53-50B.4PT1 pentamer. In each case, analytical SEC, dynamic light scattering (DLS), and nsEM revealed monodisperse populations with the expected morphology, and binding of mAbs specific to various regions of PfCSP showed the expected patterns (**Supplementary Fig. 2**). Interestingly, similar constructs that contained the entire repeat region of PfCSP failed to express (CSP L and M; **Supplementary Table 1**). In summary, we generated a series of nanoparticle immunogens displaying various CSP-derived antigens that would allow us to evaluate the contribution of each region of the protein to immunogenicity and protection.

Immunogenicity of nanoparticle immunogens comprising the CSP junctional region

To evaluate immunogenicity and the protection afforded by this series of nanoparticle immunogens, mice were injected in groups of 10 intramuscularly with 3 μg of each nanoparticle formulated with ALFQ, followed by two homologous boosts given three weeks apart (**Fig. 3c**). As benchmarks, mice were immunized with RT-I53-50 nanoparticles and non-assembled RT-I53-50A trimers. Serum was collected 1-2 weeks after each immunization and measured anti-SAmut titers by ELISA (**Fig. 3d**). Although the RT-I53-50 nanoparticles elicited significantly higher levels of antigen-specific antibodies than the RT-I53-50A trimer and CSP F nanoparticles after a single immunization, all groups had similar titers in the anti-SAmut ELISA after three immunizations.

To determine the epitopes targeted by vaccine-elicited antibodies, we conducted a peptide binding ELISA using pooled sera from each group of mice. We used a series of overlapping peptides, spanning the repeat region and CTD of PfCSP, which we refer to as peptides 20-61 and C-term (**Fig. 3e**; ref. [14]). As expected, sera from mice vaccinated with immunogens containing the CTD (i.e., all except CSP-F) showed a strong response to this domain. Also as expected, serum antibodies from RT-I53-50-vaccinated mice had a strong preference for binding to NANP-containing peptides 27 (NVDPNANPNANPNAN), 29 (NANPNANPNANPNAN), and 61 (NANPNANPNANPNKN), but did not bind well to peptides containing the junctional epitope or minor repeats. Sera from mice that received immunogens containing the junctional region displayed more balanced binding across the set of peptides, although with varying magnitudes that roughly correlated with the total number of repeats in each immunogen. For example, CSP P elicited weak responses against repeat peptides while CSP Q and R showed stronger binding across all peptides tested, including peptide 20, which spans the junctional epitope (PADGNPDPNANPNVD). CSP F, J, and K, which included more copies of the major repeat, showed stronger binding that was more balanced than RT-I53-50 but skewed more toward the major repeats (i.e., peptides 27 and 29) than CSP Q and R.

Six weeks after the second boost, we challenged the mice intravenously with 2,000 sporozoites and measured liver burden 2 days later by IVIS (**Fig. 3f**). Although all of the immunogens other than CSP P and Q provided significantly better protection than the max burden (i.e., unimmunized) control group, only CSP K reached the same level of statistical significance as RT-I53-50. Considered together with the peptide ELISA data (**Fig. 3e**), these results indicate that immunogens with higher major repeat content (i.e., RT-I53-50 and CSP F, J, K, and R) induced better protection than those focused only on the junctional region or containing a reduced number of major repeats (i.e., CSP P & Q). Furthermore, the data show that the non-assembling RT-I53-50A trimer confers less protection than the RT-I53-50 nanoparticle, and that pre-challenge anti-SAmut ELISA titers alone cannot be used to reliably predict protection[80,81]. Overall, our data demonstrate that we were able to modulate the epitope specificities of vaccine-elicited antibodies by displaying various CSP-derived antigens on I53-50, but that none of the novel immunogens was able to induce better protection than our benchmark RT-I53-50 nanoparticle immunogen.

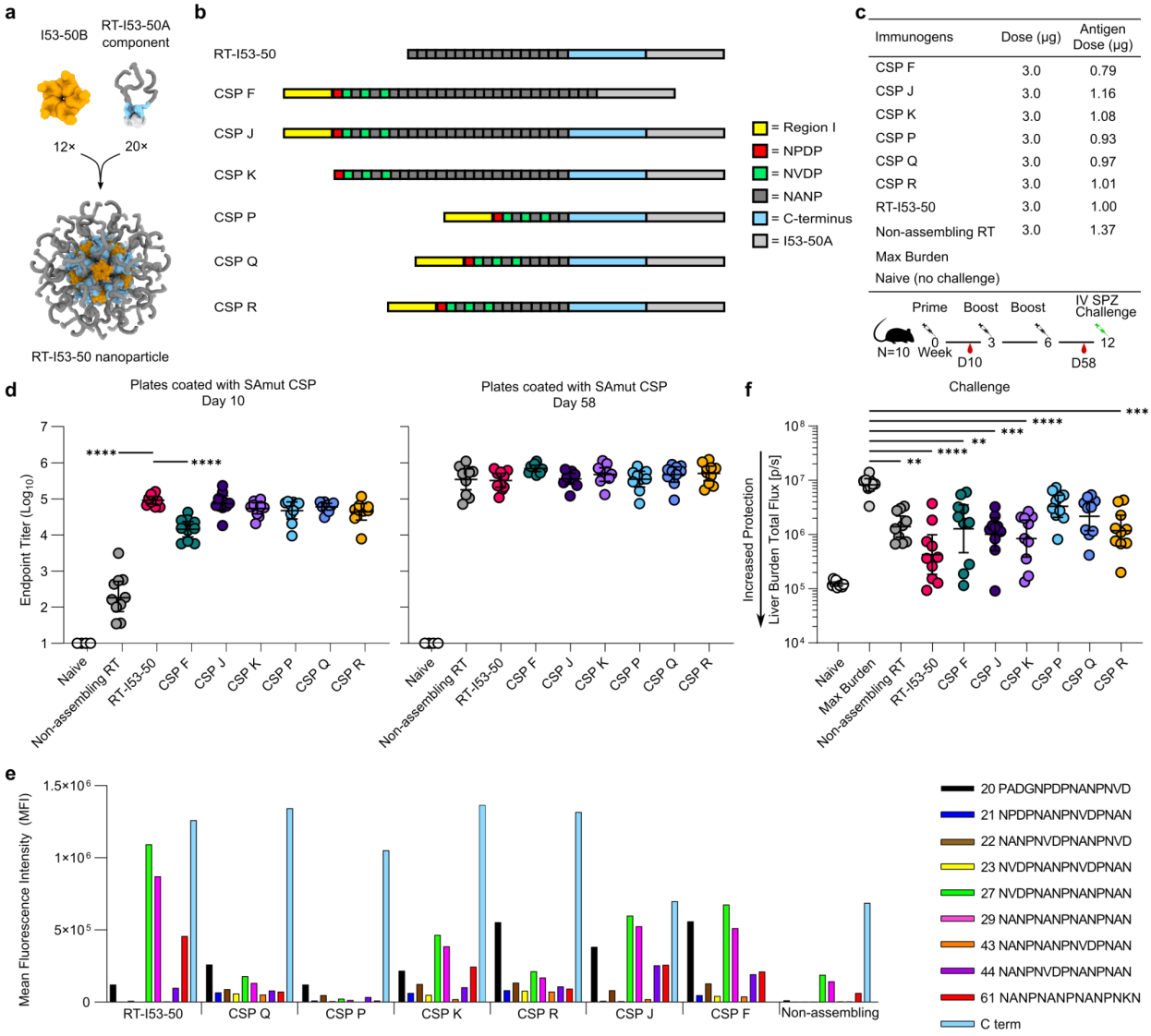

Figure 3: Design, characterization, and immunogenicity of nanoparticle immunogens comprising the CSP junctional region. a Models of the trimeric RT-I53-50A (RT in dark gray and blue, I53-50A in light gray) and pentameric I53-50B (orange) components, and an assembled RT-I53-50 nanoparticle. **b** Schematics of junctional region antigens. Each antigen was genetically fused to I53-50A. **c** Immunization regimen and details of the study. **d** Serum antibody titers against SAmut, determined by ELISA using sera obtained 1-2 weeks after the primary and third immunizations. Statistical significance was calculated by one-way ANOVA with multiple comparisons. **e** Peptide mapping ELISAs using pooled sera from each group, measured using mesoscale discovery (MSD) -multi-spot assay system.. **f** Parasite burden in the liver after challenge with transgenic sporozoites. RT-I53-50 was used as the benchmark immunogen. *, $p < 0.1$; **, $p < 0.01$; ***, $p < 0.001$; ****, $p < 0.0001$ as calculated by Kruskal-Wallis test with multiple comparisons.

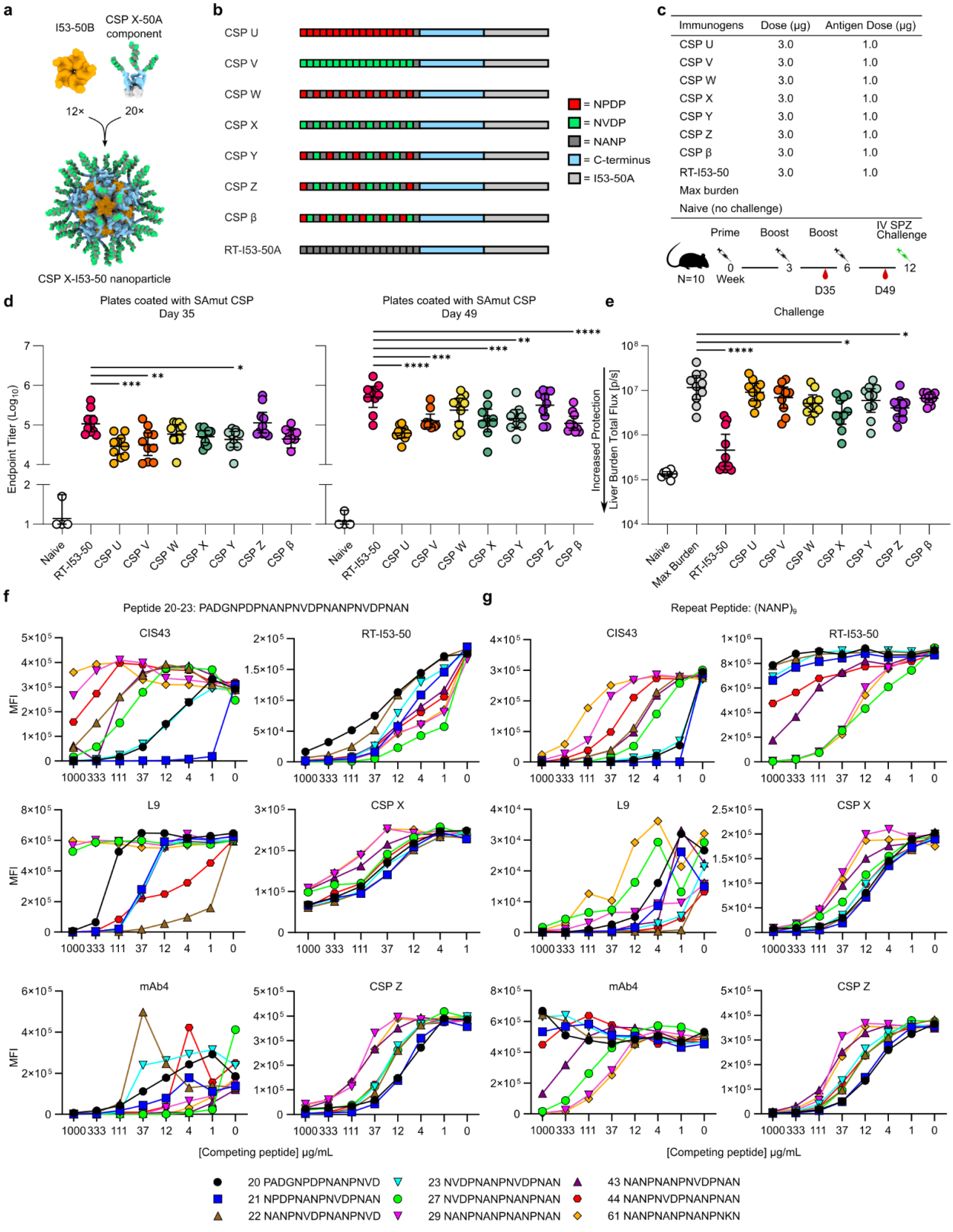
a
I53-50B
CSP X-50A component
12×
20×
CSP X-I53-50 nanoparticle
b
CSP U
CSP V
CSP W
CSP X
CSP Y
CSP Z
CSP β
RT-I53-50A
= NPDP
= NVDP
= NANP
= C-terminus
= I53-50A
c
Immunogens | Dose (μg) | Antigen Dose (μg)
CSP U | 3.0 | 1.0
CSP V | 3.0 | 1.0
CSP W | 3.0 | 1.0
CSP X | 3.0 | 1.0
CSP Y | 3.0 | 1.0
CSP Z | 3.0 | 1.0
CSP β | 3.0 | 1.0
RT-I53-50 | 3.0 | 1.0
Max burden
Naive (no challenge)
Prime
Boost
Boost
IV SPZ Challenge
N=10
0 Week
3
6
12
D35
D49
d
Plates coated with SAmut CSP Day 35
Plates coated with SAmut CSP Day 49
Endpoint Titer (Log10)
Naive
RT-I53-50
CSP U
CSP V
CSP W
CSP X
CSP Y
CSP Z
CSP β
e
Challenge
Increased Protection
Liver Burden Total Flux [p/s]
Naive
Max Burden
RT-I53-50
CSP U
CSP V
CSP W
CSP X
CSP Y
CSP Z
CSP β
f
Peptide 20-23: PADGNPDPNANPNVDPNANPNVDPNAN
CIS43
RT-I53-50
L9
CSP X
mAb4
CSP Z
MFI
1000 333 111 37 12 4 1 0
[Competing peptide] μg/mL
g
Repeat Peptide: (NANP)9
CIS43
RT-I53-50
L9
CSP X
mAb4
CSP Z
[Competing peptide] μg/mL
20 PADGNPDPNANPNVD
21 NPDPNANPNVDPNAN
22 NANPNVDPNANPNVD
23 NVDPNANPNVDPNAN
27 NVDPNANPNANPNAN
29 NANPNANPNANPNAN
43 NANPNANPNVDPNAN
44 NANPNVDPNANPNAN
61 NANPNANPNANPNKN

Figure 4: Design, characterization, and immunogenicity of non-native CSP-repeat nanoparticles. a. Models of the CSP X-I53-50A trimer (CSP X in green, dark gray, and blue; I53-50A in light gray), I53-50B (orange), and an assembled CSP X-I53-50 nanoparticle. **b** Schematics of non-native CSP-repeat antigens. Each antigen was genetically fused to I53-50A. **c** Immunization regimen and details of the study. **d** Serum antibody titers against SAmut, determined by ELISA using sera obtained after the second and third immunizations. Statistical significance was calculated by one-way ANOVA test with multiple comparisons. **e** Parasite burden in the liver after challenge with transgenic sporozoites. RT-I53-50 was used as the benchmark immunogen. *, $p < 0.1$; **, $p < 0.01$; ***, $p < 0.001$; ****, $p < 0.0001$ as calculated by Kruskal-Wallis test with multiple comparisons. **f** Peptide competition assay using pooled mouse sera from each group with peptide 20-23 as the plated antigen. **g** Peptide competition assay with the repeat peptide $(NANP)_9$ as the plated antigen.

Design, characterization, and immunogenicity of non-native CSP-repeat nanoparticles

We next designed a series of I53-50A trimers bearing non-native repeat-based antigens to attempt to further focus the vaccine-elicited immune response towards the junctional region or minor repeats (**Fig. 4a,b**). Each antigen in the series comprised 18 total repeats, always ending a major repeat to provide a native-like junction with the C-terminal domain. We designed constructs that displayed alternating forms of the CSP junctional region (CSP Y, Z), alternating junctional-major or minor-major repeats (CSP W, X), completely non-native sequences that included junctional or minor repeats only (CSP U, V) as well as a tandem junctional-minor-major repeat antigen (CSP β). All of these I53-50A fusion proteins were expressed in *E. coli*, purified using IMAC and SEC, and mixed with I53-50B to generate nanoparticle immunogens. Analytical SEC, DLS, and nsEM again indicated the formation of monodisperse I53-50-based nanoparticle immunogens (**Supplemental Fig. 3**). Antigenicity was characterized by ELISA and showed that most of the mAbs in our panel bound each of the immunogens, though most notably a decrease or loss in binding for CIS43 was observed for CSP U, V, W, and β (**Supplemental Fig. 4**).

Like our previous immunization study, we immunized groups of 10 mice three times intramuscularly with 3 μg of RT-I53-50 or each non-native repeat nanoparticle formulated with ALFQ adjuvant (**Fig. 4b,c**). In this instance, each group of mice received nearly the same number of moles of nanoparticle immunogen because of their nearly identical molecular weights. Anti-SAmut CSP titers measured by ELISA after the second and third immunizations showed that RT-I53-50 induced the highest CSP-specific antibody titers (**Fig. 4d**). CSP Z, which comprised two tandem repeats of the entire junctional region of PfCSP, elicited the highest SAmut CSP-specific antibody titers among the non-native repeat nanoparticles. As before, the mice were challenged with 2,000 sporozoites six weeks after the second boost and parasite load in the liver was measured (**Fig. 4e**). RT-I53-50, CSP-X, and CSP-Z were the only three immunogens that significantly reduced liver burden compared to the max burden control group, with RT-I53-50 providing the best protection. These results may be explained by the fact that these immunogens contained more native-like repeat cadences, while the others had higher proportions of non-native sequences of repeats such as NANP-NPDP or NPDP-NVDP (**Fig. 4b**).

To map the epitopes targeted by antibodies elicited by these three protective immunogens, we used a variation of the peptide binding ELISA in which serum antibody binding to a combined

peptide 20-23 or a major repeat peptide coated on the ELISA plate (PADGNPDPNANPNVDPNANPNVDPNAN and $(NANP)_9$, respectively) competed with binding to free peptides pre-incubated with the pooled sera (**Fig. 4f,g**). The peptides used for competition (peptides 20-61) spanned the repeat region of PfCSP. We first gauged the performance of the assay using three mAbs that bind the major, junctional, and minor repeat regions (mAb4 [ref. [14]], CIS43, and L9, respectively) and found that the preferred peptide epitopes of each mAb competed with its binding to the plated antigens as expected. Specifically, mAb4 bound $(NANP)_9$ more strongly than peptide 20-23 and exhibited the greatest reduction in binding in the presence of major repeat-containing peptides (peptides 27, 29, 61), while L9 bound peptide 20-23 more strongly and showed the greatest reduction in signal in the presence of peptides containing minor repeats (peptides 20, 21, 22, 23, 43, and 44). CIS43 bound both peptides strongly as expected[14] and showed a clear and consistent rank-ordering of peptide competition (peptide 21 > 20, 23 > 27 > 22, 43 > 44 > 29 > 61). Based on these mAb benchmarking data, we concluded that the peptide competition assay provided a sensitive readout of epitope specificity. Serum antibodies elicited by CSP X and CSP Z bound both ELISA antigens roughly equivalently, whereas the sera from mice receiving RT-I53-50 clearly bound $(NANP)_9$ more strongly than peptide 20-23 as expected. For all three immunogens, the rank-ordering of competing peptides was consistent across both ELISA antigens. Anti-RT-I53-50 sera were most strongly competed by peptides containing higher numbers of major repeats (peptides 27, 29, and 61) and less so by peptides from the junctional region (peptides 20, 21, 22, and 23). By contrast, peptides containing minor repeats and those from the junctional region most effectively prevented CSP X- and Z-elicited antibodies from binding to the plated antigens, respectively. For both of the latter two immunogens, the major repeat peptides (peptides 29, 43, and 61) provided the weakest competition.

Together, these data support several conclusions. First, synthetic repeat cadences that do not appear in PfCSP do not efficiently elicit protective antibodies in this challenge model. Second, the epitope specificity of vaccine-elicited antibodies can be tuned by displaying antigens with altered numbers or arrangements of native-like repeat sequences. Finally, immunogens that include many copies of the minor repeat alternating with the major repeat do elicit protective antibodies, but less so than RT-I53-50, which comprises only major repeats in addition to the C terminus of PfCSP.

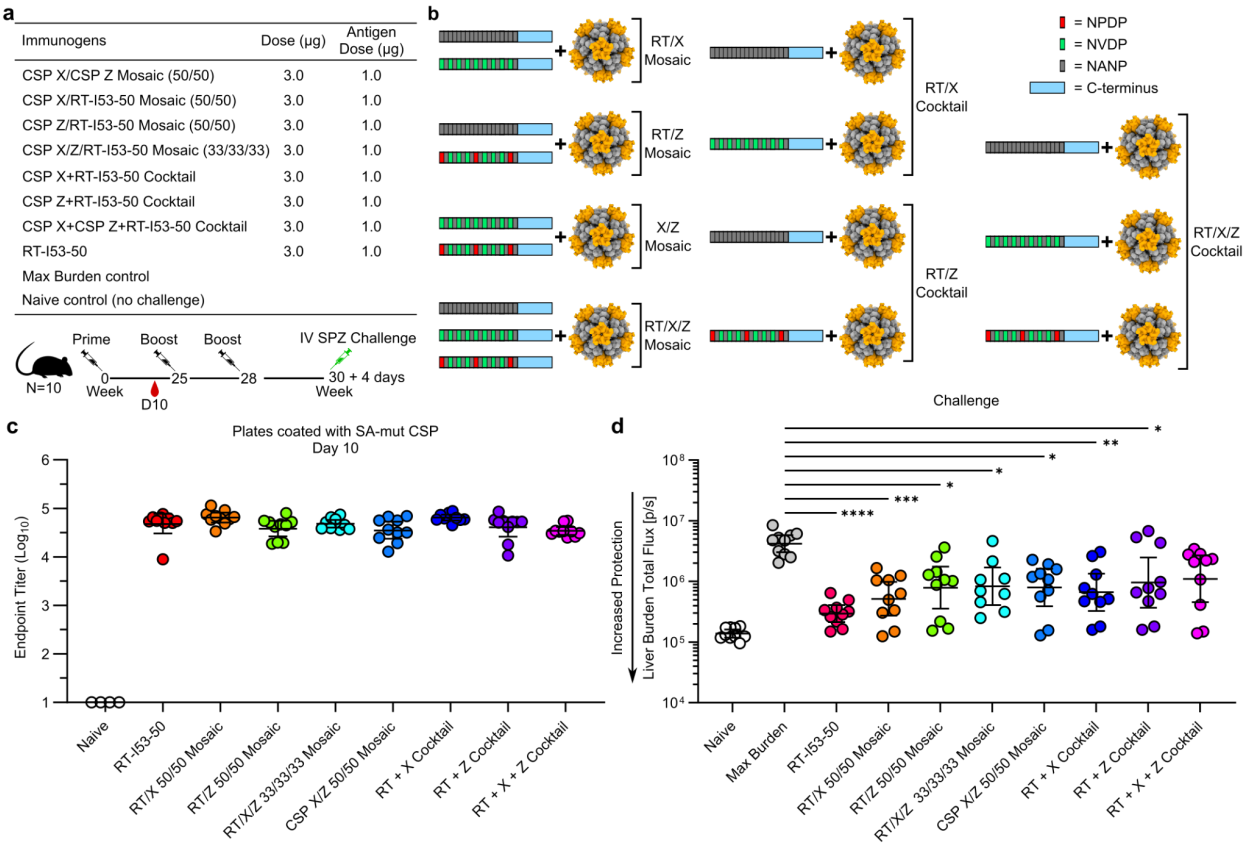

Figure 5: Immunogenicity and protection afforded by mosaic and cocktail nanoparticle immunogens. a Immunization regimen and details of the study. **b** Schematics depicting the antigenic composition of each immunogen: either mosaic nanoparticles with 33 or 50% valency of each antigen, or groups (cocktails) of monovalent nanoparticles. **c** ELISA endpoint titer of each immunogen to SAmut-coated plates post-prime. Statistical significance was calculated by one-way ANOVA test with multiple comparisons. **d** Parasite burden in the liver after challenge with transgenic sporozoites. RT-I53-50 was used as the benchmark immunogen. *, $p < 0.1$; **, $p < 0.01$; ***, $p < 0.001$; ****, $p < 0.0001$ as calculated by Kruskal-Wallis test with multiple comparisons.

Immunogenicity and protection afforded by mosaic and cocktail nanoparticle immunogens

Previous analyses have indicated that the most potently protective anti-CSP mAbs tend to be those that bind the major repeats with high affinity while also cross-reacting with the junctional and minor epitopes[15,33,82]. To explore whether we could elicit protective levels of such cross-reactive antibodies by vaccination, we conducted another mouse immunogenicity and challenge study in which we compared a series of mosaic and cocktail nanoparticle immunogens based on CSP X, CSP Z, and RT-I53-50. Several studies over the last few years have evaluated mosaic nanoparticle immunogens that co-display multiple antigenic variants on the same nanoparticle for their ability to elicit B cell and antibody responses of greater breadth than monovalent nanoparticles or mixtures thereof (“cocktails”)[63,83–95]. Two-component assemblies like I53-50 facilitate the production of mosaic nanoparticles since multiple antigens

can be co-displayed by simply adding I53-50B pentamer to mixtures of multiple different antigen-bearing I53-50A trimers[63,83–88,96,97].

We generated mosaic nanoparticles co-displaying RT and CSP X, RT and CSP Z, or CSP X and Z at 50% valency (i.e., 30 copies) each, as well as a mosaic nanoparticle co-displaying all three antigens at 33% valency (i.e., 20 copies) by adding a molar equivalent of I53-50B pentamer to appropriate mixtures of antigen-bearing I53-50A trimer components. We also made corresponding cocktail immunogens (i.e., RT + X, RT + Z, and RT + X + Z) by individually assembling and purifying each monovalent nanoparticle and then mixing them together. Analytical SEC, DLS, and nsEM indicated that the mosaic and cocktail nanoparticle immunogens assembled as intended (**Supplementary Figure 5**).

Following our previous immunization regimens, we administered 3 μg of each mosaic or cocktail nanoparticle immunogen to groups of 10 mice intramuscularly with ALFQ adjuvant, followed by two boosts (**Fig. 5a,b**). We again included RT-I53-50 as a benchmark immunogen as well as an unimmunized control group. Ten days post-prime, mice were bled and anti-SAmut CSP titers were measured by ELISA (**Fig. 5c**). All vaccine groups had similar anti SAmut CSP titers post-prime. Due to restrictions imposed during the COVID-19 pandemic, the study was put on hold after the primary immunization, resulting in an interval of 25 weeks between the prime and the first boost. Six weeks after the second boost, mice were challenged IV with 2,000 sporozoites and parasite liver load was measured by IVIS (**Fig. 5d**). Despite having similar post-prime anti-SAmut CSP titers, the immunogens conferred various reductions in liver burden compared to the mock-immunized control. RT-I53-50 was again the most protective immunogen with the lowest liver burden ($p<0.0001$), while the mosaic RT/X nanoparticle performed second-best ($p<0.001$) and the cocktail RT + X nanoparticle performed third-best ($p <0.01$). One potential reason for immunogens based on RT and CSP X being more protective compared to those based on CSP Z may be that they contain a higher proportion of native-like repeat cadences (e.g., NVDP-NANP and NANP-NANP vs. NANP-NPDP) and thus more protective epitopes, an interpretation that is also supported by our previous study (**Fig. 4**). Our data did not allow us to distinguish between the mosaic and cocktail immunogens; more detailed studies would be required to determine whether differences exist in the B cell and antibody responses elicited by each.

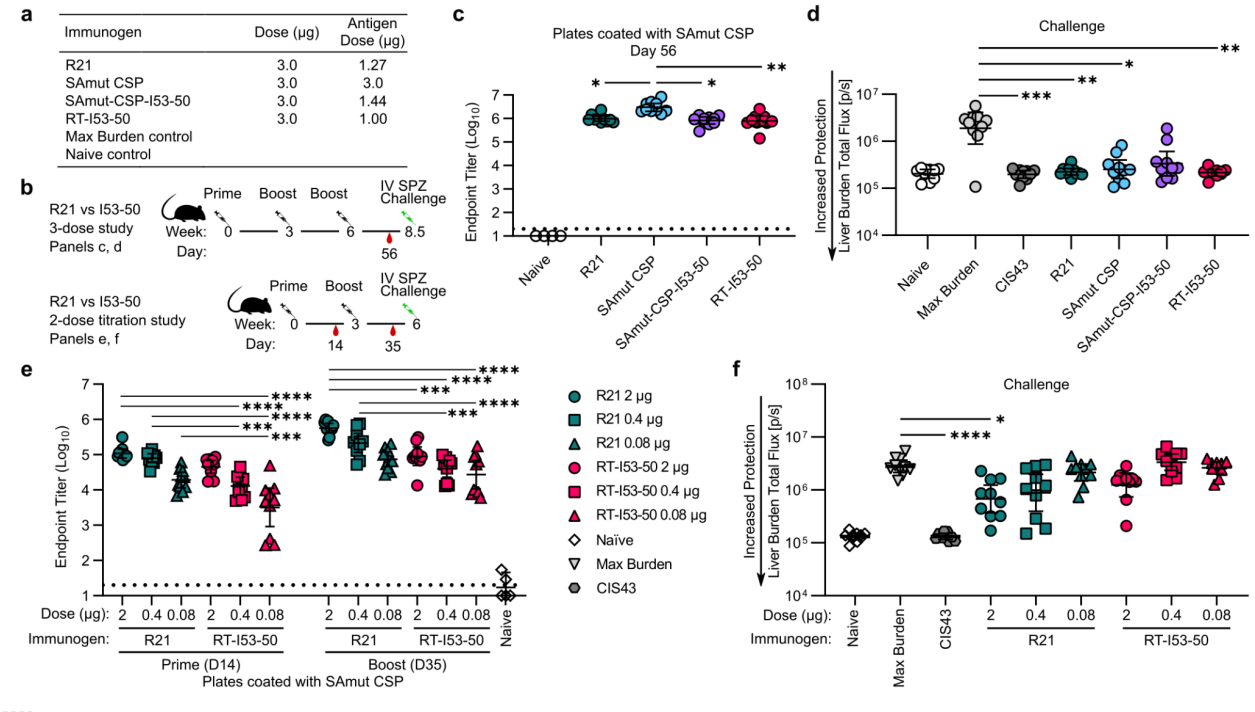

Figure 6: Comparison of R21 and RT-I53-50 adjuvanted with ALFQ. a Groups and doses used. **b** Immunization regimens and details for the three-dose and two-dose experiments. **c** ELISA endpoint titer for each immunogen in the three-dose study to SAmut-coated plates after the second boost and before the challenge. Statistical significance was calculated by one-way ANOVA test with multiple comparisons. **d** Parasite burden in the liver after three immunizations followed by challenge with transgenic sporozoites. * $p < 0.1$, ** $p < 0.01$, *** $p < 0.001$, **** $p < 0.0001$ as calculated by Kruskal-Wallis with multiple comparisons test compared to Max burden control. **e** ELISA endpoint titer for each immunogen in the two-dose titration study to SAmut-coated plates after the prime and boost immunizations. Statistical significance was calculated by one-way ANOVA test with multiple comparisons. **f** Parasite burden in the liver after two immunizations followed by challenge with transgenic sporozoites. *, $p < 0.1$; **, $p < 0.01$; ***, $p < 0.001$; **** $p < 0.0001$ as calculated by Kruskal-Wallis test with multiple comparisons compared to unimmunized (max burden) control.

Comparison of R21 and RT-I53-50 adjuvanted with ALFQ

As we repeatedly observed that RT-I53-50 conferred better protection than immunogens containing junctional or minor repeats, we compared it against R21 in a head-to-head immunogenicity and challenge study. We also included an I53-50 nanoparticle displaying full-length SAmut CSP as a genetic fusion to determine if inclusion of the NTD and the entire repeat region improved protection. A comparator group received soluble (i.e., non-particulate) SAmut CSP to control for the effect of multivalent display. The SAmut-CSP-I53-50A trimer was expressed in *E. coli*, purified by immobilized metal affinity chromatography (IMAC) and SEC, and assembled with I53-50B to form nanoparticles. The resultant SAmut-CSP-I53-50 nanoparticles were purified by SEC to remove residual components, and the purified assemblies were evaluated by DLS and analytical SEC, both of which indicated monodisperse nanoparticles of the expected size and morphology (**Supplementary Figure 6**).

Groups of 10 mice were immunized intramuscularly three times with a 5 μg total protein dose of R21, SAmut CSP, SAmut-CSP-I53-50, or RT-I53-50 formulated in ALFQ (**Fig. 6a,b**). We included a group that received 300 μg of CIS43 as a fully protective control and an unimmunized group as a negative control. Anti-SAmut CSP ELISA using sera obtained two weeks after the final immunization revealed that R21, RT-I53-50, and SAmut-CSP-I53-50 induced similar levels of anti-CSP antibodies, all three of which were lower than monomeric SAmut CSP (**Fig. 6c**). Following challenge, immunization with R21, RT-I53-50, and monomeric SAmut CSP all significantly reduced liver burden, with R21 and RT-I53-50 demonstrating complete protection using this immunization regimen (**Fig. 6d**).

To attempt to resolve potential differences in the levels of protection provided by R21 and RT-I53-50, we conducted another study in which we lowered the total protein dose to 2, 0.4, and 0.08 μg and reduced the number of immunizations to two (**Fig. 6b**). At each dose, R21 elicited higher levels of anti-SAmut CSP serum antibody titers post-prime and -boost, with comparable titers between R21 at 0.08 μg and RT-I53-50 at 2 μg (corresponding to 0.03 and 0.66 μg of RT antigen, respectively; **Fig. 6e**). This result was consistent with the parasite challenge results, with R21 at 2 μg being the only group other than the CIS43 mAb-treated control that significantly reduced liver burden compared to the mock-immunized group (**Fig. 6f**). Altogether, our data show that although immunization with RT-I53-50 and R21 in ALFQ induces equivalently robust protection after 3 doses, R21 is slightly more protective at lower doses and using a reduced number of immunizations.

Discussion

Here we analyzed the functional effects of including N-terminal, junctional region, minor, and major repeat epitopes in CSP subunit and protein nanoparticle vaccines. Our work complements and extends recent studies that have evaluated peptide-based antigens displayed on self-assembling carrier proteins or nanoparticles[39–41,43,44,52]. These studies have focused on one or a few antigens comprising epitopes from the junctional region of CSP, either alone or in combination with major repeat sequences. We employed an iterative, empirical approach in which we attempted expression of 130 constructs and evaluated liver burden protection offered by 27 different CSP-based immunogens. These immunogens displayed many different native-like or synthetic CSP-derived sequences and were compared head-to-head in a stringent intravenous sporozoite challenge model. In each challenge study, we included either RT-I53-50 or R21 so that we could compare the experimental antigens against high-performing benchmark immunogens. This strategy allowed us to directly evaluate the contribution of each region of CSP to protective immunity and explore approaches to CSP-based antigen design that had not previously been tested to our knowledge. Our data support several conclusions that may help guide the design of next-generation CSP-based vaccines.

First, by comparing a series of nanoparticles displaying the same total amount of stabilized CSP-derived antigen, but in different numbers of copies on each nanoparticle, we established a correlation between increased antigen valency and improved protection against sporozoite challenge. This result is consistent with previous work from our groups and others using viral

glycoprotein antigens[48,60,98,99], and may in part explain the improved protection offered by the full-valency R21 immunogen compared to RTS,S[5,20]. In our experiments, R21 also provided better protection than the series of SAmut-5/3 nanoparticle immunogens we tested, indicating that antigen valency is not the only determinant of immunogenicity and protection. Other salient differences between R21 and the other nanoparticles include the different T cell epitope content in each nanoparticle[100], the fact that HBsAg is a lipoprotein complex[101,102], and the displayed antigens. Regarding the latter, SAmut-5/3 contains only 8 repeats (4 major, 3 minor, 1 junctional), while R21 contains 18 major repeats, which may improve B cell receptor cross-linking, B cell activation, and the induction of anti-CSP antibodies[47]. It is also possible that inclusion of the N-terminal region of CSP in SAmut-5/3 interferes with elicitation of protective anti-repeat antibodies, as this highly disordered[103] and weakly immunogenic domain is presumably the most exposed portion of the antigen when displayed on nanoparticles.

Second, although we found that including the junctional region and minor repeats in I53-50-displayed antigens successfully induced antibodies targeting these epitopes, these immunogens consistently underperformed against parasite challenge compared to RT-I53-50, which displayed only major repeats. Furthermore, by directly comparing a series of nearly identical nanoparticle immunogens that comprised variable numbers of major repeats, we observed a correlation between increasing numbers of major repeats and improved protection. As discussed above, this correlation may be explained by improved B cell receptor cross-linking or major repeat epitope accessibility in the nanoparticles containing more major repeats. The latter explanation is supported by our observation that RT-I53-50 conferred better protection than nanoparticle immunogens comprising more major repeats that also included the junctional region and N terminus (CSP F, J, and K). The importance of the NANP repeat as a central motif in the epitopes of anti-repeat antibodies[33] was further highlighted by our non-native CSP repeat cadence nanoparticles, which again were outperformed by the benchmark RT-I53-50 nanoparticle in challenge studies. CSP X and Z were the most native-like antigens in this series, comprising repeated instances of the NVDP-NANP cadence observed in the junctional region of CSP, and were the only two that significantly reduced liver parasite burden, although not as significantly as RT-I53-50. Although several groups have reported the induction of protective responses by displaying junctional region epitopes on various nanoparticle platforms[41,44,52], few have actually done direct, side-by-side comparisons against similar vaccines that comprise only major repeats[39,42]. This complicates direct comparisons between studies, as do several other differences in the models used to evaluate protection. For example, mosquito bite challenge may be less stringent than the intravenous challenge model we used here, but may allow contributions from antibodies that cross-react with the junctional region and have distinct activities in the skin[104]. Furthermore, it is possible that the murine antibody repertoire is not suited to producing antibodies with mechanisms similar to antibodies targeting the junctional region[15], which could lead to underestimation of the performance of immunogens containing the junctional and minor epitopes. We suggest that future studies of novel CSP-based vaccines include R21 as a benchmark immunogen whenever possible.

Third, we found that the CTD was beneficial for the manufacturability and immunogenicity of our nanoparticle vaccines. There is evidence that antibodies against the CTD of CSP correlate with

protection[81,105,106], but such antibodies appear to be rarely elicited by immunization with sporozoites[78], are weakly protective as mAbs[79,107], and may be susceptible to escape by antigenic variability[78,108]. Interestingly, we found that most of our designed immunogens lacking the CTD did not express solubly in *E. coli* or were prone to aggregation, suggesting that CTD has a stabilizing effect. The one nanoparticle immunogen we were able to produce without the CTD, CSP F, elicited significantly lower antibody titers post-prime than the RT-I53-50 comparator. This result suggests that a significant fraction of the antibody response elicited by the other immunogens was directed at the CTD (which is supported by our epitope mapping data), that known T cell epitopes in the CTD augment the vaccine-elicited antibody response[109], or both. We note that other next-generation CSP-based vaccine candidates do not contain the CTD [39,40,52]. Our data recommend its inclusion, although its potential elicitation of strain-specific antibodies will need to be addressed.

Finally, comparing our I53-50-based nanoparticle immunogens to R21 indicated that properties other than the displayed antigen significantly contribute to anti-malarial immunity. RT-I53-50 reduced liver burden after challenge equivalently to R21 after three doses, establishing it as a benchmark comparator. SAmut and SAmut-I53-50 showed weaker protection, with the latter potentially being affected by N-terminal interference or differences in nanoparticle stability. A follow-up two-dose titration study between RT-I53-50 and R21 showed that R21 was superior by anti-SAmut titer and liver burden reduction at all doses compared to RT-I53-50. As the CSP-based antigen displayed by R21 and RT-I53-50 in these studies was identical, the differences observed must be due to other factors, potentially including antigen copy number[48,60,98], display geometry[110], T cell epitope content[40,111], or potential adjuvanting effects of the R21 lipoprotein complex[101]. Our head-to-head comparisons, combined with recent reports from others demonstrating robust protection from CSP-based nanoparticle vaccines that include exogenous T cell help and N-linked glycans[40], suggest that engineering these additional features into I53-50-based vaccines could improve their performance. These features may be particularly important for antigens like PfCSP that lack N-linked glycans and have substantially reduced sequence complexity compared to many viral glycoprotein antigens.

In conclusion, we extensively explored multivalent display of CSP-based antigens on self-assembling nanoparticle scaffolds. Our benchmarked studies identified several antigen design approaches that are likely not worth exploring further, such as designing non-native repeat-based sequences, while highlighting other approaches that merit further consideration. Combining these approaches on a clinically validated nanoparticle platform like I53-50 may yield an optimal CSP-based immunogen, which will be the key component of next-generation vaccines that target multiple stages of the parasite life cycle[112].

Methods

PfCSP plasmid construction and mutations

The plasmid construction of WT PfCSP was described previously[14]. Briefly, mammalian codon-optimized PfCSP was cloned into a CMV/R-expression system with a C-terminal Avi-Tag, HRV3C cleavage site, and a 6x His-tag (GenScript). Mutations to CSP and repeat truncations were generated using site-directed mutagenesis with the QuikChange XL kit (Agilent). In brief, the K66S, K67S, and R70A mutagenesis was performed on the PfCSP plasmid followed by the C25S mutagenesis. The PfCSP-C25S-SAmut-19/3 truncation was generated from the full length plasmid. The PfCSP-C25S-SAmut-5/3 truncation was generated from the PfCSP-C25S-SAmut-19/3 plasmid.

PfCSP expression and purification

PfCSP or mutants were expressed through transient transfection in HEK293E cells (National Research Council of Canada (under license)) using the Freestyle 293F expression system at 37°C, 6% CO_2 for 6 days. Protein was purified from culture supernatants using Ni-NTA affinity resin followed by size exclusion chromatography (SEC) using a HiLoad 16/600 Superdex 200 pg column (Cytiva). Fractions containing protein were pooled, concentrated, flash-frozen in liquid nitrogen, and stored at -80°C.

N-terminal sequencing

N-terminal Edman sequencing was performed at the Protein and Nucleic Acid (PAN) Biotechnology Facility at Stanford.

SAmut-5/3-SpyTag expression and purification

A codon-optimized gBlock (IDT) of the last 100bp of CSP-SAmut with a C-term 6xHisTag and SpyTag was synthesized. The gBlock was amplified using Platinum SuperFi II PCR Master Mix (Invitrogen), and PfCSP-C25S-SAmut-5/3 amplified similarly. The construct was assembled with the Infusion HD Cloning Plus kit (Takara Bio). Primer designs are available in the Key Resources Table. The construct was transformed into NEB5α *E. coli* cells (New England BioLabs) and DNA isolated for transfection by MidiPrep (Qiagen). The construct was expressed in HEK293E cells (National Research Council of Canada (under license)) , with 500ug DNA, 2mg PEI, and 38mL PBS per 1L of culture at 1 million cells/mL. Cultures were harvested after 6 days at 37°C, 5% CO_2, and 140 rpm. Supernatant was sterile filtered (0.22 μm), batch bound to Ni-NTA resin overnight at 4°C and 120 rpm, and eluted with 5mM Tris buffer containing 300 mM imidazole. The complex was concentrated using a 10 kDa Amicon® (Millipore Sigma) spin column, sterile filtered (UltraFree-CL, Millipore Sigma), and injected onto a Superdex 200 16/600 column (Cytiva) equilibrated in HEPES (5mM HEPES, 150mM NaCl, pH 7.5). Purified protein was concentrated, and flash frozen for long term storage.

SpyTag CSP-I53-50 NP assembly

Purified CSP-SAmut-5/3 protein with SpyTag was mixed with I53-50A-Spy-Catcher subunit in a 1:1 molar ratio and incubated overnight at 4˚C. The complex was purified over a Superdex 200 16x600 column (GE healthcare) in 5mM HEPES, 150mM NaCl, pH 7.5. The complex was sterile filtered (UltraFree-CL, Millipore Sigma) and combined with an equal molar ratio of I53-50B and

incubated overnight at 4˚C to form nanoparticles. As needed, L-arginine up to 150mM was added to the nanoparticles to prevent aggregation. Nanoparticles were applied to a Superose 6 increase 10/300 GL column (GE healthcare) in 5mM HEPES, 150mM NaCl, pH 7.5 buffer to isolate the nanoparticles. Concentrations. were measured with a UV-Vis spectrometer and flash frozen in liquid nitrogen for long term storage.

SpyTag CSP-SCFerritin NP assembly

Purified ferritin nanoparticles with a 6x-Histag and SpyCatcher were mixed with purified SpyTag CSP-SAmut-5/3 protein in a 1:1 molar ratio of CSP to Ferritin/SpyCatcher particle subunit. 50mM L-arginine was added to prevent precipitation, and the conjugation was allowed to run overnight at 4˚C. The complex was purified over a Superose 6 Increase 10/100 GL column in 5mM HEPES, 150mM NaCl, pH 7.5 buffer, and concentrated using a 30 kDa Amicon® (Millipore Sigma) spin column before flash freezing in liquid nitrogen.

SpyTag CSP-C4b NP assembly

Purified C4b-SpyCatcher nanoparticles were mixed in a 2:1 molar ratio of CSP:C4b in HEPES buffer (in 5mM HEPES, 150mM NaCl, pH 7.5 buffer) and the reaction was allowed to go overnight at 4˚C. The complex was purified over a Superdex 200 16x600 column in 5mM HEPES, 150mM NaCl, pH 7.5 buffer. The complex was concentrated using a 30kDa Amicon® (Millipore Sigma) spin column and flash frozen in liquid nitrogen for storage.

IgG expression and purification

Recombinant IgG were expressed through transient transfection in HEK293E cells (National Research Council of Canada (under license)) using the Freestyle 293F expression system at 37°C, 6% CO_2 for 6 days. IgG was purified from cell culture supernatant using Protein A resin (GoldBio) and eluted from resin using IgG Elution Buffer (Pierce). IgG were further purified by SEC using HiLoad 16/600 Superdex 200 pg column (GE Healthcare* now Cytiva).

PfCSP peptides

All peptides for this study were directly synthesized and biotinylated by GenScript. These include linear peptides numbered 20-61 that were 15 amino acids in length and overlapped by 11 residues spanning the central repeat region of PfCSP, a 36mer peptide $(NANP)_9$, a 27mer peptide 20-23 (PADGNPDPNANPNVDPNANPNVDPNAN), and C-Terminal domain.

Antigenicity and immunogenicity ELISAs

96-well Immulon 2HB (Thermo Scientific) microtiter plates were coated with 50 ng/mL of PfCSP or mutant overnight at 4°C. Plates were washed 4X with phosphate-buffered saline (PBS) with 0.02% Tween-20 (wash buffer). Plates were blocked with 250 µL of 10% non-fat milk and 0.02% Tween-20 in PBS (blocking buffer) for 1 hr at 37°C. Plates were washed 4X with wash buffer. CSP-binding monoclonal IgG or VRC01, a HIV Env binding antibody used as a negative control, was diluted to 20 µg/mL in blocking buffer and added to the first row of plate. IgG was diluted in

tenfold serial dilutions in blocking buffer and incubated for 1 hr at 37°C. After washing 4X with wash buffer, goat anti-human Ig-HRP (Southern Biotech) was added at a 1:3000 dilution and incubated at 37°C for 1 hr. Plates were washed 4X with wash buffer and 50 µL of SureBlue Reserve TMB Peroxidase Substrate (SeraCare) was added and incubated for 4 min followed by addition of 100 µL of 1N H_2SO_4. The optical density at 450 nm was measured using a SpectraMax M2 plate reader (Molecular Devices). Wash steps were performed using a BioTek 405 Select microplate washer. Immune responses to full-length SAmut-CSP were measured by ELISA as described above using individual mouse sera (serum from each mouse was diluted in blocking buffer to 1:20 with 10-fold serial dilutions).

Epitope Mapping and Competition ELISAs

Epitope mapping of the immune responses was performed with C-terminal domain (Genscript) and linear overlapping peptides (peptides 20-61; Genscript) that span the central repeat region of PfCSP using the MSD U-Plex Assay platform (Meso Scale Discovery) according to the manufacturer's instructions. Briefly, MSD Gold microtiter plates (Meso Scale Discovery) were blocked with PBS + 5% BSA (20 µl/well), then coated with 10 µl/well of biotinylated peptides (240 pmol, Genscript) in PBS + 1% BSA for 1 hr at room temperature. The coated plates were incubated for 2 hrs at room temperature with 10 µl of PfCSP control mAbs ($5x10^{-7}$ – 5.0 µg/mL) or polyclonal mouse sera (pooled per group then diluted in blocking buffer to 1:20 with 10-fold serial dilutions). Plates were then incubated for 1 hr at room temperature with 10 µl/well of 1.0 µg/mL of appropriate secondary (either anti-human or anti-mouse) IgG SULFO-TAG (Meso Scale Discovery) in PBS with 1% BSA/0.05% Tween-20. Plates were washed five times with PBS-Tween between each step. After a final wash, 35 µl of 1X MSD Read T Buffer (Meso Scale Discovery) was added to each well and plates were analyzed on an MSD Sector Image 2400 instrument.

Competitive ELISA was also performed using peptides 20–61. Briefly, streptavidin-coated plates (Meso Scale Discovery, MSD) were blocked with 5% BSA in PBS for 30 min at room temperature, washed five times (wash buffer, 0.05% Tween-20 in PBS), then coated for 1hr at room temperature with biotinylated-recombinant PfCSP (0.2 mg/mL, Genscript), peptide 20-23 (PADGNPDPNANPNVDPNANPNVDPNAN) or repeat peptide $(NANP)_9$ (240pmol, Genscript) in PBS with 1% BSA. PfCSP control mAbs (all at 10 ng/mL), or polyclonal mouse sera (pooled per group then diluted 1:250) were preincubated with varying concentrations (0 – 1,000 ug/mL) of selected PfCSP peptides in PBS with 1% BSA/0.05% Tween-20 for 2hrs at 37C, then added onto the rPfCSP or peptide- coated plates. ELISA was performed on the MSD platform as described above.

Expression and purification of immunogen designs

Designs were codon-optimized in pET29b, containing a His-tag expression in BL21 (DE3) or LEMO21 cells. They were transformed and transferred to ZY Autoinduction medium (ZY media, 50XM Salts, 50X5052, 1M MgSO4, and 1000X Trace metals). Cultures were incubated for 2 hr at 37°C, then the temperature was reduced to 18˚C overnight. Cultures were then centrifuged at 3,500 rpm at 4°C for 20 min in a Beckman Avanti JXN26 (Brea, CA, USA). The supernatant was discarded, and the pellet was resuspended in a buffer containing 50 mM Tris, 500 mM NaCl, 1 mM DTT, 30 mM imidazole, pH 8.0, 1mM PMSF, 10 µg/mL DNase. The suspension was

homogenized and run through a Microfluidizer (Microfluidics M-110P) to lyse and collected in a 50 mL conical. Conicals were then centrifuged at 4°C for 30 min at 4000 rpm and the supernatant was transferred to a column containing Ni-NTA resin (Qiagen, Venlo, Netherlands), pre-equilibrated with Wash Buffer (25 mM Tris pH 8.0, 500 mM NaCl, 30 mM Imidazole). The resin was washed with one column volume of wash buffer and the protein eluted with a buffer containing 50 mM Tris, 500 mM NaCl, and 500 mM imidazole. Protein solution was concentrated and underwent size exclusion chromatography (SEC) on a Superdex 200 (GE Healthcare, Chicago, Il, USA) in a buffer containing 50 mM Tris, 500 mM NaCl. Fractions containing pure protein as controlled on SDS-PAGE were pooled and concentrated for further use.

CSP-I53-50 NP assembly

CSP-I53-50A fusion proteins were sterile filtered using a 0.22 µm spin column and combined with an equal molar ratio of I53-50B and incubated for 1 hour at room temp or overnight at 4˚C with light agitation to form nanoparticles. Nanoparticles were applied to a Superose 6 increase 10/300 GL column (GE healthcare) in 50 mM Tris, 500 mM NaCl to remove unassembled components. Protein concentrations were measured using a UV-Vis spectrometer, diluted to the concentration needed for mouse immunization and flash frozen in Liquid nitrogen for long-term storage.

Negative-stain EM

CSP-I53-50 NPs were added to carbon-covered 300 or 400 mesh copper grids and stained with 2% uranyl formate. Micrographs were imaged on a Tecnai F12 Spirit microscope with a 4k FEI Eagle CCD or a Talos 120C microscope with a Ceta camera. Leginon and Appio were used to collect and process micrographs. Class average examples were generated using the 2D Classification job in CryoSparc v3.3.1.

Dynamic Light Scattering (DLS)

Dynamic light scattering (DLS) was performed to determine the hydrodynamic radii and polydispersity (PDI) of purified CSP-I53-50 immunogens. Measurements were performed on either a Wyatt DLS using a 10 mm quartz cuvette or an UNcle Nano-DSF (UNchained Laboratories) using quartz capillary cassette (UNi, UNchained Laboratories). Four to ten acquisitions were collected using auto attenuation of the laser.

Mice

Six- to eight-week-old female B6(Cg)-Tyrc-2J/J albino (B6-albino) mice were procured from The Jackson Laboratory. These animals were maintained in facilities accredited by the American Association for Accreditation of Laboratory Animal Care and cared for according to their standards. All procedures involving animals were approved by the Institutional Animal Care and Use Committees of the National Institute of Allergy and Infectious Diseases, National Institutes of Health, (Animal Study Protocols VRC-17-702 and VRC-20-0855).

Parasites and Mosquitoes

Transgenic *Plasmodium berghei* (strain ANKA 676m1C11, MRA-868) parasites expressing full-length (3D7 strain) *P. falciparum* CSP and a green fluorescent protein/luciferase fusion protein (Pb-PfCSP-GFP/LUC SPZ) were propagated and used to evaluate the efficacy of the PfCSP-based vaccines, as previously described[113]. Briefly, BALB/c mice were infected by intraperitoneal (IP) injection of Pb-PfCSP-GFP/LUC SPZ-infected RBCs. *Anopheles stephensi* (Nijmegan) mosquitoes were reared at the Laboratory of Malaria and Vector Research (National Institute of Allergy and Infectious Diseases, National Institutes of Health). Female mosquitoes were allowed to feed on the parasitized mice which were anesthetized by IP injection of ketamine (50 mg/kg) and xylazine (10 mg/kg) mixture. After feeding, mice were euthanized via CO_2 inhalation, followed by cervical dislocation. Blood fed mosquitoes were then maintained in a humidified incubator at 19–20°C and supplied with 10% sucrose. For challenge studies, sporozoites were harvested from mosquito salivary glands at day 18-21 after an infectious blood meal, as previously described[113].

Immunizations and SPZ IV Challenge

Nanoparticle immunogens and R21 were diluted in sterile PBS to the indicated doses 0.08 - 3 µg and formulated with ALFQ, a liposomal adjuvant formulation containing 3D-PHAD® and QS-21[73], in a final volume of 50 µL[114]. Female B6-albino mice were immunized intramuscularly in the quadriceps at weeks 0, 3, and 6 (or as indicated in the figure). Serum samples were collected via tail veins at the indicated time points (10 days after 1st, and 2 weeks after 2nd and 3rd immunizations) to assess immunogenicity.

Challenges were conducted 2 - 6 weeks after the final immunization as indicated, where mice were challenged intravenously via the tail vein with 2,000 freshly harvested Pb-PfCSP-GFP/LUC sporozoites[113]. Then, 40–42 hours post-challenge, mice received an IP injection of 150 µL of D-Luciferin (30 mg/mL), were anesthetized with isoflurane (5% for induction, 1-3% for maintenance). Luciferase activity in mice was visualized through imaging of whole bodies using the IVIS® Spectrum in vivo imaging system (PerkinElmer) 10 minutes post-injection. Upon completion of the experiments, mice were euthanized via CO_2 inhalation followed by cervical dislocation. To measure the burden of parasite infection in the liver, a region of interest (ROI) in the upper abdominal area (at the location of the liver) was analyzed and the total flux or bioluminescent radiance (photons/sec) emitted by Pb-PfCSP-GFP/LUC-SPZ was calculated using the manufacturer's software (Living Image 4.5, PerkinElmer).

Author Contributions

Conceptulization: J.R.F., M.Pa., M.Pe., A.H.I., R.A.S., N.P.K.; Formal Analysis: M.D.L., J.R.F., A.L.R., N.K.H., J.V.R., A.H.I., M.Pa., N.P.K.; Investigation: M.D.L., J.R.F., A.L.R., N.K.H., J.V.R., L.D.S.P., B.J.F., B.B., M.D., P.K., R.R., C.W., L.C.; Provided Adjuvant: M.R., G.R.M.; Resources Writing – Original Draft: M.D.L, A.L.R., N.K.H., J.V.R., A.H.I., M.Pa., N.P.K.; Writing – Review & Editing: all authors; Visualization: M.D.L., A.L.R., N.K.H., J.V.R., M.Pa., N.P.K.; Supervision: J.R.F., A.H.I., M.Pa., M.Pe., R.A.S., N.P.K.; Funding Acquisition: R.A.S., M.Pe., N.P.K.

Acknowledgements

We gratefully acknowledge Holger Kanzler for helpful discussions; Ahmad Salman, Alexandra Spencer, and Adrian Hill (University of Oxford) for providing the R21 vaccine; Brooke Fiala (UW) for help obtaining negative-stain electron micrographs of I53-50 nanoparticles; Kandise VanWormer, Ratika Krishnamurty, and Lance Stewart for laboratory and administrative support; and Luki Goldschmidt and Patrick Vecchiato for building and maintaining the computing infrastructure at the Institute for Protein Design. This work was supported by the Bill & Melinda Gates Foundation (INV-010680, INV-043758); the intramural research program of the Vaccine Research Center, National Institute of Allergy and Infectious Diseases, National Institutes of Health; this material is based upon work supported by the National Science Foundation Graduate Research Fellowship under Grant No. DGE-1762114; and the Audacious Project at the Institute for Protein Design.

Competing interests

The authors declare no competing interests.

References

1. *World Malaria Report 2023*. https://www.who.int/teams/global-malaria-programme/reports/world-malaria-report-2023 (2023).
2. Beeson, J. G. *et al.* Challenges and strategies for developing efficacious and long-lasting malaria vaccines. *Sci. Transl. Med.* **11**, eaau1458 (2019).
3. White, M. T. *et al.* Immunogenicity of the RTS,S/AS01 malaria vaccine and implications for duration of vaccine efficacy: secondary analysis of data from a phase 3 randomised controlled trial. *Lancet Infect. Dis.* **15**, 1450–1458 (2015).
4. Yoshida, N., Potocnjak, P., Nussenzweig, V. & Nussenzweig, R. S. Biosynthesis of Pb44, the protective antigen of sporozoites of Plasmodium berghei. *J. Exp. Med.* **154**, 1225–1236 (1981).
5. Datoo, M. S. *et al.* Safety and efficacy of malaria vaccine candidate R21/Matrix-M in African children: a multicentre, double-blind, randomised, phase 3 trial. *Lancet* **403**, 533–544 (2024).
6. The RTS,S Clinical Trials Partnership. First Results of Phase 3 Trial of RTS,S/AS01 Malaria Vaccine in African Children. *N. Engl. J. Med.* **365**, 1863–1875 (2011).
7. WHO recommends groundbreaking malaria vaccine for children at risk. https://www.who.int/news/item/06-10-2021-who-recommends-groundbreaking-malaria-vaccine-for-children-at-risk.
8. WHO recommends R21/Matrix-M vaccine for malaria prevention in updated advice on immunization. https://www.who.int/news/item/02-10-2023-who-recommends-r21-matrix-m-vaccine-for-malaria-prevention-in-updated-advice-on-immunization.
9. Coppi, A., Pinzon-Ortiz, C., Hutter, C. & Sinnis, P. The Plasmodium circumsporozoite protein is proteolytically processed during cell invasion. *J. Exp. Med.* **201**, 27–33 (2005).

10. Coppi, A. *et al.* Heparan sulfate proteoglycans provide a signal to Plasmodium sporozoites to stop migrating and productively invade host cells. *Cell Host Microbe* **2**, 316–327 (2007).
11. Cockburn, I. A. *et al.* Dendritic cells and hepatocytes use distinct pathways to process protective antigen from plasmodium in vivo. *PLoS Pathog.* **7**, e1001318 (2011).
12. Bowman, N. M. *et al.* Comparative population structure of Plasmodium falciparum circumsporozoite protein NANP repeat lengths in Lilongwe, Malawi. *Sci. Rep.* **3**, 1990 (2013).
13. Doud, M. B. *et al.* Unexpected fold in the circumsporozoite protein target of malaria vaccines. *Proc. Natl. Acad. Sci. U. S. A.* **109**, 7817–7822 (2012).
14. Kisalu, N. K. *et al.* A human monoclonal antibody prevents malaria infection by targeting a new site of vulnerability on the parasite. *Nat. Med.* **24**, 408–416 (2018).
15. Tan, J. *et al.* A public antibody lineage that potently inhibits malaria infection through dual binding to the circumsporozoite protein. *Nat. Med.* **24**, 401–407 (2018).
16. Wang, L. T. *et al.* A Potent Anti-Malarial Human Monoclonal Antibody Targets Circumsporozoite Protein Minor Repeats and Neutralizes Sporozoites in the Liver. *Immunity* **53**, 733–744.e8 (2020).
17. Flores-Garcia, Y. *et al.* The P. falciparum CSP repeat region contains three distinct epitopes required for protection by antibodies in vivo. *PLoS Pathog.* **17**, e1010042 (2021).
18. Kayentao, K. *et al.* Safety and Efficacy of a Monoclonal Antibody against Malaria in Mali. *N. Engl. J. Med.* **387**, 1833–1842 (2022).
19. Kayentao Kassoum *et al.* Subcutaneous Administration of a Monoclonal Antibody to Prevent Malaria. *N. Engl. J. Med.* **390**, 1549–1559 (2024).
20. Datoo, M. S. *et al.* Efficacy of a low-dose candidate malaria vaccine, R21 in adjuvant Matrix-M, with seasonal administration to children in Burkina Faso: a randomised controlled trial. *Lancet* **397**, 1809–1818 (2021).
21. Rappuoli, R., Bottomley, M. J., D'Oro, U., Finco, O. & De Gregorio, E. Reverse vaccinology 2.0: Human immunology instructs vaccine antigen design. *J. Exp. Med.* **213**, 469–481 (2016).
22. Papi Alberto *et al.* Respiratory Syncytial Virus Prefusion F Protein Vaccine in Older Adults. *N. Engl. J. Med.* **388**, 595–608 (2023).
23. Walsh Edward E. *et al.* Efficacy and Safety of a Bivalent RSV Prefusion F Vaccine in Older Adults. *N. Engl. J. Med.* **388**, 1465–1477 (2023).
24. Polack Fernando P. *et al.* Safety and Efficacy of the BNT162b2 mRNA Covid-19 Vaccine. *N. Engl. J. Med.* **383**, 2603–2615 (2020).
25. Baden Lindsey R. *et al.* Efficacy and Safety of the mRNA-1273 SARS-CoV-2 Vaccine. *N. Engl. J. Med.* **384**, 403–416 (2021).
26. Sadoff Jerald *et al.* Safety and Efficacy of Single-Dose Ad26.COV2.S Vaccine against Covid-19. *N. Engl. J. Med.* **384**, 2187–2201 (2021).
27. Kirchdoerfer, R. N. *et al.* Stabilized coronavirus spikes are resistant to conformational changes induced by receptor recognition or proteolysis. *Sci. Rep.* **8**, 15701 (2018).

28. Pallesen, J. *et al.* Immunogenicity and structures of a rationally designed prefusion MERS-CoV spike antigen. *Proc. Natl. Acad. Sci. U. S. A.* **114**, E7348–E7357 (2017).
29. McLellan, J. S. *et al.* Structure-based design of a fusion glycoprotein vaccine for respiratory syncytial virus. *Science* **342**, 592–598 (2013).
30. Oyen, D. *et al.* Structural basis for antibody recognition of the NANP repeats in Plasmodium falciparum circumsporozoite protein. *Proc. Natl. Acad. Sci. U. S. A.* **114**, E10438–E10445 (2017).
31. Triller, G. *et al.* Natural Parasite Exposure Induces Protective Human Anti-Malarial Antibodies. *Immunity* **47**, 1197–1209.e10 (2017).
32. Imkeller, K. *et al.* Antihomotypic affinity maturation improves human B cell responses against a repetitive epitope. *Science* **360**, 1358–1362 (2018).
33. Murugan, R. *et al.* Evolution of protective human antibodies against Plasmodium falciparum circumsporozoite protein repeat motifs. *Nat. Med.* **26**, 1135–1145 (2020).
34. Pholcharee, T. *et al.* Structural and biophysical correlation of anti-NANP antibodies with in vivo protection against P. falciparum. *Nat. Commun.* **12**, 1063 (2021).
35. Martin, G. M. *et al.* Affinity-matured homotypic interactions induce spectrum of PfCSP structures that influence protection from malaria infection. *Nat. Commun.* **14**, 4546 (2023).
36. Tripathi, P. *et al.* Cryo-EM structures of anti-malarial antibody L9 with circumsporozoite protein reveal trimeric L9 association and complete 27-residue epitope. *Structure* **31**, 480–491.e4 (2023).
37. Oyen, D. *et al.* Cryo-EM structure of P. falciparum circumsporozoite protein with a vaccine-elicited antibody is stabilized by somatically mutated inter-Fab contacts. *Sci Adv* **4**, eaau8529 (10 2018).
38. Plassmeyer, M. L. *et al.* Structure of the Plasmodium falciparum circumsporozoite protein, a leading malaria vaccine candidate. *J. Biol. Chem.* **284**, 26951–26963 (2009).
39. Langowski, M. D. *et al.* Restricted valency (NPNA)n repeats and junctional epitope-based circumsporozoite protein vaccines against Plasmodium falciparum. *npj Vaccines* **7**, 1–11 (2022).
40. Ludwig, J. *et al.* Glycosylated nanoparticle-based PfCSP vaccine confers long-lasting antibody responses and sterile protection in mouse malaria model. *NPJ Vaccines* **8**, 52 (2023).
41. Jelínková, L. *et al.* An epitope-based malaria vaccine targeting the junctional region of circumsporozoite protein. *npj Vaccines* **6**, 1–10 (2021).
42. Calvo-Calle, J. M., Mitchell, R., Altszuler, R., Othoro, C. & Nardin, E. Identification of a neutralizing epitope within minor repeat region of Plasmodium falciparum CS protein. *NPJ Vaccines* **6**, 10 (2021).
43. Atcheson, E., Hill, A. V. S. & Reyes-Sandoval, A. A VLP for validation of the Plasmodium falciparum circumsporozoite protein junctional epitope for vaccine development. *NPJ Vaccines* **6**, 46 (2021).
44. Jelínková, L. *et al.* A vaccine targeting the L9 epitope of the malaria circumsporozoite protein confers protection from blood-stage infection in a mouse challenge model. *npj Vaccines* **7**, 1–4 (2022).
45. Kucharska, I. *et al.* High-density binding to Plasmodium falciparum circumsporozoite protein repeats by inhibitory antibody elicited in mouse with human immunoglobulin repertoire. *PLoS Pathog.* **18**, e1010999 (2022).

46. Martin, G. M. *et al.* Structural basis of epitope selectivity and potent protection from malaria by PfCSP antibody L9. *Nat. Commun.* **14**, 2815 (2023).
47. Bachmann, M. F. & Jennings, G. T. Vaccine delivery: a matter of size, geometry, kinetics and molecular patterns. *Nat. Rev. Immunol.* **10**, 787–796 (2010).
48. Kato, Y. *et al.* Multifaceted Effects of Antigen Valency on B Cell Response Composition and Differentiation In Vivo. *Immunity* **53**, 548–563.e8 (2020).
49. López-Sagaseta, J., Malito, E., Rappuoli, R. & Bottomley, M. J. Self-assembling protein nanoparticles in the design of vaccines. *Comput. Struct. Biotechnol. J.* **14**, 58–68 (2016).
50. Irvine, D. J., Swartz, M. A. & Szeto, G. L. Engineering synthetic vaccines using cues from natural immunity. *Nat. Mater.* **12**, 978–990 (2013).
51. Gordon, D. M. *et al.* Safety, immunogenicity, and efficacy of a recombinantly produced Plasmodium falciparum circumsporozoite protein-hepatitis B surface antigen subunit vaccine. *J. Infect. Dis.* **171**, 1576–1585 (1995).
52. Francica, J. R. *et al.* Design of Alphavirus Virus-Like Particles Presenting Circumsporozoite Junctional Epitopes That Elicit Protection against Malaria. *Vaccines (Basel)* **9**, 272 (2021).
53. Whitacre, D. C. *et al.* P. falciparum and P. vivax Epitope-Focused VLPs Elicit Sterile Immunity to Blood Stage Infections. *PLoS One* **10**, (2015).
54. McCoy, M. E. *et al.* Mechanisms of protective immune responses induced by the Plasmodium falciparum circumsporozoite protein-based, self-assembling protein nanoparticle vaccine. *Malar. J.* **12**, 136 (2013).
55. Langowski, M. D. *et al.* Optimization of a Plasmodium falciparum circumsporozoite protein repeat vaccine using the tobacco mosaic virus platform. *Proc. Natl. Acad. Sci. U. S. A.* **117**, 3114–3122 (2020).
56. Khan, F. *et al.* Head-to-Head Comparison of Soluble vs. Qβ VLP Circumsporozoite Protein Vaccines Reveals Selective Enhancement of NANP Repeat Responses. *PLoS One* **10**, (2015).
57. Kurtovic, L. *et al.* Novel Virus-Like Particle Vaccine Encoding the Circumsporozoite Protein of Plasmodium falciparum Is Immunogenic and Induces Functional Antibody Responses in Mice. *Front. Immunol.* **12**, 641421 (2021).
58. Bale, J. B. *et al.* Accurate design of megadalton-scale two-component icosahedral protein complexes. *Science* **353**, 389–394 (2016).
59. Ueda, G. *et al.* Tailored design of protein nanoparticle scaffolds for multivalent presentation of viral glycoprotein antigens. *Elife* **9**, e57659 (2020).
60. Marcandalli, J. *et al.* Induction of Potent Neutralizing Antibody Responses by a Designed Protein Nanoparticle Vaccine for Respiratory Syncytial Virus. *Cell* **176**, 1420–1431.e17 (2019).
61. Brouwer, P. J. M. *et al.* Enhancing and shaping the immunogenicity of native-like HIV-1 envelope trimers with a two-component protein nanoparticle. *Nat. Commun.* **10**, 4272 (2019).
62. Walls, A. C. *et al.* Elicitation of Potent Neutralizing Antibody Responses by Designed Protein

Nanoparticle Vaccines for SARS-CoV-2. *Cell* **183**, 1367–1382.e17 (2020).
63. Boyoglu-Barnum, S. *et al.* Quadrivalent influenza nanoparticle vaccines induce broad protection. *Nature* **592**, 623–628 (2021).
64. Song, J. Y. *et al.* Immunogenicity and safety of SARS-CoV-2 recombinant protein nanoparticle vaccine GBP510 adjuvanted with AS03: interim results of a randomised, active-controlled, observer-blinded, phase 3 trial. *EClinicalMedicine* **64**, 102140 (2023).
65. Pancera, M. & Weidle, C. Circumsporozoite proteins with increased expression in mammalian cells. *US Patent* (2024).
66. Singh, A. P. *et al.* Plasmodium circumsporozoite protein promotes the development of the liver stages of the parasite. *Cell* **131**, 492–504 (2007).
67. Yang, X. *et al.* Modifications that stabilize human immunodeficiency virus envelope glycoprotein trimers in solution. *J. Virol.* **74**, 4746–4754 (2000).
68. Walls, A. C. *et al.* Cryo-electron microscopy structure of a coronavirus spike glycoprotein trimer. *Nature* **531**, 114–117 (2016).
69. Kirchdoerfer, R. N. *et al.* Pre-fusion structure of a human coronavirus spike protein. *Nature* **531**, 118–121 (2016).
70. Singh, S. K. *et al.* The Plasmodium falciparum circumsporozoite protein produced in Lactococcus lactis is pure and stable. *J. Biol. Chem.* **295**, 403–414 (2020).
71. Collins, K. A., Snaith, R., Cottingham, M. G., Gilbert, S. C. & Hill, A. V. S. Enhancing protective immunity to malaria with a highly immunogenic virus-like particle vaccine. *Sci. Rep.* **7**, 46621 (2017).
72. Zakeri, B. *et al.* Peptide tag forming a rapid covalent bond to a protein, through engineering a bacterial adhesin. *Proc. Natl. Acad. Sci. U. S. A.* **109**, E690–7 (2012).
73. Alving, C. R., Peachman, K. K., Matyas, G. R., Rao, M. & Beck, Z. Army Liposome Formulation (ALF) family of vaccine adjuvants. *Expert Rev. Vaccines* **19**, 279–292 (2020).
74. Raghunandan, R. *et al.* Characterization of two in vivo challenge models to measure functional activity of monoclonal antibodies to Plasmodium falciparum circumsporozoite protein. *Malar. J.* **19**, 113 (2020).
75. Kraft, J. C. *et al.* Antigen- and scaffold-specific antibody responses to protein nanoparticle immunogens. *Cell Rep Med* **3**, 100780 (2022).
76. de Groot, A. S. *et al.* Human T cell recognition of polymorphic epitopes from malaria circumsporozoite protein. *J. Immunol.* **142**, 4000–4005 (1989).
77. Good, M. F. *et al.* Construction of synthetic immunogen: use of new T-helper epitope on malaria circumsporozoite protein. *Science* **235**, 1059–1062 (1987).
78. Scally, S. W. *et al.* Rare PfCSP C-terminal antibodies induced by live sporozoite vaccination are ineffective against malaria infection. *J. Exp. Med.* **215**, 63–75 (2018).
79. Beutler, N. *et al.* A novel CSP C-terminal epitope targeted by an antibody with protective activity against Plasmodium falciparum. *PLoS Pathog.* **18**, e1010409 (2022).

80. Seaton, K. E. *et al.* Subclass and avidity of circumsporozoite protein specific antibodies associate with protection status against malaria infection. *NPJ Vaccines* **6**, 110 (2021).
81. Dobaño, C. *et al.* Concentration and avidity of antibodies to different circumsporozoite epitopes correlate with RTS,S/AS01E malaria vaccine efficacy. *Nat. Commun.* **10**, 2174 (2019).
82. Thai, E. *et al.* Molecular determinants of cross-reactivity and potency by VH3-33 antibodies against the Plasmodium falciparum circumsporozoite protein. *Cell Rep.* **42**, (2023).
83. Dosey, A. *et al.* Combinatorial immune refocusing within the influenza hemagglutinin RBD improves cross-neutralizing antibody responses. *Cell Rep.* **42**, 113553 (2023).
84. Walls, A. C. *et al.* Elicitation of broadly protective sarbecovirus immunity by receptor-binding domain nanoparticle vaccines. *Cell* **184**, 5432–5447.e16 (2021).
85. Brinkkemper, M. *et al.* Co-display of diverse spike proteins on nanoparticles broadens sarbecovirus neutralizing antibody responses. *iScience* **25**, 105649 (2022).
86. Sliepen, K. *et al.* Induction of cross-neutralizing antibodies by a permuted hepatitis C virus glycoprotein nanoparticle vaccine candidate. *Nat. Commun.* **13**, 7271 (2022).
87. Kang, Y.-F. *et al.* Quadrivalent mosaic HexaPro-bearing nanoparticle vaccine protects against infection of SARS-CoV-2 variants. *Nat. Commun.* **13**, 2674 (2022).
88. Hutchinson, G. B. *et al.* Nanoparticle display of prefusion coronavirus spike elicits S1-focused cross-reactive antibody response against diverse coronavirus subgenera. *Nat. Commun.* **14**, 6195 (2023).
89. Kanekiyo, M. *et al.* Mosaic nanoparticle display of diverse influenza virus hemagglutinins elicits broad B cell responses. *Nat. Immunol.* **20**, 362–372 (2019).
90. Wang, E. *et al.* Designed mosaic nanoparticles enhance cross-reactive immune responses in mice. *bioRxiv* (2024) doi:10.1101/2024.02.28.582544.
91. Cohen, A. A. *et al.* Mosaic sarbecovirus vaccination elicits cross-reactive responses in pre-immunized animals. *bioRxiv* (2024) doi:10.1101/2024.02.08.576722.
92. Hills, R. A. *et al.* Multiviral Quartet Nanocages Elicit Broad Anti-Coronavirus Responses for Proactive Vaccinology. *bioRxiv* (2023) doi:10.1101/2023.02.24.529520.
93. Cohen, A. A. *et al.* Mosaic RBD nanoparticles protect against challenge by diverse sarbecoviruses in animal models. *Science* **377**, eabq0839 (2022).
94. Cohen, A. A. *et al.* Mosaic nanoparticles elicit cross-reactive immune responses to zoonotic coronaviruses in mice. *Science* **371**, 735–741 (2021).
95. Cohen, A. A. *et al.* Construction, characterization, and immunization of nanoparticles that display a diverse array of influenza HA trimers. *PLoS One* **16**, e0247963 (2021).
96. Wargacki, A. J. *et al.* Complete and cooperative in vitro assembly of computationally designed self-assembling protein nanomaterials. *Nat. Commun.* **12**, 883 (2021).
97. Read, B. J. *et al.* Mannose-binding lectin and complement mediate follicular localization and enhanced immunogenicity of diverse protein nanoparticle immunogens. *Cell Rep.* **38**, (2022).

98. Malhi, H. *et al.* Immunization with a self-assembling nanoparticle vaccine displaying EBV gH/gL protects humanized mice against lethal viral challenge. *Cell Rep Med* **3**, 100658 (2022).
99. Ols, S. *et al.* Multivalent antigen display on nanoparticle immunogens increases B cell clonotype diversity and neutralization breadth to pneumoviruses. *Immunity* **56**, 2425–2441.e14 (2023).
100. Wu, Y., Ding, Y. & Shen, C. A Systematic Review of T Cell Epitopes Defined from the Proteome of Hepatitis B Virus. *Vaccines (Basel)* **10**, (2022).
101. Liu, H. *et al.* Cryo-EM structures of human hepatitis B and woodchuck hepatitis virus small spherical subviral particles. *Sci Adv* **8**, eabo4184 (2022).
102. Peterson, D. L., Nath, N. & Gavilanes, F. Structure of hepatitis B surface antigen. Correlation of subtype with amino acid sequence and location of the carbohydrate moiety. *J. Biol. Chem.* **257**, 10414–10420 (1982).
103. Geens, R. *et al.* Biophysical characterization of the Plasmodium falciparum circumsporozoite protein's N-terminal domain. *Protein Sci.* **33**, e4852 (2024).
104. Aguirre-Botero, M. C. *et al.* Cytotoxicity of human antibodies targeting the circumsporozoite protein is amplified by 3D substrate and correlates with protection. *Cell Rep.* **42**, 112681 (2023).
105. Ubillos, I. *et al.* Baseline exposure, antibody subclass, and hepatitis B response differentially affect malaria protective immunity following RTS,S/AS01E vaccination in African children. *BMC Med.* **16**, 197 (2018).
106. Suscovich, T. J. *et al.* Mapping functional humoral correlates of protection against malaria challenge following RTS,S/AS01 vaccination. *Sci. Transl. Med.* **12**, (2020).
107. Wang, L. T. *et al.* Protective effects of combining monoclonal antibodies and vaccines against the Plasmodium falciparum circumsporozoite protein. *PLoS Pathog.* **17**, e1010133 (2021).
108. Neafsey, D. E. *et al.* Genetic Diversity and Protective Efficacy of the RTS,S/AS01 Malaria Vaccine. *N. Engl. J. Med.* **373**, 2025–2037 (2015).
109. Hayashi, C. T. H. *et al.* Antibodies elicited by Plasmodium falciparum circumsporozoite proteins lacking sequentially deleted C-terminal amino acids reveal mouse strain and epitopes specific differences. *Vaccine* (2023) doi:10.1016/j.vaccine.2023.10.009.
110. Ellis, D. *et al.* Antigen spacing on protein nanoparticles influences antibody responses to vaccination. Preprint at (2023).
111. Alexander, J. *et al.* The optimization of helper T lymphocyte (HTL) function in vaccine development. *Immunol. Res.* **18**, 79–92 (1998).
112. Zavala, F. RTS,S: the first malaria vaccine. *J. Clin. Invest.* **132**, (2022).
113. Flores-Garcia, Y. *et al.* Optimization of an in vivo model to study immunity to Plasmodium falciparum pre-erythrocytic stages. *Malar. J.* **18**, 426 (2019).
114. Beck, Z., Torres, O. B., Matyas, G. R., Lanar, D. E. & Alving, C. R. Immune response to antigen adsorbed to aluminum hydroxide particles: Effects of co-adsorption of ALF or ALFQ adjuvant to the aluminum-antigen complex. *J. Control. Release* **275**, 12–19 (2018).

Supplementary Figures

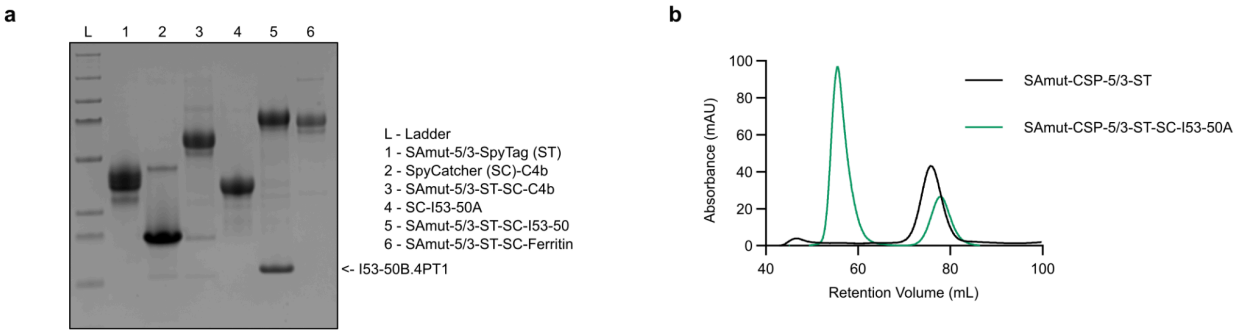

Figure S1: Supplemental characterization data for stabilized SAmut-5/3 on nanoparticles. a SDS-PAGE of SpyCatcher (SC) and SpyTag (ST) constructs before and after conjugation. **b** Overlaid SEC chromatograms of unconjugated SAmut-5/3-ST and conjugated SAmut-5/3-ST-SC-I53-50A component.

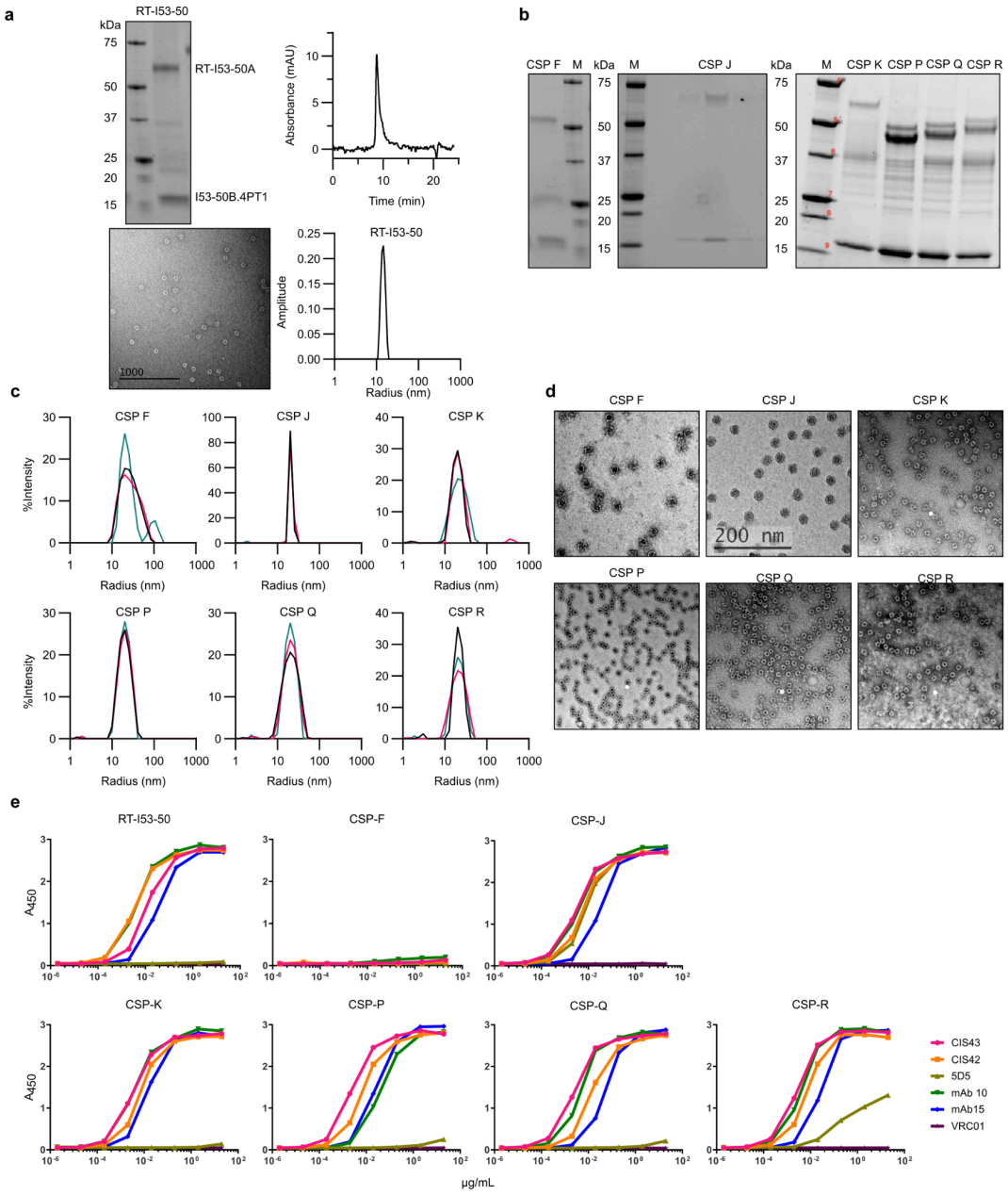

Figure S2: Supplemental characterization data for I53-50 nanoparticle immunogens comprising the CSP junctional region. a (Clockwise, from upper left) SDS-PAGE, SEC, nsEM, and DLS of purified RT-I53-50 nanoparticles used in Figure 3. **b** SDS-PAGE, **c** DLS, and **d** nsEM for additional nanoparticle immunogens used in Figure 3. **e** Antigenicity ELISA curves for each nanoparticle immunogen against a panel of mAbs targeting the junctional epitope (CIS43 & CIS42), Region I (5D5), the major repeats (mAb10), and the C-terminal domain (mAb15). VRC01 was used as a negative control.

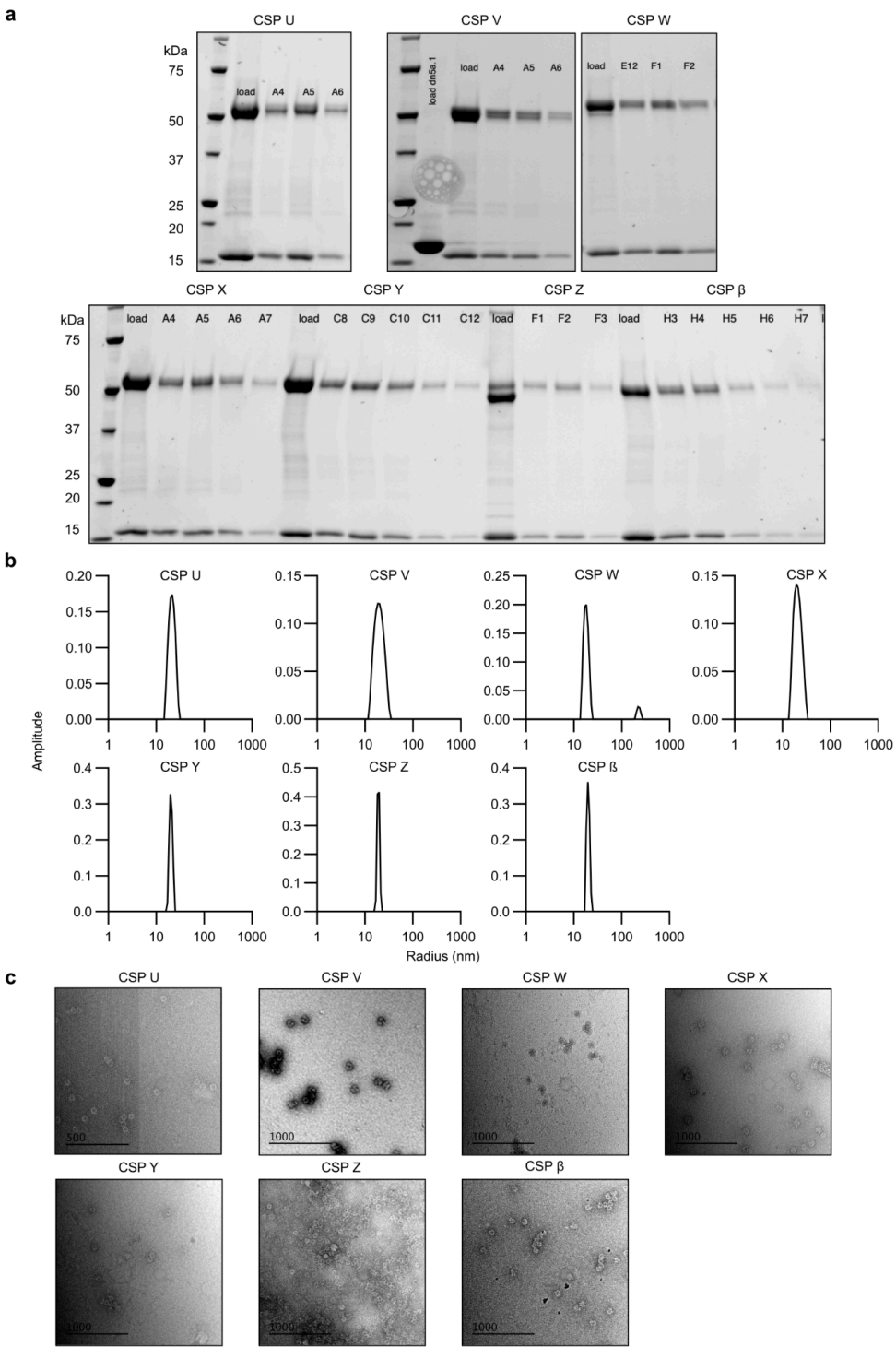

Figure S3: Supplemental characterization data for I53-50 nanoparticle immunogens comprising non-native CSP repeats. a SDS-PAGE, **b** DLS, and **c** nsEM of nanoparticles used for immunization in non-native CSP repeat study.

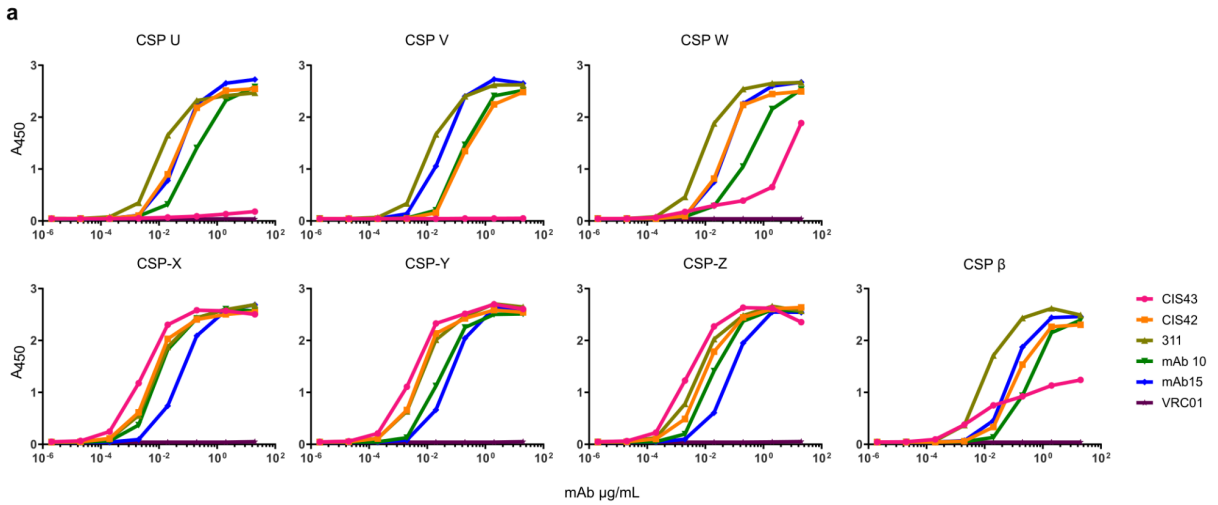

Figure S4. Non-native CSP I53-50 nanoparticle antigenicity. Antigenicity ELISA curves for each nanoparticle immunogen against a panel of mAbs targeting the junctional epitope (CIS43 & CIS42), Region I (5D5), the major repeats (mAb10), and the C-terminal domain (mAb15). VRC01 was used as a negative control.

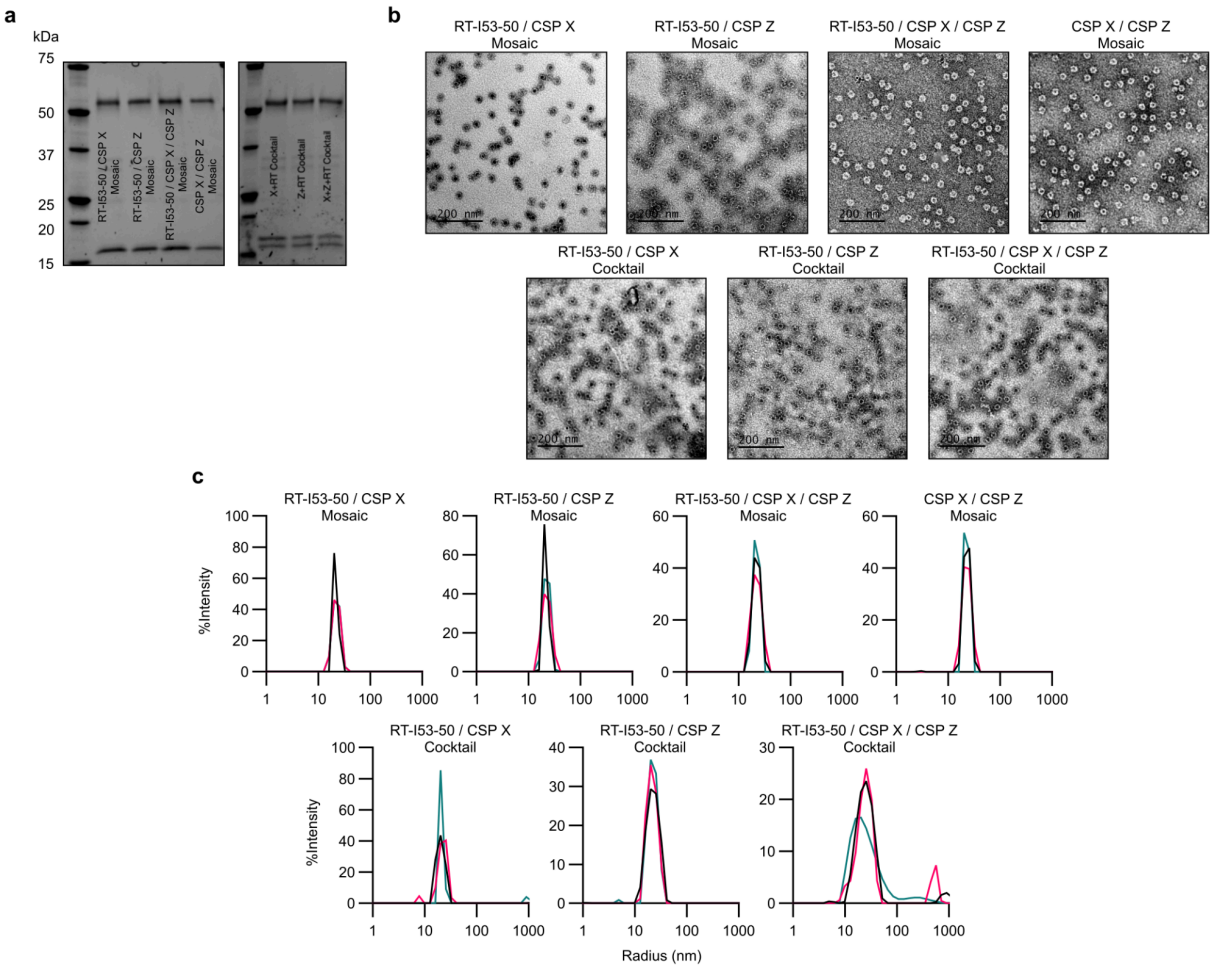

Figure S5: Supplemental characterization data for CSP mosaic and cocktail nanoparticles. a SDS-PAGE, **b** nsEM, and **c** DLS data for cocktail and mosaic CSP-repeat nanoparticles.

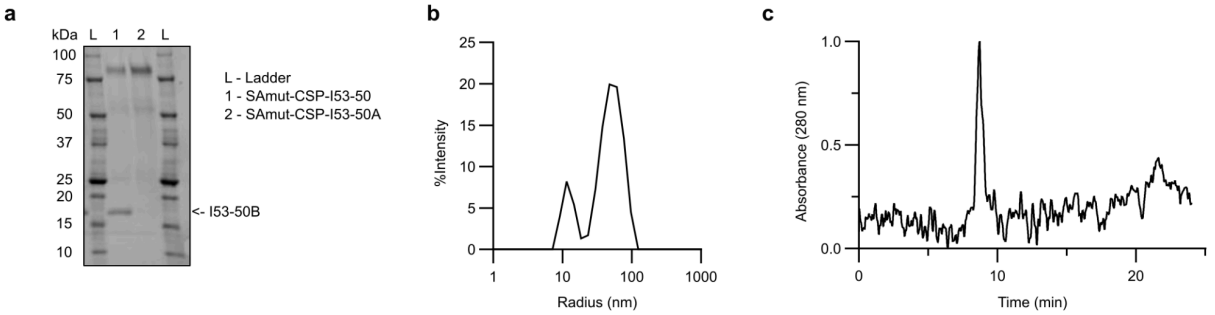

Figure S6. Supplemental characterization data for SAmut-CSP-I53-50. a SDS-PAGE, **b** DLS, and **c** Analytical SEC chromatogram of SAmut-CSP-I53-50 nanoparticle used for immunizations in Figure 6.

Chapter 2: Glycosylated Circumsporozoite protein (CSP) nanoparticles enhance the early anti-CSP B cell response and improve protection against sporozoite challenge

This chapter is in preparation as:
Courtney McDougal[1,12], Mark D. Langowski[2,3,4,12], Daria Nikolaeva[5], Chengbo Chen[11], Adian Valdez[2], Rashmi Ravichandran[2], Mariah Lofgren[6], Marlon Dillon[5], Delante Sanders[5], Alvaro Molina-Cruz[5], Darrell J. Irvine[6,7,8,9,10], Azza H. Idris[8], Kelly Lee[11], Robert A. Seder[5,*], Marion Pepper[1,*], Neil P. King[2,3*] **Glycosylated Circumsporozoite protein (CSP) nanoparticles enhance the early anti-CSP B cell response and improve protection against sporozoite challenge.**

[1]Department of Immunology, University of Washington, Seattle, WA, USA
[2]Institute for Protein Design, University of Washington, Seattle, WA, USA
[3]Department of Biochemistry, University of Washington, Seattle, WA, USA
[4]Graduate Program in Molecular and Cellular Biology, University of Washington, Seattle, WA, USA
[5]Vaccine Research Center, National Institute of Allergy and Infectious Diseases, National Institutes of Health, Bethesda, MD, USA
[6]Department of Biological Engineering, Massachusetts Institute of Technology, Cambridge, MA, USA
[7]Consortium for HIV/AIDS Vaccine Development, The Scripps Research Institute, La Jolla, CA, USA
[8]The Ragon Institute of Massachusetts General Hospital, Massachusetts Institute of Technology, Harvard University, Cambridge, MA, USA
[9]Koch Institute for Integrative Cancer Research, Massachusetts Institute of Technology, Cambridge, MA, USA
[10]Howard Hughes Medical Institute, Chevy Chase, MD, USA
[11]Department of Medicinal Chemistry, University of Washington, WA, USA
[12]These authors contributed equally: Courtney McDougal, Mark D. Langowski
*Corresponding authors

Introduction

Malaria caused by *Plasmodium falciparum* inflicts a significant public health burden globally, causing most of the estimated 608,000 deaths in 2022, 95.4% of which occurred in Africa[1]. Over 11.7 million deaths caused by malaria have been averted from 2000 to 2022, primarily through seasonal malaria chemoprevention (SMC) and the use of insecticide treated bednets, but growing drug and insecticide resistance threaten these gains[1]. Two vaccines recently recommended by the WHO, RTS,S/AS01 and R21/Matrix-M, have shown great promise with vaccine efficacies of 55.8% and 68% after 1 year, respectively[2,3]. Both vaccines display a truncated segment of the major surface antigen of the sporozoite stage, the circumsporozoite protein (CSP), and display ~18 NANP major repeats and the C-terminal domain on Hepatitis B S antigen virus-like particles[4,5]. These vaccines are currently being distributed in areas of moderate-to-high malaria transmission intensity, and will further aim to reduce case incidence and death in children[1]. However, these vaccines require three doses to achieve a high anti-CSP

titer, and because their antibody titers rapidly wane[3,6–8], a yearly booster is required to maintain efficacy.

The presence of oligomannose glycans on antigens and nanoparticles has been shown to be important for their efficient trafficking to the germinal center (GC) follicle[9,10]. We have shown that engineering N-linked oligomannose glycans on the surface of a computationally designed nanoparticle platform, I53-50[11], exhibits a density-dependent effect in nanoparticle trafficking to GC follicles[10]. This occurs through the mannose-binding lectin (MBL) pathway of complement, where oligomannose-bearing antigens and nanoparticles are opsonized complement through MBL, traffic to lymph nodes (LNs), and are taken up by subcapsular sinus macrophages, transported into the follicle to follicular dendritic cells (FDCs) where they are protected from protease activity inside the follicle[12], and can then be presented to GC B cells[9,10]. We also recently reported on RT-I53-50, a two-component icosahedral nanoparticle which displays 60 copies of the RT antigen found in RTS,S(Langowski et al. 2024, *In review*). This nanoparticle is statistically equal in liver burden reduction to R21 after 3 doses in mice after transgenic parasite challenge, but performs worse than R21 after 2 doses. One question is if improved trafficking of oligomannose I53-50 can provide benefit to CSP antigens displayed on this platform.

Another group has already shown that the presence of oligomannose on HpFerritin displaying CSP repeats (145S-HpFerritin) may improve protection in mice against parasite challenge relative to non-glycosylated HpFerritin[13]. This may be due in part to the trafficking benefits of the MBL complement pathway, as well as the reduction of anti-scaffold responses and the increase in anti-CSP repeat responses, which result in an increased level of anti-CSP repeat bone marrow-derived plasma cells (PCs)[13]. In line with increased levels of bone marrow PCs, 145S-HpFerritin immunized mice exhibited sterile protection against bite challenge with transgenic parasites up to nearly a half year after immunization, though no head-to-head comparisons were made against non-glycosylated nanoparticles, or nanoparticles bearing different glycoforms. Thus, it is unknown whether the benefits observed were due to shielding the scaffold with glycans or by MBL complement, or both.

Here we describe a series of experiments using glycosylated RT-I53-50 nanoparticles (RT.2-I53-50-3gly or -4gly, **Figure 1a**) and compare them directly with non-glycosylated and less mannosylated forms to determine the phenotype of B cell responses generated in mice by both nanoparticles, and how the presence of these glycoforms affects protection against sporozoite challenge.

Results

Design and characterization of CSP glycosylated nanoparticles

We have shown that glycosylated I53-50 nanoparticles (I53-50A-4gly) bearing oligomannose can more efficiently traffic to germinal centers via the mannose-binding lectin pathway of the complement system resulting in increased follicular dendritic cell (FDC) localization and improve germinal center (GC) responses[10]. We therefore hypothesized that displaying RT on

glycosylated I53-50 nanoparticles may improve anti-CSP B cell responses and thus result in improved protection against parasite challenge.

To accommodate the fusion of RT to I53-50A-4gly, the trimeric component containing four N-linked glycan sequons, we added a flexible 8GS linker to its C-terminus and named this construct RT.2-I53-50A-4gly (**Fig. 1a**). We also produced a variant, RT.2-I53-50A-3gly (**Fig. 1a**), deleting the first N-linked glycan sequon that was proximal to the nanoparticle interface and reduced nanoparticle assembly efficiency in our previous study[10], and a "bare" non-glycosylated variant RT.2-I53-50A. When fully assembled with its corresponding component I53-50B.4PT1[14], RT.2-I53-50-4gly and RT.2-I53-50-3gly display 60 total copies of RT.2, and 240 and 180 total glycans on their surfaces, respectively (**Fig. 1a, b**).

RT.2-I53-50A-4gly and -3gly components were expressed in Expi293F cells under native conditions which should result in primarily complex type glycans, or with kifunensine, an inhibitor of mannosidase processing which results in a 100% oligomannose N-linked glycan composition[15,16], and subsequently purified by immobilized metal affinity chromatography (IMAC) and size exclusion chromatography (SEC). RT.2-I53-50A-4gly and -3gly were assembled *in vitro* with I53-50B.4PT1 in a 1.1:1 ratio and excess components were separated by SEC (**Fig. 1c**). Nanoparticle purity was assessed by SDS-PAGE and was confirmed as being >95% pure (**Fig. 1e**). The presence of assembled nanoparticles was confirmed by dynamic light scattering (DLS), with diameters ranging from 36-38 nm, and negative-stain electron microscopy (nsEM) (**Fig. 1d, f**).

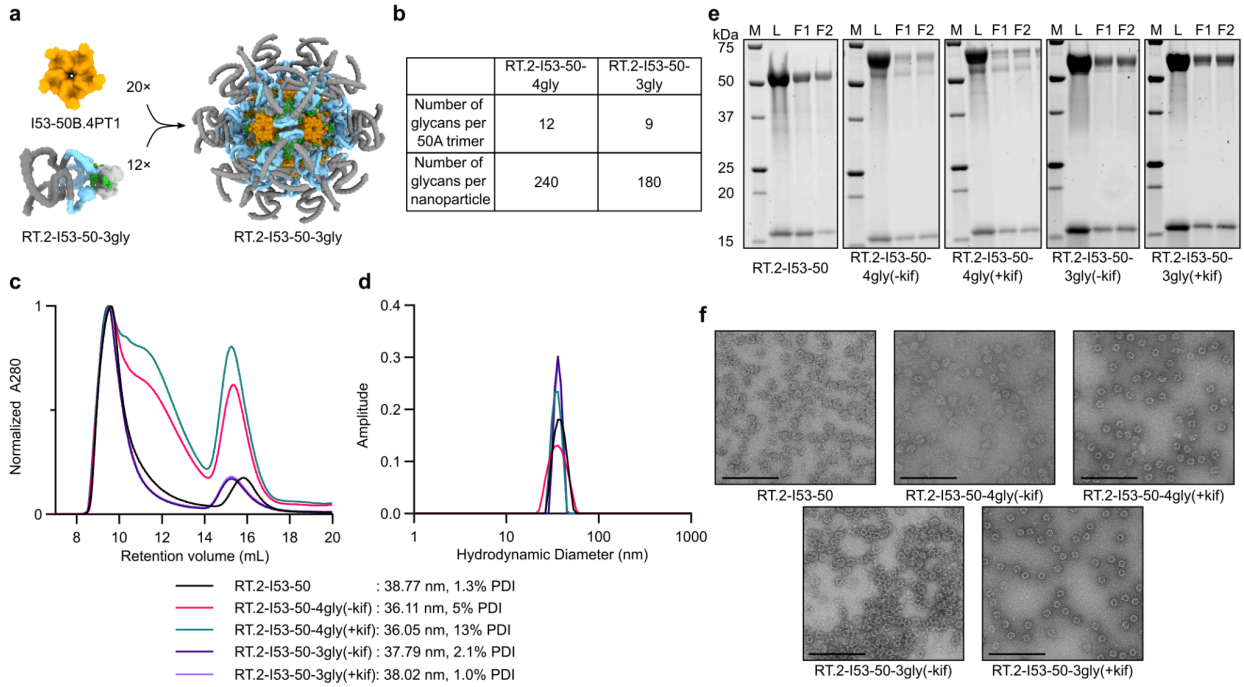

Figure 1. Design and characterization of RT.2-I53-50 glycosylated nanoparticles. a AF3 model for RT.2-I53-50A-3gly (major repeats in gray, CSP C-terminus light blue, I53-50A in light gray, and

$GlcNAc_2Man_6$ glycans in green) and I53-50B.4PT1 (orange). A fully assembled nanoparticle (right) displays 60 copies of RT antigen. **b** Numbers of glycans per trimer and nanoparticle for 4gly and 3gly variants. **c** Size exclusion chromatography (SEC) traces on a Superose 6 Increase 10/300 GL column. The first peak corresponds to the assembly, and the second peak corresponds to excess components. **d** Hydrodynamic diameter of Hydrodynamic diameter of nanoparticles as determined by dynamic light scattering (DLS). **e** SDS-PAGE for bare and glycosylated RT.2-I53-50 nanoparticles; M = marker, L = load, F1 & F2 = fractions pooled for immunization studies. **f** Negative-stain electron micrographs for nanoparticles at 57k magnification. Black bar inset in the lower left for each micrograph corresponds to 200 nm size.

Glycoprofiling of CSP glycosylated nanoparticles

We next determined the glycan composition of our RT.2-I53-50-4gly and -3gly nanoparticles. Previous glycoprofiling of antigenless I53-50-4gly revealed an occupancy of >75% complex glycans at all sites when prepared under native conditions without kifunensine[10]. Purified RT.2-I53-50A-4gly and -3gly expressed under native conditions (native) or in the presence of kifunensine (mannose) were treated with PNGase F, an enzyme which cleaves all N-linked glycans types, and resulted in a gel shift for both components expressed under native conditions or in the presence of kifunensine (**Fig. 2a**). Treatment with Endo H, which cleaves oligomannose glycans, revealed a complete gel shift for kifunensine treated preparations, and unexpectedly a partial gel shift for native preparations indicating the presence of oligomannose glycans (**Fig. 2a**).

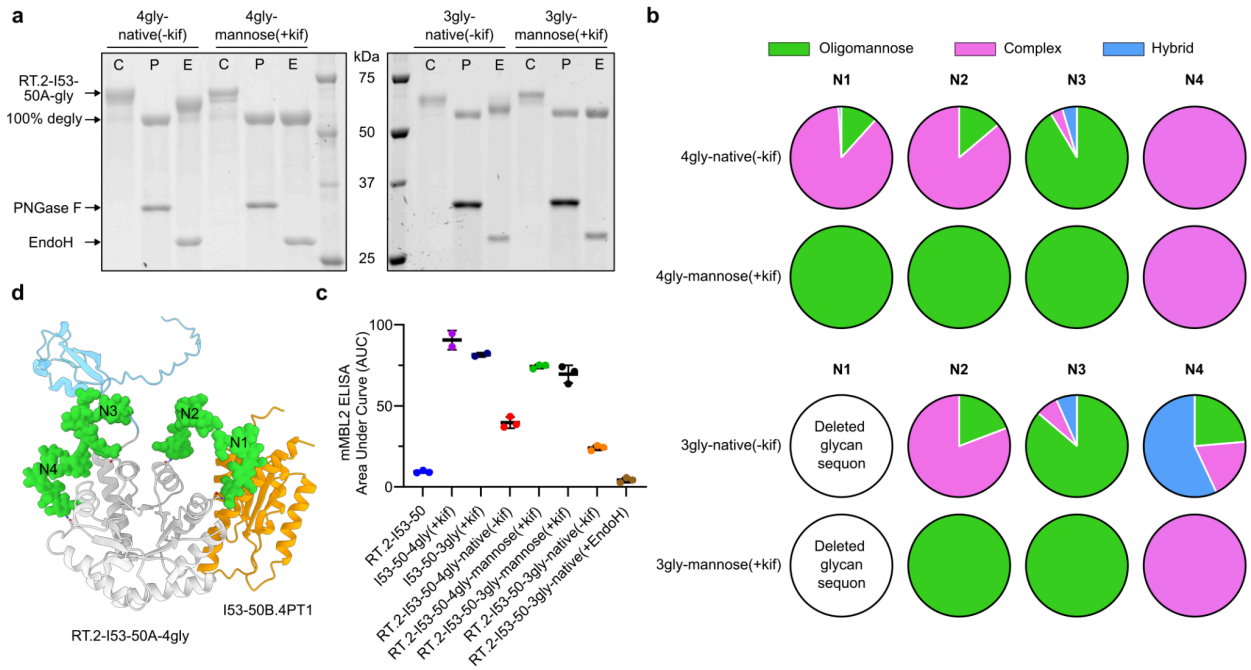

Figure 2. Glycoprofiling of RT.2-I53-50 glycosylated nanoparticles. a Control untreated (C), PNGase F (P), and Endo H (E) treated glycosylated RT.2-I53-50 nanoparticles. SDS-PAGE was run under denaturing conditions. **b** Bottom-up mass spectrometry data for glycosylated RT.2-I53-50A component at each sequon. **c** Model of RT.2-I53-50 minimal asymmetric unit. CSP-C terminus in light blue, I53-50A in light gray, glycans in green, and I53-50B.4PT1 in orange. **d** Anti-mouse MBL2 ELISA average (n=3 technical replicates) area under the curve (AUC) measurements against RT.2-I53-50

nanoparticles with and without glycans, and in comparison to non-antigen bearing I53-50-4gly and -3gly preparations made with kifunensine. RT.2-I53-50-3gly-native(+EndoH) is a native preparation treated with Endo H to remove all oligomannose glycans. Mean and standard deviation are plotted.

Analysis of N-linked glycosylation occupancy by mass spectrometry showed that both RT.2-I53-50-4gly-mannose and RT.2-I53-50-3gly-mannose had 100% oligomannose at all N-linked glycan positions as expected, except for position 4 which could not be fully characterized due to issues with peptide cleavage preferences, confounding analysis (**Fig. 2b**). Positions 1 and 2 were >75% complex for RT.2-I53-50-4gly-native and RT.2-I53-50-3gly-native, but position 3 was >75% oligomannose confirming the gel shift results that oligomannose is present on these native preparations (**Fig. 2b**). These results were further confirmed by an enzyme-linked immunosorbent assay (ELISA) using murine mannose-binding lectin 2 (MBL2) which showed binding against both native and mannose nanoparticles, with a dose dependent effect depending on the number of glycans and presence of mannose (**Fig. 2d**). Native preparations of nanoparticles treated with Endo H did not bind MBL2 as expected (**Fig. 2d**). We hypothesized that the presence of mannose in native preparations is likely due to the fusion point of the RT antigen, which is directly adjacent to position 3 and likely sterically occludes mannosidase enzymes from processing oligomannose glycans at this position (**Fig. 2c**), a phenomenon observed in many viral glycoproteins[17,18].

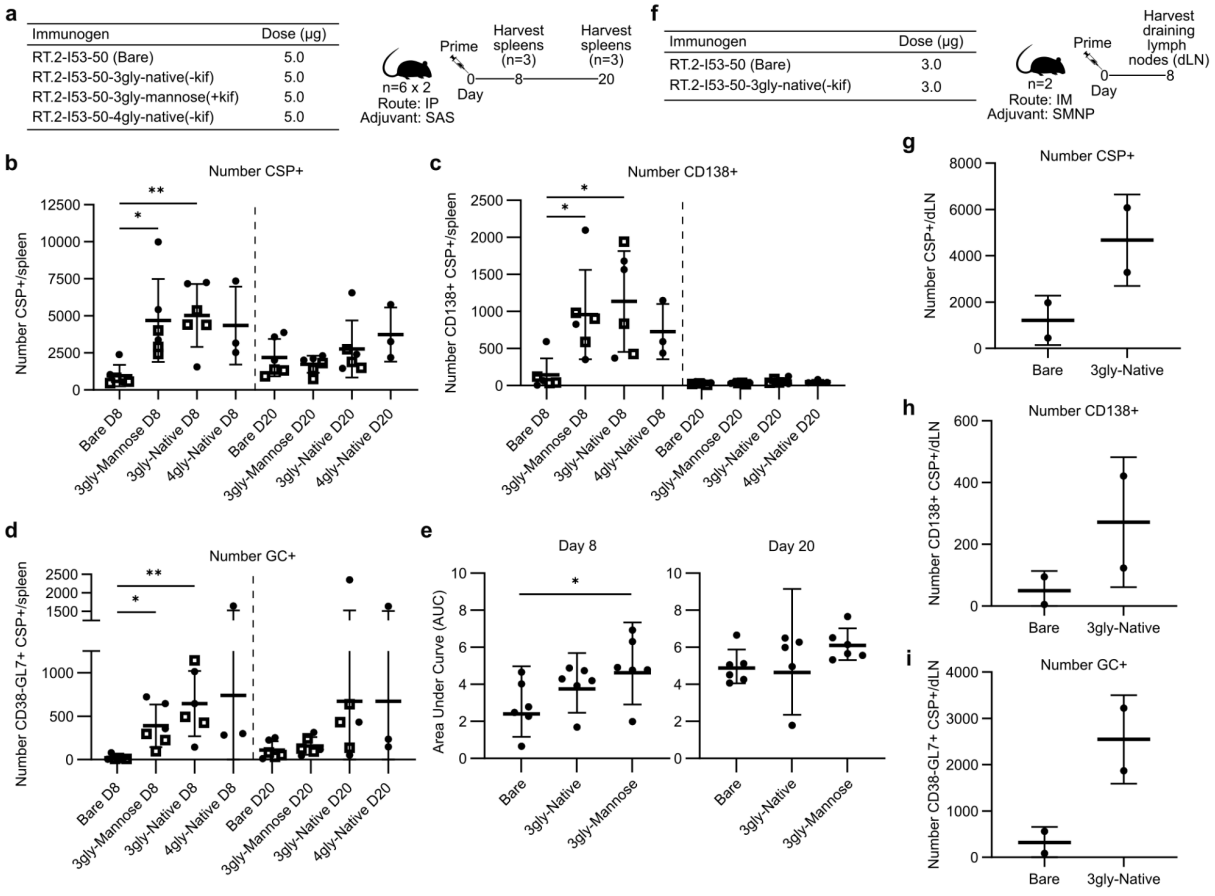

Figure 3. Anti-CSP B cell responses after immunization with bare and glycosylated RT.2-I53-50. **a** Study design for nanoparticles adjuvanted with SAS. Dose refers to the amount of RT antigen (total dose of nanoparticle was 15 μg). **b** CSP+, **c** CSP+CD138+ (plasmablast), and **d** CSP+ GC B cell numbers from splenocytes 8 and 20 days after immunization in SAS adjuvant. **e** Anti-CSP ELISA AUC at days 8 and 20. **f** Study design for nanoparticles adjuvanted with SMNP. Dose refers to total nanoparticle administered. **g** CSP+, **h** CSP+CD138+ (plasmablast), and **i** CSP+ GC B cell numbers from cells isolated from dLNs. Mean and standard deviation are plotted for all graphs. *, $p < 0.1$; **, $p < 0.01$; ***, $p < 0.001$; **** $p < 0.0001$ as calculated by Kruskal-Wallis test with multiple comparisons.

RT.2-I53-50 nanoparticles displaying oligomannose glycans improve early anti-CSP B cell responses

Having extensively characterized our RT.2-I53-50 glycosylated nanoparticles, we next evaluated them in mouse models. We immunized mice intraperitoneally (IP) with 15 μg of RT.2-I53-50 (bare), RT.2-I53-50-3gly-native, RT.2-I53-50-3gly-mannose(+kif), or RT.2-I53-50-4gly-native formulated in SAS adjuvant (Sigma Aldrich; **Fig. 3a**), which contains a TLR4 agonist and squalene as a water-in-oil emulsion. We focused on the 3gly variants as they were much easier to produce due to their improved assembly efficiency with no trailing shoulder present (**Fig. 1**), but also included 4gly-native to determine if we observed differences between their differing numbers of glycans. Spleens were harvested to determine the anti-CSP B cell response at days 8 and 20. At day 8, mice immunized with RT.2-I53-50-3gly groups showed a significantly increased number of CSP+ B cells (**Fig. 3b**), CSP+ plasmablasts (**Fig. 3c**), and CSP+ GC B cells (**Fig. 3d**). Anti-CSP antibody titers were significantly higher only for RT.2-I53-50-3gly-mannose as compared to bare nanoparticles (**Fig. 3e**). RT.2-I53-50-4gly-native also showed a trend for an increased number of these B cell populations at day 8, but was not included in statistical analyses due to its smaller group size (**Fig. 3b-d**). At day 20, no significant differences in B cell phenotype or antibody titers were observed between the bare or glycosylated nanoparticles.

To account for differences in splenic vs lymph node architecture, and to remain consistent with planned parasite challenge studies, we next analyzed the B cell responses in draining lymph nodes (dLNs) after intramuscular immunization with SMNP adjuvant[19] (**Fig. 3f**). In a small pilot study, mice immunized with 3 μg of RT.2-I53-50-3gly-native had higher numbers of CSP+ B cells, CSP+ plasmablasts, and CSP+ GC B cells when compared with bare RT.2-I53-50 groups 8 days after immunization (**Fig. 3g-i**). Another pilot study with SMNP, including RT.2-I53-50-3gly-native(+EndoH) which should have only complex glycans present on its surface, showed a decrease in the number of CSP+ B cells, CSP+ plasmablasts, and CSP+ GC B cells as compared to groups that contained oligomannose (**Supplementary Fig. 1**). Overall, our data show that 8 days after immunization, glycosylated RT.2-I53-50 nanoparticles with oligomannose exhibit and increased number of CSP-specific plasmablasts and GC B cells when compared to bare, non-glycosylated nanoparticles, and that this effect is consistent between lymphocytes from the spleen and dLNs, and with different adjuvants.

Glycosylated RT.2-I53-50 improves protection against parasite challenge

We immunized mice intramuscularly with RT.2-I53-50-3gly-native, RT.2-I53-50-3gly-mannose, RT.2-I53-50 bare, and our benchmark *E. coli* derived RT-I53-50-Ec (Langowski et al. 2024, *In review*), all formulated in Adjuplex carbopol polymer[20], to determine if we could see differences in parasite liver burden reduction when formulated with a non-saponin containing adjuvant (**Fig. 4a**). Immunized mice were challenged IV with 2000 transgenic *P. berghei*-PfCSP-GFP/Luc sporozoites three weeks after boost immunization and liver burden was measured by an *in vivo* imaging system (PerkinElmer, ref.[21]). All groups of immunized mice showed a significant reduction in liver burden when compared to an untreated control, but the two glycosylated groups showed the most significant levels of liver burden reduction (**Fig. 4b**).

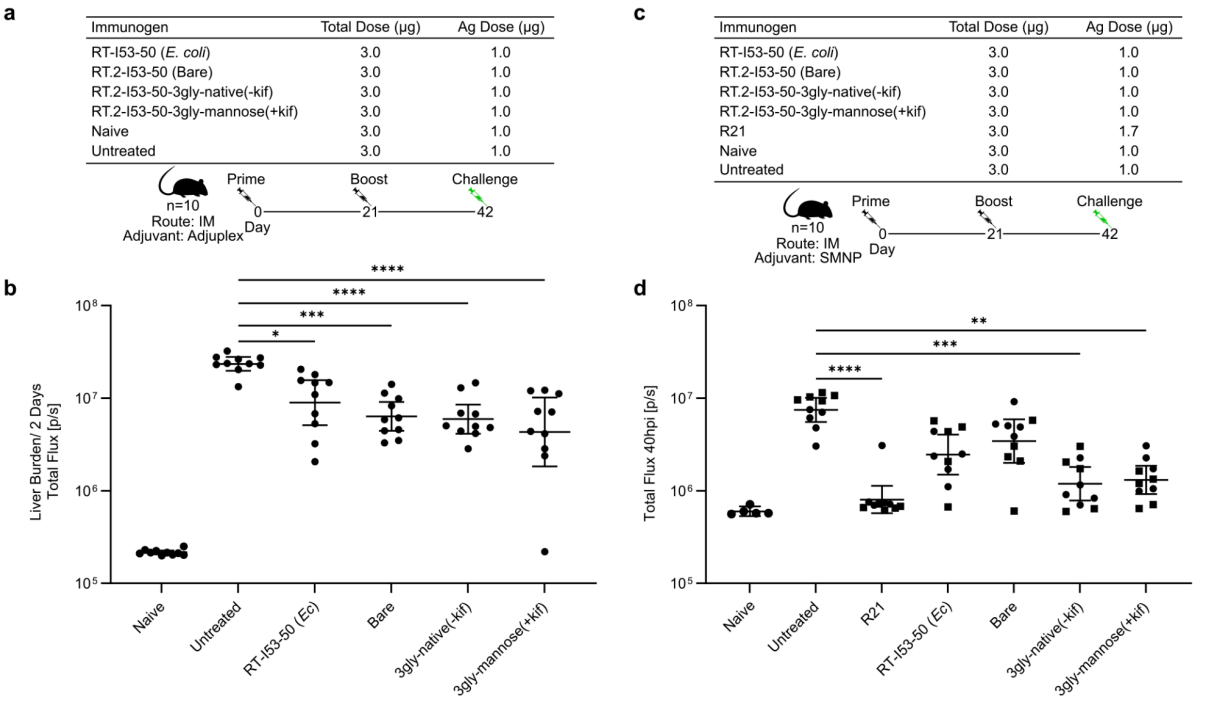

Figure 4. Pb-PfCSP transgenic parasite challenge in mice immunized with non-glycosylated or glycosylated RT.2-I53-50 nanoparticles. **a** Study design for mice immunized with listed nanoparticles in SAS adjuvant. **b** Parasite burden in the liver after challenge with transgenic sporozoites in the SAS adjuvant study. **c** Study design for mice immunized with listed nanoparticles in SMNP adjuvant. **d** Parasite burden in the liver after challenge with transgenic sporozoites in the SMNP adjuvant study. R21 is also adjuvanted in SMNP. Geometric mean and 95% confidence interval are plotted for all graphs. *, $p < 0.1$; **, $p < 0.01$; ***, $p < 0.001$; **** $p < 0.0001$ as calculated by Kruskal-Wallis test with multiple comparisons and directly compared to the untreated control.

For our next experiment, we compared if glycosylated RT.2-I53-50 could achieve significant levels of protection similar to R21 after two doses, which we previously did not achieve with RT-I53-50-*Ec* (Langowski et al. 2024, *In review*). The same set of nanoparticles, including R21, were all formulated with 5 µg of SMNP, an immunostimulatory complex (ISCOM) adjuvant containing saponin [19] similar to Matrix M, and mice were immunized twice and challenged three weeks later (**Fig. 4c**). Only groups immunized with R21 and the two glycosylated

RT.2-I53-50-3gly groups had significantly reduced liver burden when compared to untreated control, and no significant reduction was observed for both non-glycosylated RT-I53-50-*Ec* or Bare RT.2-I53-50 (**Fig. 4d**). There were no differences in liver burden when comparing R21 and the glycosylated groups, though it should be noted that R21 still had the lowest liver burden overall. Our data shows that mice immunized with glycosylated RT.2-I53-50 nanoparticles can have a significant liver burden reduction after only two doses, and that this reduction is non-inferior to R21. It is possible that this is due to a combination of MBL complement deposition and shielding the I53-50 scaffolding with glycans.

Discussion

Here, we demonstrated mice immunized with RT.2-I53-50 nanoparticles bearing oligomannose show improvements in early antigen-specific GC B cell responses. These results also translated to a challenge with transgenic parasites, with oligomannose bearing nanoparticles showing significant liver burden reduction compared to bare RT.2-I53-50. Our results confirm reports by others that oligomannose nanoparticles displaying CSP repeats show improved functional outcomes[13], and that this may be a general strategy that can be applied to recombinant *P. falciparum* vaccines that do not naturally contain occupied N-linked glycans, though it should be noted that the role of natural glycosylations on *Plasmodium* proteins is unclear and up for debate[22].

The fusion of complement C3d and derived peptides has been shown to increase immune responses toward model and clinically relevant antigens such as hen-egg lysozyme[23], amyloid peptides[24], and HIV[25–27], among others[28–30]. Genetic fusion of the p28 peptide derived from C3d that binds complement receptor 2 (CR2)[31], to *P. berghei* CSP as a molecular adjuvant, was shown to protect mice against sporozoite challenge[32]. It is unclear how this could be applied to human vaccination, as fusion of human complement derived peptides or proteins could present challenges in regulatory approval. RT.2-I53-50-3gly-mannose and -native nanoparticles were both able to bind an essential component of the complement pathway, MBL2, without the need for the genetic fusion of human-derived peptides or proteins. Another advantage is that RT.2-I53-50-3gly-native did not require kifunensine treatment to produce oligomannose glycoforms on its surface, though its overall levels were less than the kifunensine treated RT.2-I53-50-3gly-mannose preparations (**Fig. 2**). This may be advantageous for manufacture as it is unlikely that treatment with an enzyme like kifunensine would allow for production of cost efficient malaria vaccines.

The presence of oligomannose in both RT.2-I53-50-3gly preparations was reflected in the mouse MBL2 ELISA in a dose-dependent response, showing that recombinant MBL2 could potently bind nanoparticles that contained 100% mannose glycans, with weaker binding for RT.2-I53-50-3gly-native and -4gly-native preparations as the N3 glycan position was the only position that contained >75% mannose glycans, which differed from our original antigen-less I53-50-4gly construct[10]. This was further confirmed by cleaving mannose glycans from RT.2-I53-50-3gly-native(+EndoH), abrogating MBL2 binding. The presence of oligomannose at position N3 is likely due to sterics blocking processing by mannosidase enzymes, as the bulky and flexible RT.2 antigen is fused directly next to this position. We observed this phenomenon in

several native preparations, and the reproducibility of this glycosylation pattern is consistent with viral glycoproteins that also have site-specific N-linked mannose glycosylation due to this steric occlusion of mannosidases by crowding of local glycan and protein environments[17,18,33]. It should also be noted that despite the presence of the large and flexible RT.2 antigen, MBL2 was able to access the surface of the nanoparticles for binding. RT.2-I53-50-3gly nanoparticles did however, exhibit a slightly decreased level of MBL2 binding as compared to I53-50-3gly and -4gly nanoparticles alone. It is also possible that other C-lectin type receptors that bind oligomannose such as DC-SIGN may influence the innate immune response[34], but that is not in the scope of this work.

Oligomannose on RT.2-I53-50-3gly nanoparticles may allow for their opsonization by MBL complement pathways and improve trafficking to the GC. Indeed, we observed that both RT.2-I53-50-3gly-native and mannose nanoparticles compared to bare RT.2-I53-50 showed enhanced B cell responses at early time points after vaccination in both SAS (Sigma Aldrich) and SMNP [19] adjuvant. When adjuvanted in SAS adjuvant, significant increases at day 8 in the number of CSP+ B cells, CD138+ plasmablasts, and CSP+CD38-GL7+ GC B cells were observed from isolated splenocytes, and higher anti-CSP IgG titers in RT.2-I53-50-3gly-native and -mannose groups, though only the latter was statistically significant (**Fig. 3**). Interestingly, these responses wane when examined at day 20 with no differences between bare and glycosylated groups. This may be due to this time point being close to the resolution of a typical GC response[35], though it may depend on other factors such as the antigen itself or the adjuvant used. We also saw an increase in GC B cell responses from dLNs in mice immunized IM with RT.2-I53-50-3gly-native adjuvanted in SMNP, confirming that this effect is observed in different lymphatic architectures.

When compared to an infection control after 2 immunizations, though R21 lowest parasite liver burden, RT.2-I53-50-3gly-native and -mannose had significant liver burden reduction in SMNP adjuvant, which is something we did not observe with RT-I53-50-Ec in this study or in our previous one(Langowski et al. 2024, *In review*). This could be due to a stronger plasmablast response observed in glycosylated groups, resulting in higher circulating titers of anti-CSP antibodies that may be important for protection, but this will need to be determined by future ELISA experiments to see if there are any differences. It is thought that immunization with CSP repeats may favor short-lived plasmablast responses as observed with other malaria antigens[36], which results in the rapid decay of anti-CSP titers[37]. Though this increase in short-lived plasmablasts may be improving protection in glycosylated over bare nanoparticles in the short term, it remains to be seen whether these antibodies level sustain protection against challenge at later time points or if long-lived plasma cells (LLPCs) populations are elevated as seen in 145S-HpFerritin[13]. Short-lived plasmablasts also generally secrete lower-affinity antibodies[38], but it remains to be seen if there are differences in antibody quality between non-glycosylated and glycosylated RT.2-I53-50, and future avidity ELISA experiments will be carried out to determine this is the case.

An outstanding question still is whether these functional benefits are directly related to the presence of oligomannose interacting with MBL. Julien and colleagues showed that a decrease

in anti-scaffold responses due to glycosylation on HpFerritin may have improved anti-CSP responses[13], but did not determine the effects of MBL complement binding or its trafficking to the GC. For example, though HBsAg derived from yeast contains large N-linked oligomannose glycans, it traffics to GCs via non-MBL complement pathways[10]. It is unclear what the glycosylation status of R21 used in this study, and this will need to be explored in future experiments. Responses toward immunogenic viral glycoproteins on I53-50 and other computationally designed nanoparticles have shown little benefit when masking nanoparticle surfaces[39], but it is unknown whether this applies to antigens such as the CSP repeats. Experiments with influenza HA bearing paucimannose, oligomannose, or complex glycoforms have shown HAs with paucimannose and oligomannose had higher HA titers than complex preparations, but complex glycans had higher virus neutralization and protection against influenza challenge[40]. It is unclear as to whether the presence of different glycoforms on RT.2-I53-50-3gly would affect the results seen in this study in the same way. A pilot study (**Supplementary Figure 1**) showed that RT.2-I53-50-3gly-native(+EndoH), which only contained complex glycans, showed lower B cell responses similar to bare RT.2-I53-50, indicating that the benefits observed in RT.2-I53-50-3gly-native and -mannose groups may be due to the presence of oligomannose. We have future experiments planned with RT.2-I53-50-3gly-native(+EndoH) that will hopefully elucidate whether the removal of oligomannose reduces anti-CSP B cell responses and functional protection against parasite challenge.

In conclusion, this study provides evidence that the incorporation of oligomannose glycans on the surface of RT.2-I53-50 nanoparticles enhances early GC B cell responses and significantly improves protection against malaria in a mouse model. This effect is likely mediated by the interaction of oligomannose with MBL complement, leading to improved nanoparticle trafficking and antigen presentation. Importantly, the presence of oligomannose on native preparations of RT.2-I53-50-3gly nanoparticles offers a practical approach for vaccine development. While further investigations are needed to fully elucidate the mechanisms responsible for the observed improvements and to assess the long-term efficacy of this strategy, our findings highlight the potential of oligomannose-bearing nanoparticles as a promising platform for the development of next-generation malaria vaccines with enhanced immunogenicity and protective capacity.

Methods

Molecular modeling

RT.2-I53-50-3gly nanoparticle was predicted with AlphaFold3 [41] with $GlcNAc_2Man_6$ glycans at each N-linked glycan sequon. The full nanoparticle was modeled with ChimeraX 1.6 software (UCSF).

Plasmid synthesis

Plasmids for I53-50B.4PT1 and RT-I53-50A were constructed using the pET29b+ vector as previously described[14]. For mammalian expressed non-glycosylated and glycosylated components, genetic fusions of the RT antigen were fused by an 8-residue GS linker (RT.2) to I53-50 or I53-50A-4gly (RT.2-I53-50A or RT.2-I53-50-4gly), the latter of which was based off of a previously described construct with four N-linked glycan sequons[10]. RT.2-I53-50-3gly variants

were produced by mutating the first glycan sequon to the original I53-50A sequence[11]. Constructs were codon optimized for mammalian expression with a prolactin signal sequence and a C-terminal hexahistidine tag, and inserted into a pCMV/R vector (XbaI and AvrII restriction sites) and produced by Genscript.

Protein expression

I53-50B.4PT1 and RT-I53-50A component was expressed as previously described in *E.coli*[11,14]. RT.2-I53-50A and RT.2-I53-50-glycosylated plasmids were used to transiently transfect Expi293F cells by using PEI-MAX (Polysciences). RT.2-I53-50-glycosylated were expressed without (referred to as “native” preparations) and with 5 μM kifunensine, the latter of which results in 100% oligomannose glycoforms (designated “mannose”). Kifunensine treated preparations were supplemented with 25 mM glucose to improve N-linked glycan occupancy.

RT.2-I53-50A component purification

After expression, mammalian cultures were centrifuged and supernatant was collected for downstream purification. Ni Sepharose excel resin was added (10 mL per 200 mL supernatant) for batch binding supernatant from RT.2-I53-50A and RT.2-I53-50A-glycosylated components, and flow through was collected via a gravity column. Resin was subsequently washed with 10 column volumes (CVs) of 50 mM Tris, 500 mM NaCl, 20 mM Imidazole, 0.75% CHAPS, pH 8.0 (wash buffer). Bound components were eluted with 50 mM Tris, 500 mM NaCl, 300 mM Imidazole, 0.75% CHAPS, pH 8.0 (elution buffer) in two 2.5 CV fractions, the first of which contained the protein of interest. Eluates for components were purified by size exclusion chromatography (SEC) using a Superdex 200 Increase 10/300 GL column (Cytiva) in 25 mM Tris, 150 mM NaCl, 0.75% CHAPS, pH 8.0 (Component sizing buffer). 1 mL fractions were collected for peaks of interest that corresponded to the correct molecular weight of the components, and their purity was determined by SDS-PAGE. Component concentrations were determined by UV-vis (Cary 3500, Agilent) and low endotoxin content confirmed by Endosafe Endotoxin Testing Cartridges (Charles River).

RT.2-I53-50 nanoparticle assembly and purification

Purified RT.2-I53-50A (bare and glycosylated) were assembled *in vitro* in a 1.1:1 ratio with I53-50B.4PT1 in 25 mM Tris, 150 mM NaCl, 5% Glycerol pH 8.0 (Assembly buffer) at a total molar concentration of 20-50 μM as previously described[14], and left overnight at 4°C on a rocking shaker. Nanoparticles were purified from excess component by SEC using a Superose 6 Increase 10/300 GL column (Cytiva) in Assembly buffer. Fractions corresponding to the correct molecular weight of the fully formed assemblies were collected for downstream analysis. Purity was determined by SDS-PAGE and concentration by UV-vis (Cary 3500, Agilent).

Dynamic Light Scattering (DLS)

Measurements for nanoparticles were performed on an UNcle Nano-DSF (UNchained Laboratories) using quartz capillary cassettes (UNi, UNchained Laboratories). Four acquisitions were collected using auto attenuation of the laser, and the UNcle analysis software (UNchained

Laboratories) was used to determine the hydrodynamic diameter and polydispersity index (PDI) of assemblies.

Negative-stain electron microscopy (nsEM)
Assembled nanoparticles at a concentration of 50 µg/mL were added to carbon-covered 400 mesh copper grids (Electron Microscopy Sciences) and stained with 2% uranyl formate. Micrographs were imaged on a Talos 120C microscope with a Ceta camera.

Glycan profiling by glycosidase gel shifts
After denaturation, RT.2-I53-50A-glycosylated components or nanoparticles N-linked glycosylation content was determined by treatment with PNGase F (NEB) which cleaves all N-linked glycoforms, and Endo H (EndoH, NEB) which only cleaves oligomannose. These samples were run by SDS-PAGE and their gel shifts after treatment were compared to an untreated control. A shift in molecular weight after treatment with Endo H indicated the presence of oligomannose.

Glycan profiling by mass spectrometry (MS)
N-linked glycosylation profiles at each RT.2-I53-50A-glycosylated N-linked glycan sequon was determined by MS as previously described[10].

Murine Mannose-binding lectin 2 (MBL2) enzyme-linked immunosorbent assay (ELISA)
Nunc MaxiSorp ELISA plates (ThermoFisher) were coated with 50 µL of 1 µg/mL RT.2-I53-50 or RT.2-I53-50-glycosylated nanoparticles in Phosphate buffered saline (PBS), in triplicate, and left covered overnight in a cold room. The next day, the plates were washed 3x with PBS + Tween-20 0.05% (PBS-T). Recombinant MBL2 (Bio-Techne Corporation) was diluted in D-PBS with calcium and magnesium + 1% Bovine Serum Albumin (blocking buffer), diluted 1:2 down the column of the plate, and incubated for 1 hour at 37°C. After incubation, plates were washed 3x with PBS-T, and anti-MBL2 antibody (14D12, Abcam) in block buffer at a concentration of 2 µg/mL was added to each well and incubated at room temperature for 1 hour. Plates were washed 4x with PBS-T, and secondary antibody HRP conjugate (anti-rat IgG:HRP, BioRad) at a 1:6000 dilution in blocking buffer was added to each well and incubated for 1 hour at room temperature. 50 µL of TMB substrate was added to each well and developed for 5 minutes, and subsequently neutralized with sulfuric acid stop solution. Absorbance at 450 nm was measured using an Epoch Microplate reader (Biotek) and values plotted and calculated using GraphPad Prism (GraphPad Software).

Adjuvants
For the first B cell phenotyping study, nanoparticles were formulated with Sigma Adjuvant System (SAS, Sigma-Aldrich) in a 1:1 ratio. For studies involving SMNP[19], nanoparticle immunogens were formulated with 5 µg of SMNP in a final volume of 50 µL. For Adjuplex formulations, nanoparticles were formulated with 10% Adjuplex[20].

Immunizations and analyses for B cell phenotyping experiments

Experiments with SAS adjuvant were formulated with 5 μg of antigen (approximately 15 μg of total nanoparticle) and delivered intraperitoneally (IP), and experiments with SMNP adjuvant were formulated with 3 μg of total nanoparticle and delivered intramuscularly (IM) . For SAS adjuvant experiments, female B6-albino mice were immunized and spleens were harvested to isolate splenocytes at 8 and 20 days post immunization. For SMNP adjuvant experiments, mice were immunized and draining lymph nodes (dLNs) were harvested to isolate lymphocytes 8 days after immunization. Isolated cells were stained with probes for CSP+ B cells, CD138+CSP+ Plasmablasts, and CD38-GL7+ GC B cells. Antibody titers were measured against a soluble CSP construct coated on ELISA plates.

Parasites and mosquitoes

Transgenic *Plasmodium berghei* (strain ANKA 676m1C11, MRA-868) parasites expressing full-length (3D7 strain) *P. falciparum* CSP and a green fluorescent protein/luciferase fusion protein (Pb-PfCSP-GFP/LUC SPZ) were propagated and used to evaluate the efficacy of the PfCSP-based vaccines, as previously described[21]. Briefly, BALB/c mice were infected by intraperitoneal (IP) injection of Pb-PfCSP-GFP/LUC SPZ-infected RBCs. *Anopheles stephensi* (Nijmegan) mosquitoes were reared at the Laboratory of Malaria and Vector Research (National Institute of Allergy and Infectious Diseases, National Institutes of Health). Female mosquitoes were allowed to feed on the parasitized mice which were anesthetized by IP injection of ketamine (50 mg/kg) and xylazine (10 mg/kg) mixture. After feeding, mice were euthanized via CO_2 inhalation, followed by cervical dislocation. Blood fed mosquitoes were then maintained in a humidified incubator at 19–20°C and supplied with 10% sucrose. For challenge studies, sporozoites were harvested from mosquito salivary glands at day 18-21 after an infectious blood meal, as previously described[21].

Immunizations and sporozoite challenge studies

RT-I53-50, RT.2-I53-50, and RT.2-I53-50-glycosylated nanoparticle immunogens were diluted in buffer to the indicated doses with either Adjuplex or SMNP adjuvants. R21 in the second challenge study was also formulated with SMNP. Female B6-albino mice were immunized intramuscularly in the quadriceps at weeks 0 and 3 weeks. Challenges were conducted 3 weeks after the final immunization as indicated, where mice were challenged intravenously via the tail vein with 2,000 freshly harvested Pb-PfCSP-GFP/LUC sporozoites as previously described[21]. Then, 40–42 hours post-challenge, mice received an IP injection of 150 μL of D-Luciferin (30 mg/mL), were anesthetized with isoflurane (5% for induction, 1-3% for maintenance). Luciferase activity in mice was visualized through imaging of whole bodies using the IVIS® Spectrum in vivo imaging system (PerkinElmer) 10 minutes post-injection. A group of uninfected control mice were referred to as naive, and infected control mice referred to as untreated, were used for each challenge experiment. Upon completion of the experiments, mice were euthanized via CO_2 inhalation followed by cervical dislocation. To measure the burden of parasite infection in the liver, a region of interest (ROI) in the upper abdominal area (at the location of the liver) was analyzed and the total flux or bioluminescent radiance (photons/sec) emitted by Pb-PfCSP-GFP/LUC-SPZ was calculated using the manufacturer's software (Living Image 4.5, PerkinElmer).

Quantitative and statistical analysis

Statistical differences between mouse groups were determined by parametric and non-parametric one-way ANOVA analysis with multiple comparisons test using GraphPad Prism (GraphPad Software).

References

1. *World Malaria Report 2023*. https://www.who.int/teams/global-malaria-programme/reports/world-malaria-report-2023 (2023).
2. The RTS,S Clinical Trials Partnership. First Results of Phase 3 Trial of RTS,S/AS01 Malaria Vaccine in African Children. *N. Engl. J. Med.* **365**, 1863–1875 (2011).
3. Datoo, M. S. *et al.* Safety and efficacy of malaria vaccine candidate R21/Matrix-M in African children: a multicentre, double-blind, randomised, phase 3 trial. *Lancet* **403**, 533–544 (2024).
4. Gordon, D. M. *et al.* Safety, immunogenicity, and efficacy of a recombinantly produced Plasmodium falciparum circumsporozoite protein-hepatitis B surface antigen subunit vaccine. *J. Infect. Dis.* **171**, 1576–1585 (1995).
5. Collins, K. A., Snaith, R., Cottingham, M. G., Gilbert, S. C. & Hill, A. V. S. Enhancing protective immunity to malaria with a highly immunogenic virus-like particle vaccine. *Sci. Rep.* **7**, 46621 (2017).
6. White, M. T. *et al.* Immunogenicity of the RTS,S/AS01 malaria vaccine and implications for duration of vaccine efficacy: secondary analysis of data from a phase 3 randomised controlled trial. *Lancet Infect. Dis.* **15**, 1450–1458 (2015).
7. RTS,S Clinical Trials Partnership. Efficacy and safety of RTS,S/AS01 malaria vaccine with or without a booster dose in infants and children in Africa: final results of a phase 3, individually randomised, controlled trial. *Lancet* **386**, 31–45 (2015).
8. Datoo, M. S. *et al.* Efficacy and immunogenicity of R21/Matrix-M vaccine against clinical malaria after 2 years' follow-up in children in Burkina Faso: a phase 1/2b randomised controlled trial. *Lancet Infect. Dis.* (2022) doi:10.1016/S1473-3099(22)00442-X.
9. Tokatlian, T. *et al.* Innate immune recognition of glycans targets HIV nanoparticle immunogens to germinal centers. *Science* **363**, 649–654 (2019).
10. Read, B. J. *et al.* Mannose-binding lectin and complement mediate follicular localization and enhanced immunogenicity of diverse protein nanoparticle immunogens. *Cell Rep.* **38**, 110217 (2022).
11. Bale, J. B. *et al.* Accurate design of megadalton-scale two-component icosahedral protein complexes. *Science* **353**, 389–394 (2016).
12. Aung, A. *et al.* Low protease activity in B cell follicles promotes retention of intact antigens after immunization. *Science* **379**, eabn8934 (2023).
13. Ludwig, J. *et al.* Glycosylated nanoparticle-based PfCSP vaccine confers long-lasting

antibody responses and sterile protection in mouse malaria model. *npj Vaccines* **8**, 1–14 (2023).

14. Wargacki, A. J. *et al.* Complete and cooperative in vitro assembly of computationally designed self-assembling protein nanomaterials. *Nat. Commun.* **12**, 883 (2021).
15. Elbein, A. D., Tropea, J. E., Mitchell, M. & Kaushal, G. P. Kifunensine, a potent inhibitor of the glycoprotein processing mannosidase I. *J. Biol. Chem.* **265**, 15599–15605 (1990).
16. Elbein, A. D., Kerbacher, J. K., Schwartz, C. J. & Sprague, E. A. Kifunensine inhibits glycoprotein processing and the function of the modified LDL receptor in endothelial cells. *Arch. Biochem. Biophys.* **288**, 177–184 (1991).
17. Behrens, A.-J. & Crispin, M. Structural principles controlling HIV envelope glycosylation. *Curr. Opin. Struct. Biol.* **44**, 125–133 (2017).
18. Allen, J. D. *et al.* Site-specific steric control of SARS-CoV-2 spike glycosylation. *Biochemistry* **60**, 2153–2169 (2021).
19. Silva, M. *et al.* A particulate saponin/TLR agonist vaccine adjuvant alters lymph flow and modulates adaptive immunity. *Sci. Immunol.* **6**, eabf1152 (2021).
20. Wegmann, F. *et al.* The carbomer-lecithin adjuvant Adjuplex has potent immunoactivating properties and elicits protective adaptive immunity against influenza virus challenge in mice. *Clin. Vaccine Immunol.* **22**, 1004–1012 (2015).
21. Flores-Garcia, Y. *et al.* Optimization of an in vivo model to study immunity to Plasmodium falciparum pre-erythrocytic stages. *Malar. J.* **18**, 426 (2019).
22. Gowda, D. C. & Miller, L. H. Glycosylation in malaria parasites: what do we know? *Trends Parasitol.* **40**, 131–146 (2024).
23. Dempsey, P. W., Allison, M. E., Akkaraju, S., Goodnow, C. C. & Fearon, D. T. C3d of complement as a molecular adjuvant: bridging innate and acquired immunity. *Science* **271**, 348–350 (1996).
24. Movsesyan, N. *et al.* DNA epitope vaccine containing complement component C3d enhances anti-amyloid-beta antibody production and polarizes the immune response towards a Th2 phenotype. *J. Neuroimmunol.* **205**, 57–63 (2008).
25. Koch, M. & Baum, J. The mechanics of malaria parasite invasion of the human erythrocyte – towards a reassessment of the host cell contribution. *Cell. Microbiol.* **18**, 319–329 (2016-3).
26. Ross, T. M., Xu, Y., Green, T. D., Montefiori, D. C. & Robinson, H. L. Enhanced avidity maturation of antibody to human immunodeficiency virus envelope: DNA vaccination with gp120-C3d fusion proteins. *AIDS Res. Hum. Retroviruses* **17**, 829–835 (2001).

27. Bale, S. *et al.* Fusion of the molecular adjuvant C3d to cleavage-independent native-like HIV-1 Env trimers improves the elicited antibody response. *Front. Immunol.* **14**, 1180959 (2023).
28. Pompa-Mera, E. N., Arroyo-Matus, P., Ocaña-Mondragón, A., González-Bonilla, C. R. & Yépez-Mulia, L. Protective immunity against enteral stages of Trichinella spiralis elicited in mice by live attenuated Salmonella vaccine that secretes a 30-mer parasite epitope fused to the molecular adjuvant C3d-P28. *Res. Vet. Sci.* **97**, 533–545 (2014).
29. Galvez-Romero, G., Salas-Rojas, M., Pompa-Mera, E. N., Chávez-Rueda, K. & Aguilar-Setién, Á. Addition of C3d-P28 adjuvant to a rabies DNA vaccine encoding the G5 linear epitope enhances the humoral immune response and confers protection. *Vaccine* **36**, 292–298 (2018).
30. Li, B. *et al.* Enhancing the immunogenicity of lipid-nanoparticle mRNA vaccines by adjuvanting the ionizable lipid and the mRNA. *Nat. Biomed. Eng.* 1–18 (2023) doi:10.1038/s41551-023-01082-6.
31. Tsokos, G. C., Lambris, J. D., Finkelman, F. D., Anastassiou, E. D. & June, C. H. Monovalent ligands of complement receptor 2 inhibit whereas polyvalent ligands enhance anti-Ig-induced human B cell intracytoplasmic free calcium concentration. *J. Immunol.* **144**, 1640–1645 (1990).
32. Bergmann-Leitner, E. S. *et al.* C3d-defined complement receptor-binding peptide p28 conjugated to circumsporozoite protein provides protection against Plasmodium berghei. *Vaccine* **25**, 7732–7736 (2007).
33. Casalino, L. *et al.* Beyond shielding: The roles of glycans in the SARS-CoV-2 spike protein. *ACS Cent. Sci.* **6**, 1722–1734 (2020).
34. Gao, C. *et al.* Differential recognition of oligomannose isomers by glycan-binding proteins involved in innate and adaptive immunity. *Sci. Adv.* **7**, eabf6834 (2021).
35. Matz, H. C., McIntire, K. M. & Ellebedy, A. H. Persistent germinal center responses: slow-growing trees bear the best fruits. *Curr. Opin. Immunol.* **83**, 102332 (2023).
36. Krishnamurty, A. T. *et al.* Somatically hypermutated Plasmodium-specific IgM(+) memory B cells are rapid, plastic, early responders upon malaria rechallenge. *Immunity* **45**, 402–414 (2016).
37. Cockburn, I. A. & Seder, R. A. Malaria prevention: from immunological concepts to effective vaccines and protective antibodies. *Nat. Immunol.* **19**, 1199–1211 (2018).
38. Nutt, S. L., Hodgkin, P. D., Tarlinton, D. M. & Corcoran, L. M. The generation of antibody-secreting plasma cells. *Nat. Rev. Immunol.* **15**, 160–171 (2015).

39. Kraft, J. C. *et al.* Antigen- and scaffold-specific antibody responses to protein nanoparticle immunogens. *Cell Rep Med* **3**, 100780 (2022).
40. Lin, S.-C. *et al.* Different immunity elicited by recombinant H5N1 hemagglutinin proteins containing pauci-mannose, high-mannose, or complex type N-glycans. *PLoS One* **8**, e66719 (2013).
41. Abramson, J. *et al.* Accurate structure prediction of biomolecular interactions with AlphaFold 3. *Nature* **630**, 493–500 (2024).

Supplementary Figures

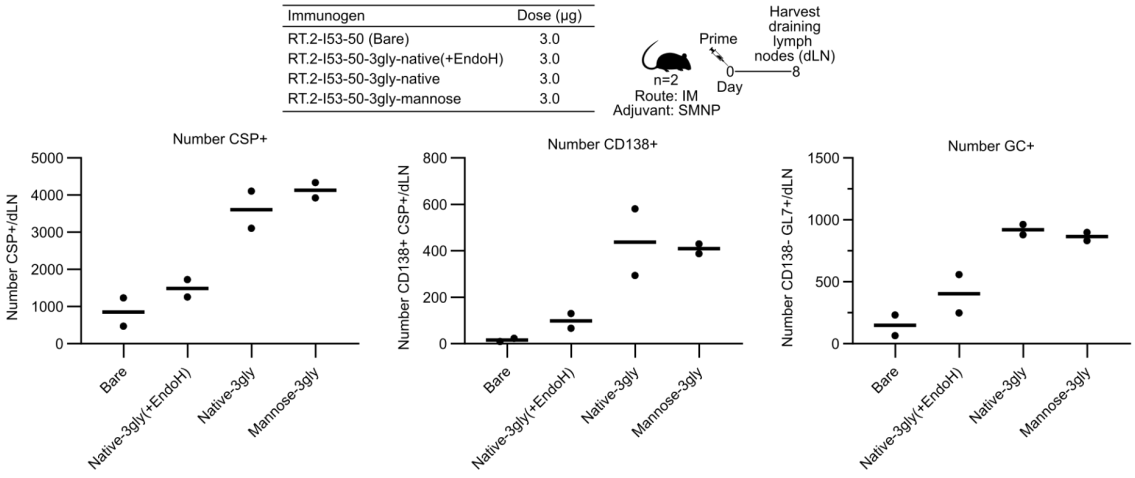

Supplementary Figure 1. Removal of oligomannose glycan on RT.2-I53-50-3gly-native results in a B cell phenotype similar to bare nanoparticles. Mice were intramuscularly immunized with 3 µg of RT.2-I53-50 nanoparticles listed and formulated with 5 µg SMNP adjuvant. RT.2-I53-50-3gly-native(+EndoH) refers to an Endo H treated nanoparticle that contains no oligomannose glycans. Draining lymph nodes were harvested 8 days after immunization and cells were stained and populations of CSP+, CSP+ plasmablasts (CD138+), and CSP+ GC B cells (CD38-GL7+) were determined by flow cytometry.

Chapter 3: Circumsporozoite protein (CSP) germline-targeting vaccines for *P. falciparum* malaria

This chapter is in preparation as:
Mark D. Langowski*, Jahyun Koo*, Wilma Lee, Nicholas K. Hurlburt, Sai Sundar Rajan Raghavan, M. Nathan Yoo, Sebastian Ols, Stefan Clarke, Robert A. Seder, Andrew Ward, Marie Pancera, Facundo D. Batista, Neil P. King;
Circumsporozoite protein (CSP) germline-targeting vaccines for P. falciparum malaria.

Affiliations:
Institute for Protein Design, University of Washington, Seattle, WA, USA
Department of Biochemistry, University of Washington, Seattle, WA, USA
Graduate Program in Molecular and Cellular Biology, University of Washington, Seattle, WA, USA
Vaccine and Infectious Disease Division, Fred Hutchinson Cancer Center, Seattle, WA, USA
Vaccine Research Center, National Institute of Allergy and Infectious Diseases, National Institutes of Health, Bethesda, MD, USA
Department of Integrative Structural and Computational Biology, The Scripps Research Institute, La Jolla, CA, USA

Introduction

The WHO reported that in 2022 malaria caused an estimated 249 million cases and 608,000 deaths, with a majority of these deaths being caused by *Plasmodium falciparum* in children under 5 years of age. Public health efforts have reduced these numbers over the last two decades through use of interventions such as insecticide-treated bed nets and widespread seasonal malaria chemoprevention (SMC), but these successes are threatened by the emergence of growing insecticide and drug resistance[1]. This necessitates the need for the development of additional interventions such as highly efficacious vaccines to mitigate this significant public health burden.

After the bloodmeal of an infected Anopheles mosquito, the *P. falciparum* sporozoite stage must travel through the skin, blood, and into the liver to establish an infection, which then progresses to its erythrocytic stage and infects red blood cells (RBCs), and is where symptomatic malaria illness occurs. As such, many vaccine efforts aim to intervene at the sporozoite stage to provide sterilizing immunity and break this life cycle chain. The primary target of pre-erythrocytic vaccines is the circumsporozoite protein (CSP), which is the most abundant protein on the surface of sporozoites and is important for its development[2], motility[3], and infection of hepatocytes[4]. CSP is an intrinsically disordered protein composed of three domains: an N-terminal domain with a conserved KLKQP (Region I) sequence found at its C-terminal end, a central tetrapeptide repeat domain starting with a single junctional sequence (NPDP) and consisting of downstream major (NANP) and minor (NVDP) repeats, and a structured C-terminal domain that adopts an alpha-thrombospondin repeat fold with a GPI anchor[5]. The world's most advanced malaria vaccines, RTS,S/AS01 and R21/Matrix-M, display only major repeats and the

C-terminal domain on HepBsAg virus-like particles (VLPs), and have been recommended by the WHO for use in children and infants in Africa for the prevention of malaria with efficacy ranging from 55.8 and 68% at standard sites, respectively[6,7]. Though implementation of these vaccines are likely to further reduce malaria burden, there are concerns with their antibody durability and quality, the latter of which may be due to the lack of inclusion of recently elucidated protective epitopes that target the junctional NPDP and minor NVDP repeats.

Solved structures of monoclonal antibodies (mAbs) isolated from individuals immunized with RTS,S or attenuated sporozoite vaccines have revealed that protective mAbs primarily target the CSP major, minor, and junctional repeats, typically in type I beta-turn or pseudo310 turn conformations[8–12]. Clinical trials involving passive immunization of two of these mAbs, the NPDP-targeting CIS43LS and NVDP-targeting L9LS, have shown significant efficacy against malaria infection in controlled human malaria infection (CHMI) trials, and in the field, providing a proof-of-concept that antibodies targeting these two epitopes can be efficacious at low serum concentrations[13–16]. Based on these results, numerous groups have developed preclinical vaccine candidates that include these epitopes in hopes that they can improve the efficacy of CSP vaccines[17–22]. However, current transgenic parasite challenge mouse models have not shown a clear improvement in protection as compared to R21, RTS,S-like vaccines, or others that only contain major repeats[21,23]. One possible reason for this is that CSP repeats are inherently flexible and act independently as their own structural units[24,25], and thus simple genetic fusion of these known epitopes may not be sufficient to generate antibodies that target protective epitope conformations. For example, protective mAb CIS43 targets the junctional NPDPNANPNVDP sequence, but non-protective mAb CIS42 binds the same sequence in a different conformation, so it is likely that immunization with this sequence could generate a polyclonal response that induces both types of antibodies. Thus, one strategy would be to “lock” the CIS43 epitope in a stable conformation and thus disallow binding of CIS42.

A significant fraction of vaccine-elicited mAbs use *IGHV3-33* and *IGKV1-5* genes, such as L9, and have evolved Fab-Fab homotypic antibody contacts that improve the apparent affinity of these antibodies for CSP repeats as they bind next to each other and form ordered structures[11,26–30], and these matured homotypic contacts are important for mediating protection in transgenic parasite mouse challenge models[28]. Though these studies have shown that immunization with PfCSP can induce these antibodies, it is unclear how to specifically target them with flexible repeats as the specific geometry for their binding cannot be enforced. To date, there is only one study that has explored immunogens that can specifically induce these mutations in a controlled manner using homotypic mAb 1210 fused to 5.5 NANP repeats via a flexible linker and displayed as a 60mer on lumazine synthase (1210-NANP5.5-LS), such that half of these repeats would be bound by the fused 1210 Fab, and the other half of the repeats would be available for BCR engagement[31]. One possible way to further improve upon this concept would be to use protein design methods to produce an immunogen that does not require the fusion of a human Fab to an antigen, and scaffolds epitopes such as L9 or 1210 to enforce the geometry required to induce these Fab-Fab homotypic contacts without the formation of a pre-immune complex.

Epitope-based vaccine design is a promising way to elicit a potent immune response against protective epitopes. Most of these have been designed against epitopes from viral fusion glycoproteins such as RSV F or HIV using Rosetta-based protein design and yeast-display approaches, with varying levels of success in producing neutralizing responses in animal models[32–39]. More recent deep-learning based protein design methods, such as RFDiffusion[40], are an additional tool in generating novel backbones with high accuracy to their design model, and one application is motif-scaffolding for stabilizing epitopes in specific conformations. Deep-learning enabled motif-scaffolding holds promise for the display of stabilized CSP repeat conformations as this has been generally a more difficult task for Rosetta-based methods.

Here we describe the use of deep learning-based models, RFDiffusion and ProteinMPNN[40,41], to design immunogens that display stabilized protective CSP repeat epitopes of CIS43 and L9. These immunogens are highly stable, bind to their target antibody with equal or greater affinity as compared to their native epitopes, and show reduced or no binding to less protective antibodies. Immunization of germline-CIS43 knock-in mice with CIS43 immunogens shows that they are able to induce antibody responses with similar maturation pathways as to the original mature CIS43 antibody. L9 immunogens can also induce the recruitment of germline-L9 B cells to the germinal center, and structural determination reveals the precise scaffolding of the L9 Fab-Fab epitope.

Results

Design and of CIS43 epitope immunogens:
We hypothesized that we could use RFDiffusion to generate a backbone that would buttress the CIS43 epitope (NPDPNANPNVDPN) and stabilize its conformation, thus disfavoring the generation of off-target antibodies such as CIS42 (**Fig. 1a-c**). We first used the crystal structure of CIS43 in complex with its native epitope and attempted to diffuse 25-35 residues around either side of the peptide to buttress the epitope (**Fig. 1c**). Upon filtering 3750 designs for ≤0.3Å RMSD of the target epitope in the diffused backbone to the input structure, we noticed only 837 designs passed this filter (22% passing, **Supplementary Fig. 1a**). We hypothesized that this low number of designs was due to RFdiffusion being unable to properly pack secondary structure against polar/charged residues (Asp 3, Asn 5, and Asn 11) in the original CIS43 epitope (**Supplementary Fig. 1b**). Thus, we used three total inputs to try and generate proposed backbones: the native peptide and two “hydrophobic” inputs (hphobic1 & hphobic2) where residues 3, 5, or 11 were replaced with leucines to promote the packing of secondary structure on the side of the epitope that faced away from the antibody paratope (**Supplementary Fig. 1b**). RFdiffusion was run using these three inputs in complex with a CIS43 antibody model mutated to its inferred-germline sequence (iGL-CIS43; ref.[42]) and we tested multiple parameter combinations in order to generate a significant amount of prospective backbones (**Supplementary Fig. 1a**). A total of 11,236 backbones were generated and were filtered on 1) ≤0.3Å RMSD of the target motif in the diffused backbone to the reference structure, and 2) zero antibody backbone clashes with the newly diffused immunogen.

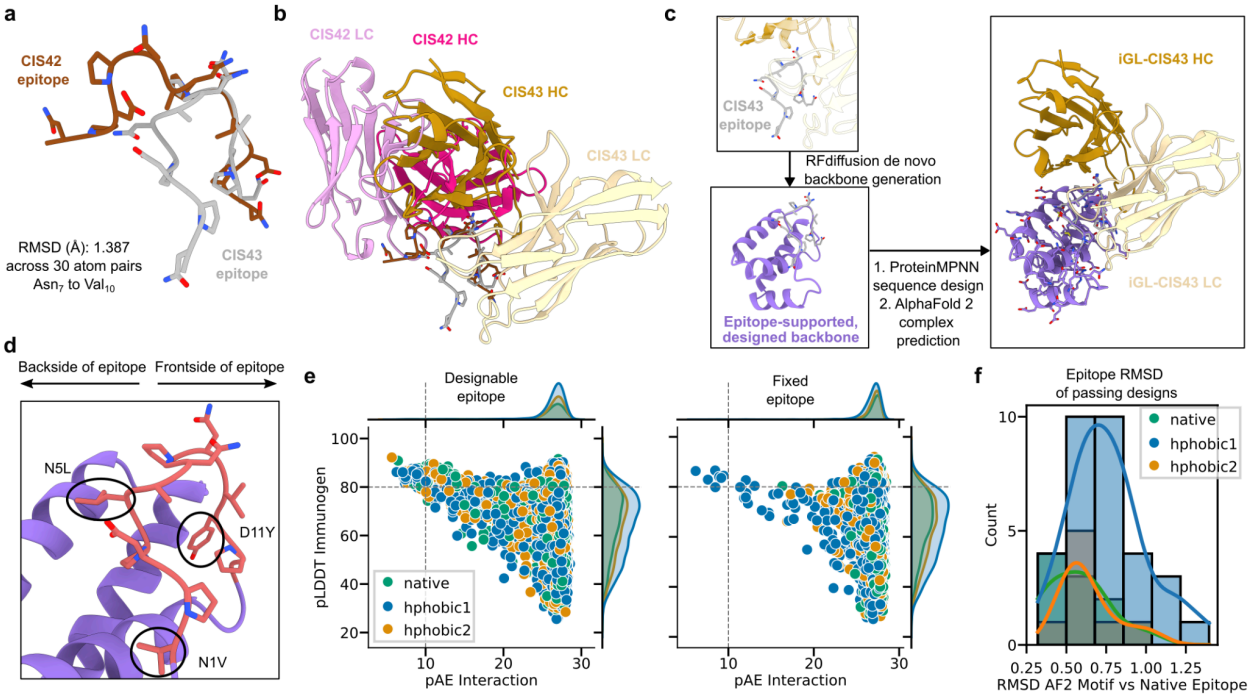

Figure 1. Design of CIS43 epitope germline-targeting immunogens. a Overlaid structures of NPDPNANPNVDPN peptides in bound CIS43 (gray, PDB ID: 6B5M) and CIS42 (brown, PDB: 6B5R) structures. **b** CIS43 and CIS42 antibody-peptide structures highlighting the different angles of approach of these two antibodies. **c** Design pipeline for CIS43 immunogens. *De novo* backbone around the epitope (gray) was generated with RFdiffusion (purple), sequence designed, and AF2-predicted in complex with iGL-CIS43 (inferred-germline CIS43; dark gold, wheat). **d** Example AF2 model of residues designed on the backside of the supported epitope (red). Circled residues are sites that were polar or charged in the original epitope structure, but were allowed to be designable and were thus mutated to small hydrophobics that pack against supporting helices. **e** RFdiffusion was performed with fully native CIS43 epitopes (green), and "hydrophobic" (hphobic) inputs (blue, yellow) to promote de novo backbone packing on the backside of the epitope. These backbones were then sequence designed (MPNN-FR) and epitopes were allowed to be fully designable or fixed at important positions. Scatterplots of all AlphaFold2 predicted MPNN-FR designs from designable (left) and fixed (right) epitope sets. Dashed lines indicate cutoffs used for filtering (pLDDT immunogen > 80, pAE interaction with antibody < 10). **f** Histogram of passing designs (total n=50; 44 from designable, and 6 from fixed sets).

837 designs from the native peptide input (22% passing), 1732 from hphobic1 input (46.2% passing), and 1106 from hphobic2 input (29.5% passing), for a total of 3675 designs, passed these filters and were used for subsequent sequence design using a ProteinMPNN and Rosetta FastRelax protocol (ProteinMPNN-FR; ref.[43]) with two subsets for design: 1) "designable," whereby design was allowed on the entire diffused immunogen, including the epitope; and 2) "fixed," where the entire epitope was fixed, except for hphobic inputs which allowed design at mutated input positions (e.g., residues 3, 5, or 11 of the input epitope). The generated sequences were then predicted with an AlphaFold2 (AF2) initial guess protocol[43,44], and filtered on >80 pLDDT of the immunogen and <10 pAE of interaction with CIS43 (**Fig. 1c,e**). In general, we observed that predictions that came from hphobic1 and hphobic2 designs that were allowed

to be fully designable had the greatest success rates for a total of 44 designs from the designable set (0.46% passing) and 6 designs from the fixed set (0.06% passing, **Fig. 1e,f**). A majority of these passing designs had mutations on the backside of the epitope at residues that aren't directly involved in CIS43 contacts, replacing originally polar/charged residues with small or large hydrophobic residues that can more easily pack against supporting secondary structure (**Fig. 1d**).

Screening and characterization of CIS43 epitope immunogens:
Designs that passed AF2 metrics were expressed in BL21(DE3) *E. coli* and purified by immobilized metal affinity chromatography (IMAC). All designs contained a significant amount of purified protein at the expected molecular weight (MW) in their IMAC eluate as assessed by SDS-PAGE, except for design #90 (**Fig. 2a**). We further purified IMAC eluates by size exclusion chromatography (SEC) and found 29 of 50 designs (58%) were monodisperse with a significant peak at their expected retention volumes (**Fig. 2b**). SEC fractions were collected and were pure as assessed by SDS-PAGE (**Fig. 2b**), and 280 nm absorbance was measured to determine concentrations for binding experiments.

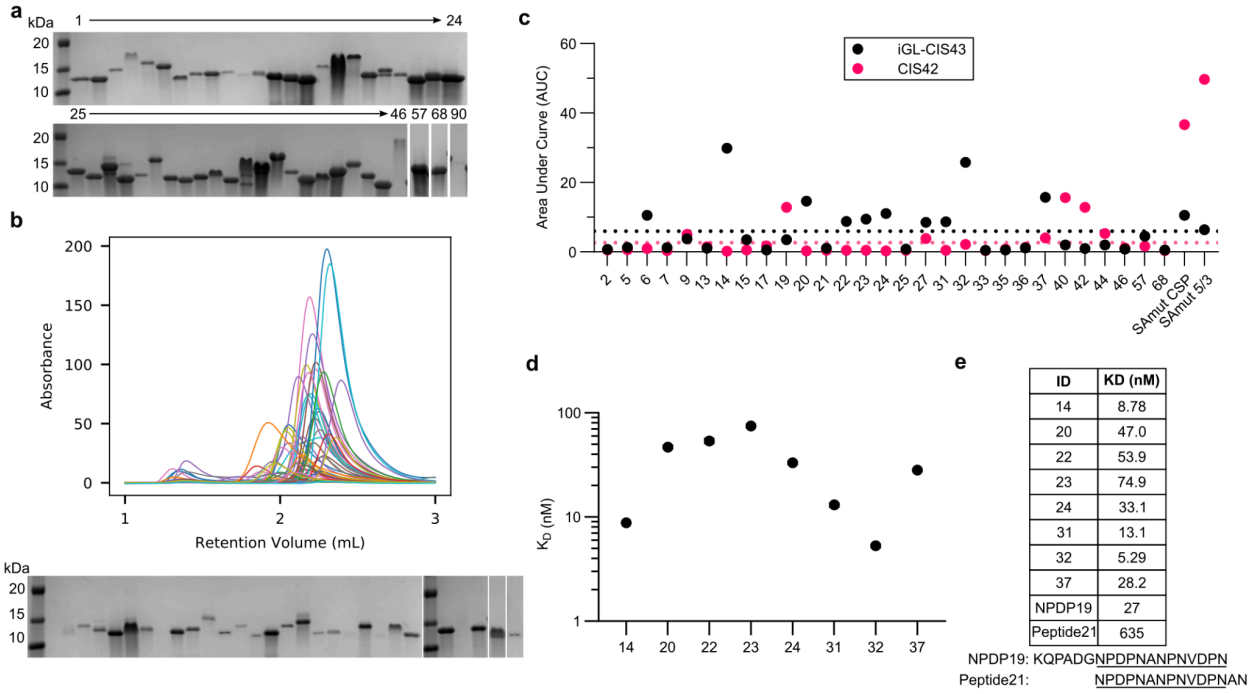

Figure 2. Screening and characterization of CIS43 epitope immunogens. a SDS-PAGE of IMAC eluates. **b** Overlaid SEC chromatograms of all 50 designs (top), and corresponding SDS-PAGE gel confirming purity (bottom). **c** BLI AUC for 29 designs at 100 nM concentration tested for binding against ProA tips loaded with either iGL-CIS43 or CIS42. Dashed lines indicate mean AUC values. **d** BLI-determined K_D values for 8 selected designs. **e** iGL-CIS43 KD values against immunogens in comparison to the reported values for native peptides NPDP19 and Peptide21.

We performed biolayer interferometry (BLI) using ProteinA tips to assess if our CIS43 immunogens could bind to IgG of inferred-germline of CIS43 (iGL-CIS43), while having little or no binding to CIS42. A soluble and stable full-length CSP (SAmut CSP), and a construct with a

truncated repeat region that contained primarily junctional and minor repeat epitopes (SAmut 5/3) were used as controls. As an initial screen, loaded IgG tips were dipped into 100 nM of immunogen or control to determine if there was reactivity to either mAb. Our controls behaved as expected with a binding shift observed for both SAmut CSP and SAmut 5/3 against either iGL-CIS43 or CIS42. Significant binding shifts, analyzed as an area under the curve (AUC) greater than the mean iGL-CIS43 AUC of all immunogens, were observed in 10 of the 29 designs tested (**Fig. 2c**). Of these 10 designs (designs 14, 32, 37, 20, 24, 6, 23, 22, 31, 27), only two had CIS42 AUCs greater than the mean CIS42 AUC indicating detectable off-target binding at this immunogen concentration (**Fig. 2c**). This same screen was performed against mature CIS43 in comparison to iGL-CIS43 and we found that for all constructs, mature CIS43 bound with a higher shift as compared to iGL-CIS43 at 100 nM of immunogen (**Supplementary Fig. 2**). Enzyme linked immunosorbent assay (ELISA) using iGL-CIS43 and CIS42 mAbs tested for binding against plated immunogens also confirmed the results and general trends of the BLI screen, showing potent binding to iGL-CIS43, though a higher level of CIS42 reactivity was observed for certain designs (32, 31, 22) as compared to the BLI experiment (**Supplementary Fig. 2**).

Based on this data we down-selected seven designs that had high-specificity for iGL-CIS43 (14, 20, 22, 23, 24, 31, 32) and one design (37) that had appreciable binding to CIS42 for affinity measurements by BLI across a concentration range of 100 nM to 1.56 nM. iGL-CIS43 affinities for all immunogens tested were close to or better than the reported affinities for NPDP19 or Peptide21 (27 and 635 nM, respectively; **Fig. 2d-e, Supplementary Fig. 3a**). Background level binding for CIS42 was observed at this concentration range for all but design 37, consistent with the previous screening experiments (**Supplementary Fig. 3b)**. Altogether these results show that CIS43 epitope-specific immunogens designed with RFdiffusion and MPNN-FR can bind their target antibody with high specificity.

Design and characterization of immunogen-fused nanoparticles:
The multivalent display of antigens and immunogens on nanoparticles is known to improve vaccine-elicited responses by improving B cell cross-linking for activation, vaccine trafficking, and antigen presentation[45]. Our group has leveraged these benefits by use of computationally designed self-assembling protein nanoparticles and shown that they can generate potent antibody responses against antigens from SARS-CoV-2, RSV F, and many others[46–48]. We decided to move forward with design 14, hereafter referred to as 14-glCIS43, for genetic fusion on two-component nanoparticle platforms: the tetrahedral T33-dn10[49] and icosahedral I53-50[50]. 14-glCIS43 (**Fig. 3a**) was selected because it was highly specific toward iGL-CIS43 and had no reactivity to CIS42 in both the BLI and ELISA experiments (**Fig. 2c**, **Supplementary Fig. 2 & 3**), and only differed from the CIS43 epitope by three mutations (**Fig. 3b**). 14-glCIS43 was genetically fused via an 8-residue GS linker to trimeric components T33-dn10A and I53-50A (**Fig. 3c**).

These constructs were expressed in *E. coli*, purified by IMAC and SEC, and their purity was verified by SDS-PAGE (**Supplementary Fig. 4a**). Nanoparticles for 14-glCIS43-T33-dn10 were assembled by mixing 14-glCIS43-T33-dn10A and T33-dn10B in a 1:1 molar ratio.

14-glCIS43-I53-50 nanoparticles were assembled by mixing 14-glCIS43-I53-50A and I53-50B.4PT1 in a 1.1:1 molar ratio[51]. Assembled nanoparticles were purified by SEC to remove residual components and both had peaks at their expected retention volumes (**Figure 3b**), and negative-stain electron microscopy (nsEM) showed nanoparticles of the expected morphologies (**Fig. 3c**, **Supplementary Fig. 4c**). We next tried surface plasmon resonance (SPR) on these nanoparticles to assess nanoparticle binding specificity, and found that both 14-glCIS43-T33_dn10 and 14-glCIS43-I53-50 had strong binding to iGL-CIS43 and had weak-to-no binding for CIS42 across a concentration range of 100 nM to 0.09 nM (**Figure 3d**). These results confirmed that 14-glCIS43 retained its binding specificity when presented on multivalent nanoparticles.

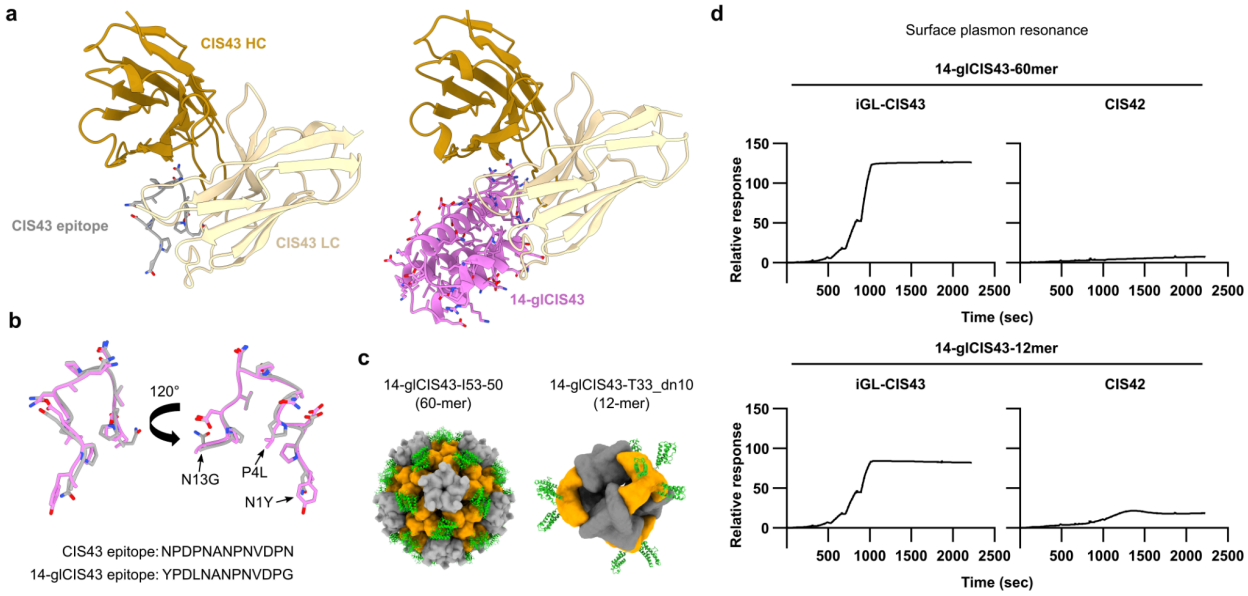

Figure 3. Design and characterization of 14-glCIS43 immunogen-fused nanoparticles. a Comparison of CIS43 antibody and peptide co-crystal structure (left), to AF2-predicted 14-glCIS43 model in complex with iGL-CIS43 (right). **b** Overlaid peptide 21 structure (gray) on corresponding motif in 14-glCIS43 (pink). Differences in residues are highlighted with arrows. **c** AF2-predicted models for 14-glCIS43-I53-50 (left) and 14-glCIS43-T33_dn10 (right) nanoparticles. Images are not to scale. 14-glCIS43 fused via a flexible linker is shown in green. **d** SPR sensorgrams of nanoparticle immunogens across a concentration range of 100 to 0.09 nM against iGL-CIS43 and CIS42.

Assessment of 14-glCIS43 nanoparticles in an iGL-CIS43 knock-in mouse model:
An iGL-CIS43 knock-in mouse model has previously shown that immunization of mice with minimal CIS43 epitope conjugated to keyhole limpet hemocyanin (KLH) can recruit iGL-CIS43 B cells to germinal centers (GCs) more efficiently than full-length PfCSP immunization[42]. We used this model to determine if monomeric or nanoparticle 14-glCIS43 immunogens could recruit iGL-CIS43 B cells to GCs and produce antibodies with similar features as mature CIS43. Knock-in heavy-chain (HC) and kappa-chain (LC) iGL-CIS43 B cells were adoptively transferred into congenic mice at a precursor frequency of $1{:}10^5$ and these mice were immunized intraperitoneally (IP) with 10 µg PfCSP, 14-glCIS43 (1mer), 14-glCIS43-T33_dn10 (12mer), and 14-glCIS43-I53-50 (60mer), all formulated in Alum (**Fig. 4a**). Splenocytes were isolated and

analyzed by flow cytometry at day 13 and 28 (**Supplementary Figure 5a**), and CSP^{+}CD45.2^{+}GC^{+} B cells were sequenced at day 28 (**Fig. 4a**). GC B cells (CD38^{low}, CD95^{+}) were detected in all groups at day 13, with PfCSP and 14-glCIS43-60mer groups being significantly higher than 14-glCIS43-1mer (**Fig. 4b**). Significantly more transferred CD45.2+ B cells were recruited to GCs by 14-glCIS43-12mer as compared to all other groups, with 14-glCIS43-60mer being the only other group with appreciable levels of these cells (**Fig. 4b,c**), and a majority of CD45.2^{+} GC B cells reacted with CSP tetramer probes (**Fig. 4b**). On day 28, only 14-glCIS43-60mer had on-going GCs with CD45.2^{+}PfCSP^{+} GC B cells, and these cells were sorted for HC and LC sequencing (**Fig. 4c,d**).

Sequencing from 14-glCIS43-60mer immunized mice showed similar somatic hypermutations (SHMs) observed from in the original CIS43[9], and an engineered variant developed with this knock-in model, CIS43.D3[42]. Important SHMs M34I$_{HC}$, G54D$_{HC}$, V102L$_{HC}$, and Q95H$_{LC}$ were all observed at high frequencies in sorted cells (**Fig. 4d**), though it should be noted that important mutations N52K$_{HC}$, K59R$_{HC}$, and T94S$_{LC}$ were observed at lower frequencies compared to previous work[42]. Altogether, this data shows that immunization with CIS43 epitope immunogen 14-glCIS43-60mer can activate and recruit transferred, knock-in iGL-CIS43 B cells to GCs and sequences sorted from these B cells reflect similar SHMs observed in CIS43 and CIS43.D3.

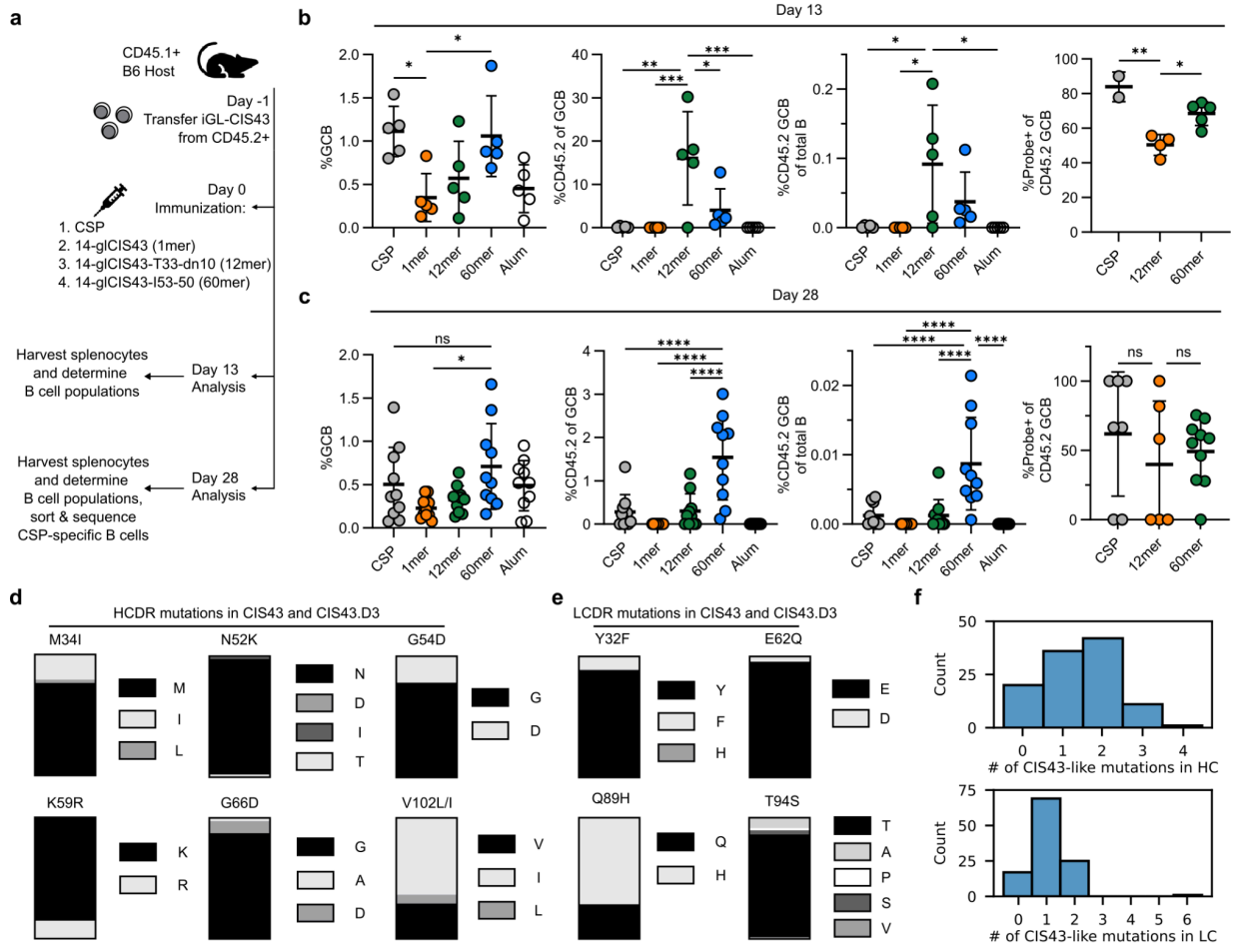

Figure 4. Immunization with 14-glCIS43 nanoparticle immunogens leads to activation and recruitment of knock-in CIS43 B cells to germinal centers (GCs). a Study schematic for 14-glCIS43 immunizations with knock-in iGL-CIS43 mice. **b** Day 13 and **c** Day 28 flow cytometry graphs for splenocytes from immunized mice. These graphs indicate total GC B cells, CD45.1 or CD45.2 GC B cells, and PfCSP reactive (Probe^{+}) CD45.2 GC B cells. **d** Counts of HCDR and **e** LCDR somatic hypermutations (SHMs) at important positions isolated from mice immunized with 14-glCIS43-60mer. The first residue refers to the germline, and the second residue the mutation found in either CIS43 or CIS43.D3. **f** Total number of CIS43-like SHMs found in individual sorted sequences. Average of 1.42 HC and 1.11 LC mutations per sequence.

Design and characterization of de novo immunogens targeting the L9 Fab-Fab epitope: We designed additional immunogens to scaffold epitopes from potent CSP repeat mAb L9 using the same RFdiffusion and ProteinMPNN pipeline used for CIS43 (**Figure 1c**). Three L9 Fabs are bound in the original structure to three consecutive NPNV repeats (**Fig. 5a**; ref.[26,27]), and the placement of two of these epitopes in their pre-arranged geometry is likely required to select for homotypic interfab contacts of L9-like antibodies. We selected our input as two consecutive L9 Fabs as we believed it easier to scaffold as compared to three. Two epitopes for L9 Fabs were scaffolded continuously (NPNVDPNANPNVD) or discontinuously (NPNVD and NPNVD) with supporting de novo backbone generated by RFdiffusion (**Fig. 5a,b; Supplementary Fig. 6a**). 19 hits that passed AF2 metrics and RMSD filtering were from the discontinuous set, and 9 from the continuous set, for a total of 28 designs ordered for screening (**Supplementary Fig. 6a**). Constructs were expressed in *E. coli*, purified (**Supplementary Fig. 6b-d**), and tested for their binding by BLI and showed a majority of designs bound to L9 (**Supplementary Fig. 6e**). The four designs with the largest binding shift against L9 in the BLI screen (17, 19, 21, and 28) were selected for testing by mass photometry to determine if they bound two L9 Fabs at once. Three of the four designs, 19, 21, and 28, all showed a significant peak corresponding to the weight of two L9 Fabs bound to one immunogen (**Supplementary Fig. 6f**) and were selected for biophysical and structural characterization.

We examined the down-selected designs by negative-stain electron microscopy (nsEM), and one of these designs in the presence of L9 Fabs, 19 (hereafter referred to as 19-ifL9), exhibited 2D class averages and a volume reconstruction (not shown) reminiscent of the original homotypic L9 structure (**Fig. 5a**). Surface plasmon resonance (SPR) confirmed strong binding to L9 with little-to-no off-rate, and weaker but appreciable binding to the inferred-germline L9 which cannot form homotypic contacts (**Fig. 5c**). Circular dichroism (CD) spectroscopy confirmed the alpha helical profile of the design (**Fig. 5d**). We were able to obtain a high resolution cryo-electron microscopy (cryo-EM) structure of 3.1Å for 19-ifL9 in a complex with two L9 Fabs that closely matched the original input structure and the AF2 prediction model (**Fig. 5b, e**), with an epitope Cα root mean square deviation (RMSD) of 0.660Å. The cryo-EM density also confirmed similar rotameric conformations present in the 19-ifL9 structure Fabs as compared to the original structure (**Fig. 5f**). In sum, we designed immunogens capable of binding two L9 Fabs in a prearranged orientation and recapitulate the mode of binding to a high degree of accuracy as confirmed by cryo-EM.

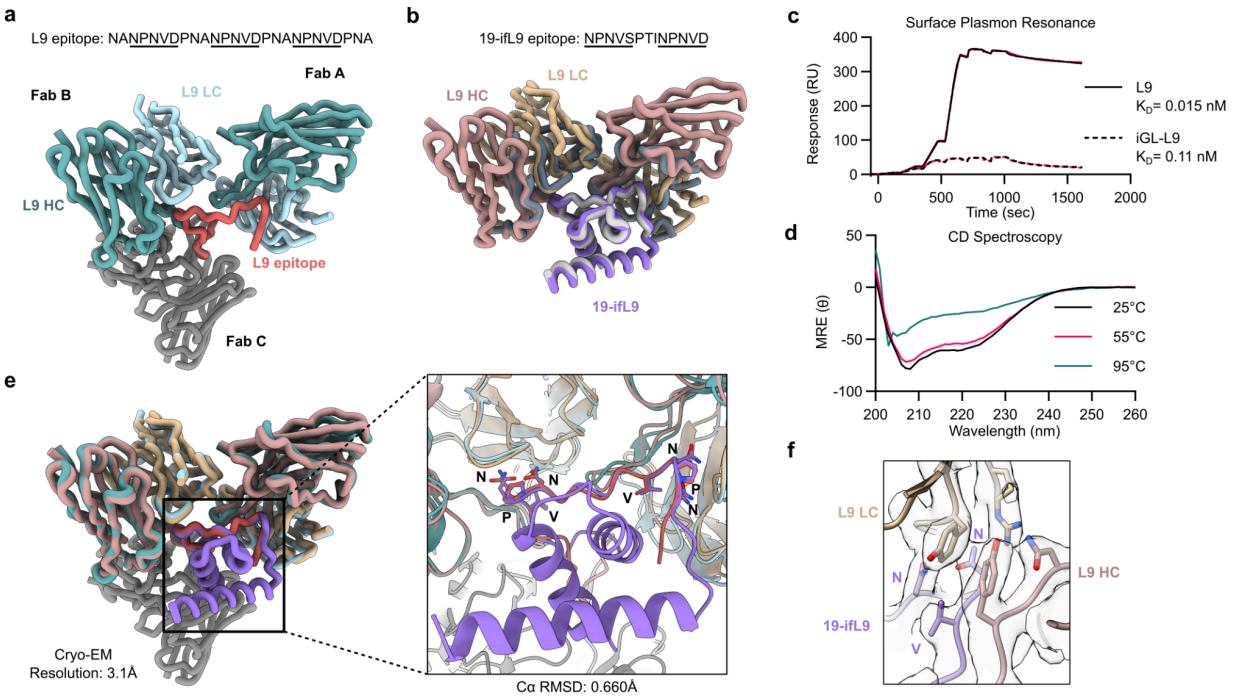

Figure 5. Biophysical characterization of designed immunogens targeting the homotypic Fab epitope of L9. **a** Cryo-EM structure (PDB ID: 8EH5) of three L9 Fabs bound to recombinant CSP at its minor repeats. Underlined residues indicate repeats with the greatest buried surface area (BSA) when bound. The third Fab is in gray as its epitope was not used for design. **b** Cryo-EM structure for design 19-ifL9 bounds to two L9 Fabs. The 19-ifL9 backbone generated prior to sequence design is overlaid in white and L9 inputs in slate gray. **c** SPR sensorgrams and apparent affinities of 19-ifL9 tested for binding against L9 and iGL-L9 loaded on a ProA sensor chip. Curve fits are underlaid in magenta. **d** CD spectrum at three temperatures for 19-ifL9 confirming alpha helical profile. **e** 19-ifL9 cryo-EM structure overlaid with original L9 input structure. Cα RMSD of scaffolded epitope to the original structure was 0.660Å. Cryo-EM map resolution was 3.1Å. **f** 19-ifL9 and L9 models fitted in cryo-EM density at the interface between adjacent Fabs.

ifL9 immunogens activate and recruit knock-in iGL-L9 B cells to the GC:
Immunization with PfCSP or the minimal epitope for the L9 complex would be unlikely to elicit L9-like antibodies at a high frequency due to the flexible conformations of the repeats, which may only present two NPNV epitopes in close proximity a fraction of the time, which would be required to select for and mature Fab-Fab contacts. Thus, we wanted to determine if our designed ifL9 immunogens, when compared to flexible repeat antigens like PfCSP, could more potently activate and recruit transferred CD45.2 iGL-L9 B cells to the germinal centers of congenic CD45.1 mice. We fused 19-ifL9, 21-ifL9, and 28-ifL9 to I53-50 to produce 60mer nanoparticles similar to our iGL-CIS43 study (**Fig. 2c & 3a**), and compared them to PfCSP and Peptide22-Keyhole Limpet Hemocyananin (Pep22-KLH), which contains the two NPNV repeat epitopes that can bind consecutive L9 Fabs conjugated to a KLH carrier. Eight days after immunization, all mice showed a significant increase in total GC B cells, but the most significant recruitment of transferred-in CD45.2 in the GCs of recipient CD45.1 mice were observed in

groups immunized with ifL9-60mers, with significantly more CD45.2 GC B cells from the 19-ifL9-60mer group (**Fig. 6a,b**). Of these CD45.2+ GC B cells from ifL9-60mers, a significant fraction were reactive to CSP probes (**Fig. 6a,b**). These data suggest that ifL9-60mers, with their NPNV epitopes scaffolded in pre-arranged binding geometry, can more easily recruit iGL-L9 precursors to the GC of recipient mice as compared to flexible repeats. This result may be due to selection of contacts required for homotypic Fab L9 contacts which will need to be further investigated.

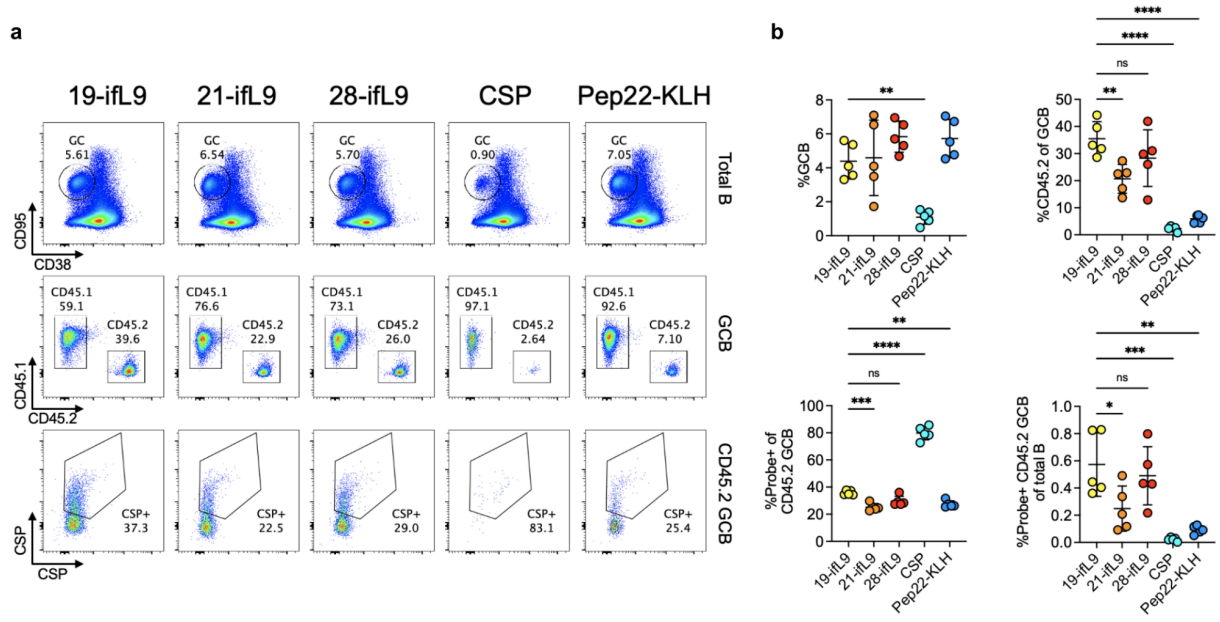

Figure 6. Immunization with 19-ifL9-60mer leads to potent activation and recruitment of knock-in iGL-L9 B cells to germinal centers (GCs). a CD45.1 mice with transferred-in CD45.2 iGL-L9 B cells were immunized with 19-ifL9-60mer or CSP and Peptide22-KLH controls. Splenocytes were harvested at day 8 and analyzed by flow cytometry. **b** Percentage of total GC B cells, CD45.2+ GC B cells, CSP+CD45.2+ GC B cells, and CSP+CD45.2+ GC B cells as a fraction of total B cells.

Discussion

Designed, epitope-based immunogens have largely scaffolded epitopes with secondary structure[32,33,36,39,52], and more complicated discontinuous epitopes or loops[38,53–55], by grafting them into existing proteins using Rosetta software, or by using idealized secondary structural elements around motifs to scaffold epitopes without the need for existing proteins[37]. Deep learning based backbone generation methods like RoseTTAfold hallucination and inpainting[56], and RFdiffusion used here[40], can scaffold RSV F epitopes with completely de novo topologies without any pre-specification of existing or idealized structural elements[57]. Scaffolding loop epitopes is a difficult protein design task owing to their inherent flexibility. Structural characterization has shown *Pf*CSP repeat epitopes form short, transient turn-based motifs in their unbound forms[24,58]. Early attempts tried to mimic these conformations for vaccines[59], but no other reports to date have attempted to scaffold PfCSP repeats from bound or unbound structures. Here, we report the design of multiple immunogens via deep learning based protein

design methods display CIS43 and L9 epitopes, bind specifically to their targets in multiple binding assays, can activate and recruit target knock-in inferred-germline B cells to the GC, and for L9 designs can be verified as atomically accurate by cryo-EM compared to design AF2 prediction models.

Our ability to specifically design immunogens that can bind specific conformations of PfCSP repeat antibodies provides a new strategy to improve the quality of the antibody response. Passively transferred CIS43 or L9 can be protective at concentrations as low as 50 μg/mL in humans[14,16,60], which is far lower than the 188 μg/mL of anti-CSP repeat from RTS,S/AS01B vaccines protected from CHMI[61]. It is hard to make direct comparisons in this case as RTS,S also contains the C-terminus of CSP, but this may be indicative that a significant fraction of RTS,S induced repeat antibodies are of low quality. Vaccination with flexible repeats, regardless of whether they target the junctional NPDP, minor NVDP, or major NANP repeats, may thus prove insufficient in generating potent antibody responses. Our designed immunogens are highly specific, with 14-glCIS43-60mer showing potent binding in SPR experiments to iGL-CIS43, and no binding to mature CIS42 at equivalent concentrations. This immunogen would in theory preferentially activate precursors of protective antibodies like CIS43 while avoiding the activation of non-protective CIS42 altogether, thus improving the overall quality of the polyclonal response. 14-glCIS43-60mer activated and recruited iGL-CIS43 to recipient GCs, but future experiments with knock-in iGL-CIS42 B cells are planned to determine if 14-glCIS43-60mer can maintain this specific activation *in vivo*.

Though we did not use serum or test monoclonals elicited by immunization with our CIS43 or L9 immunogens for their functional activity against parasites, the presence of CIS43-like mutations in antibodies generated by 14-glCIS43 immunogens suggest that activity is possible. Future experiments are planned to characterize the generated monoclonals and determine if they exhibit functional activity *in vitro* or *in vivo*. Interestingly, though CIS43-like mutations were observed from 14-glCIS43-60mer immunized mice, they were at a lower overall frequency compared to the flexible minimal epitope in a previous study (**Fig. 4f**, ref.[42]). For example, $N52K_{HC}$ in HCDR2 is an important mutation for binding to the junctional epitope and was observed at 28.6% frequency at day 28 post immunization, but was not observed in our study (**Fig. 4d**). However, other CIS43 or CIS43.D3 SHMs such as $V102L/I_{HC}$ in HCDR3, and $Q89H_{LC}$ in LCDR3 were observed at high frequency as in the previous study (**Fig. 4d,e**). It is unclear as to whether this is due to random chance or if scaffolding this epitope changes local dynamics and thus disrupts certain interactions that would be made in native context, and will need to be addressed in future studies.

Homotypic interfab antibodies utilizing *IGHV3-33/IGKV1-5* genes like L9 present an interesting challenge in eliciting the specific SHMs associated with their formation and contributions to protection. These mutations in L9 are rare[27,62], and it would be unlikely that the display of flexible PfCSP repeats would elicit these types of antibodies at high frequencies as each repeat acts as its own unit[25]. Immunization with a homotypic antibody fused to PfCSP repeats on a nanoparticle, 1210-NANP5.5-LS, when compared to PfCSP, showed that serum from mice with humanized antibody repertoires were no different at *in vitro* parasite inhibition showing no

benefit to this strategy in the polyclonal response, but did isolate a potent antibody that utilized homotypic contacts[31]. 19-ifL9 scaffolds two NPNV epitopes to a high degree of accuracy as evidenced by cryo-EM that matches the AF2 model to Cα 0.660Å RMSD (**Fig. 5e**), and the fusion of this immunogen on 19-ifL9-60mer is able to activate and recruit transferred-in iGL-L9 B cells to recipient GCs with significantly higher levels than Peptide22-KLH and PfCSP which display native, flexible epitopes (**Fig. 6**). This suggests that there is selection for homotypic contacts with 19-ifL9-60mer due to the pre-arranged geometry required for binding, but sequencing of sorted and paired B cell HC and LCs will be required to determine the presence of L9-like mutations. Assessment of 19-ifL9-60mer in a platform like Kymice[63] will also be required to determine if L9-like antibodies can be preferentially elicited in a more diverse and competitive B cell environment. Another advantage of 19-ifL9-60mer over 1210-NANP5.5-LS is that it doesn't require the formation of a pre-immune complex derived from humans, which may be a hurdle in vaccine development and approval.

The ability to scaffold flexible loop epitopes, as demonstrated here with PfCSP, represents a significant achievement in rational vaccine design. By precisely presenting these epitopes in defined conformations, we can selectively engage and activate B cell precursors with specific features known to be critical for protection. This approach offers a powerful strategy to elicit high-quality antibody responses against *P. falciparum*, paving the way for the development of more effective vaccines against malaria.

Methods

RFdiffusion for de novo generation of backbones

RFdiffusion[40] was run using the following input parameters: Sampling of noise scale values from 0 to 1.0 in 0.25 increments, binder_ncontacts and interface_ncontact potentials, a guide potential value of 2, a quadratic guide decay, total timesteps of n=200 with a final step at 25 for CIS43 designs, and total timesteps of n=50 with a final step at 1 for L9 designs.

ProteinMPNN-FastRelax (ProteinMPNN-FR) & ProteinMPNN-MultiSeq (ProteinMPNN-MS)

ProteinMPNN-FR and ProteinMPNN-MS were run using the pipeline outlined by Bennett *et al.*[43]. Briefly, ProteinMPNN[41] is run on RFdiffusion designs for sequence design with or without residues fixed. In the ProteinMPNN-FR protocol, this backbone is then relaxed using PyRosetta and one additional sequence is generated for this backbone. In the ProteinMPNN-MS protocol, multiple sequences for the original RFdiffusion backbone are generated without any relaxation step.

AlphaFold2 Initial Guess

AlphaFold2 Initial Guess was run as described by Bennett *et al*.[43]. Briefly, this modified protocol provides initialized coordinates based on the input RFdiffusion backbone with the sequences provided by ProteinMPNN-FR or -MS, as opposed to starting from the origin in a typical AlphaFold2 prediction run[44]. No multiple sequence alignment (MSA) is generated and predictions are run as a single sequence input with a variable number of recycles (default=3)

using Model 1 weights. The receptors (CIS43 and L9 Fabs) were templated based on the input structure for prediction.

Computational design and filtering pipeline for immunogens

RFdiffusion was run using cleaned (removed heteroatoms) and renumbered inputs for the CIS43 (PDB ID: 6B5M) and L9 (PDB ID: 8EH5) structures. For CIS43, RFdiffusion was run with 25-35 residues generated on either side of the NPDPNANPNVDPN epitope with inputs described in **Figure 1**. For L9 continuous and discontinuous epitope inputs, 25-45 residues were generated on either side of the NPNVD epitopes, and the discontinuous input had 3-15 residues in between NPNVD epitopes. Both immunogens were designed in the context of their Fabs. CIS43 designs were filtered on 0.3Å RMSD to the input epitope structure and 0 backbone clashes with the Fab, and L9 designs were filtered on 0.5Å RMSD to the input and 0 backbone clashes with the Fab.

Filtered designs were then sequence designed using ProteinMPNN-FR for CIS43 with epitopes fixed or designable as described in **Figure 1**. For L9, both ProteinMPNN-FR and -MS protocols were used for sequence design and were completely designable at the epitopes. The generated sequences were then used for AF2 Initial Guess prediction using 3 recycles for CIS43 designs, and 6 recycles for L9 designs. Designs for CIS43 were filtered on AF2 pLDDT values for the immunogen > 80 and pAE of interaction with CIS43 < 10. Designs for L9 were filtered on the same metrics in complex with L9 Fabs. Note that for L9, the second asparagine position was often mutated by ProteinMPNN to tyrosine and this was reverted to asparagine as in the original epitope for passing designs.

Plasmid synthesis

Sequences for passing designs were codon optimized for *E. coli* expression and ordered as synthetic genes (eBlocks, Integrated DNA Technologies) with BsaI overhangs for insertion via Golden Gate Assembly into vector LM0627, a modified pET vector that contains a 6xHis-Tag and a SNAC-tag[64] as described by Wicky et al.[65].

Protein expression and purification for screening

Assembled vectors were cloned into *E. coli* (BL21, New England Biolabs) in a 96 well PCR plate format with 1 µL of plasmid combined with 6 µL of competent cells, and transformed by standard heat-shock protocol described by the manufacturer. Transformed cells grown overnight in LB medium with kanamycin were used to inoculate 2 x 900 µL of Terrific Broth II in round-bottom deep well plates. Inoculated plates were sealed with breathable film (Breathe-EASIER, Diversified Biotech) and incubated on Heidolph shakers at 1200 RPM at 37°C for 1.5 hours, and subsequently induced with 10 µL of 100 mM Isopropyl β-D-1-thiogalactopyranoside and left shaking overnight at room temperature. Cultures were then lysed using BugBuster® Protein Extraction Reagent (Merck) and lysate was clarified by centrifugation at 4000 x g for 10 minutes. Supernatants were applied to 100 µL of nickel resin (Ni-NTA Superflow, QIAGEN) washed with Tris buffered saline (TBS) with 20 mM imidazole. Target protein was eluted with 250 µL using

TBS with 300 mM Imidazole, and SDS-PAGE (Criterion TGX Stain-Free Precast Gels, Bio-Rad) was used to confirm presence and purity of proteins.

Size exclusion chromatography (SEC) was run on Ni-NTA eluates using a Superdex 75 Increase 5/150 GL column (Cytiva) and fractions were collected in 0.25 mL volumes. Fractions of interest were picked based on Absorbance at 280 nm and purity was verified by SDS-PAGE. Protein concentrations were determined by 280 nm absorbance (Take3 Trio, Biotek).

Scaled up expression and purification for down-selected designs were run using a similar protocol. Expression volume was scaled up to 50 mL, sonicated on ice for lysis, Ni-NTA resin 1-2 mL for purification, and SEC using a Superdex 75 Increase 10/300 GL column (Cytiva). Purified samples had their concentrations determined using a 10 mm pathlength quartz cuvette in a UV-vis spectrophotometer (Cary 3500, Agilent).

Antibody expression and purification

IgG1 antibodies in this manuscript were expressed and purified using ProteinA resin (TurboCHO Antibody Expression, Genscript).

Biolayer interferometry (BLI)

BLI was performed using an Octet Red 96 or Octet R8 system (Sartorius), at 22°C and shaking at 1000 rpm. CIS43, iGL-CIS43, CIS42, L9, and 224 antibodies were diluted in kinetics buffer (HEPES Buffered Saline-EP+ with 0.1% bovine serum albumin) to a final concentration of 5 µg/mL before loading onto Protein A (ProA) biosensors (Sartorius). For screening, IgG loaded ProA biosensors were dipped into 100 nM of immunogens diluted in kinetics buffer, and dissociated in blank kinetics buffer. For affinity determination, loaded ProA tips were dipped into 50 nM to 1.56 nM of immunogen for 200 second association, and 200 second dissociation. Affinity values were determined by 1:1 fitting using Sartorius BLI analysis software.

Enzyme-linked immunosorbent assay (ELISA) for glCIS43 immunogens

Immunogens were coated on HisSorb plates (QIAGEN) with 50 ng of design per well (one design per plate column) and full-length SAmut CSP and SAmut CSP5/3 (Langowski et al. 2024 *In review*) as positive controls, and left at 4C overnight. Plates were washed with Phosphate Buffered Saline pH 7.4 + Tween 20 0.05% (PBS-T) three times. 100 µL of PBS-T with 5% Casein (Blocking buffer) was added to each well and left at room temperature for 30 minutes. Plates were washed again with PBS-T three times. Primary antibodies for iGL-CIS43 and CIS42 were diluted at a starting concentration of 4 µg/mL down in 10-fold increments to 0.004 µg/mL for each design and were incubated at room temperature for 30 minutes. Plates were washed with PBS-T, and secondary antibody (Goat anti-human IgG HRP, SouthernBiotech) was diluted 1:6000 in PBS-T, 100 µL added per well, and incubated for 30 minutes at room temperature. Plates were washed three times with PBS-T and 90 µL of TMB substrate was subsequently added to each well and then neutralized with 1N HCl solution (90 uL) after 5 minutes. Absorbance at 450 nm was measured using an Epoch Microplate reader (Biotek) and values plotted and calculated using GraphPad Prism (GraphPad Software).

Surface Plasmon Resonance (SPR)

For 14-glCIS43 nanoparticles and L9 immunogens, binding kinetics were determined by SPR on a Biacore8K (Cytiva). IgG antibodies were loaded onto Biacore Sensor Chip Protein A (Cytiva) using HBS-EP+ Buffer (Cytiva). Immunogens were diluted in HBS-EP+ buffer and binding kinetics were determined by a single-cycle kinetics protocol using 100 nM diluted 4-fold down the plate. Affinity values were determined by 1:1 fitting using Cytiva SPR analysis software.

Expression, purification, and assembly of nanoparticle immunogens

Designs 14-glCIS43, 19-ifL9, 21-ifL9, and 28-ifL9 were codon-optimized and genetically fused to the N-terminus of I53-50A[50] or T33_dn10A[49] and inserted into the pET29b+ vector, which contains a 6xHis-tag at its C-terminus. These genetically fused components were transformed into BL21(DE3) *E. coli* (NEB) and single colonies were picked for inoculating starter cultures. Starter cultures were added to Terrific Broth II medium with kanamycin and were incubated for 2.5 hr at 37°C, and subsequently induced with 0.1 mM IPTG and temperature was reduced to 18°C for overnight induction. Cultures were then harvested by centrifugation at 4000 x g at 4°C and the supernatant was discarded, and the pellet was resuspended in a buffer containing 50 mM Tris, 250 mM NaCl, 20 mM imidazole, pH 8.0, and 1mM PMSF. The re-suspended pellet was sonicated at 65% amplitude on ice for 3 minutes. The lysate was cleared by centrifugation at 14,500 x g for 30 minutes at 4°C. The resulting supernatant was used for purification by 1-3 mL of Ni-NTA resin (QIAGEN) that was pre-equilibrated with a wash buffer (50 mM Tris, 250 mM NaCl, and 20 mM imidazole, pH 8.0) and flow through was collected. The resin was washed again with 5-10 column volumes of wash buffer. Bound protein was eluted using an elution buffer (50 mM Tris, 250 mM NaCl, 300 mM Imidazole pH 8.0) and eluted protein was then purified by SEC using a Superdex 200 Increase 10/300 GL column (Cytiva). Protein purity was verified by SDS-PAGE and concentrations determined by 280 nm absorbance measurements.

For nanoparticle assembly, purified components were mixed with their corresponding B components (I53-50B or T33_dn10B) as previously described[49–51]. Assemblies were purified by SEC to remove residual components using a Superose 6 Increase 10/300 GL column for I53-50 nanoparticles, and a Superdex 200 Increase 10/300 GL for T33_dn10 nanoparticles. Protein concentrations were measured by UV-vis (Cary 3500, Agilent).

Negative-stain electron microscopy (nsEM)

I53-50 and T33_dn10 nanoparticles were added to carbon-covered 400 mesh copper grids (Electron Microscopy Sciences) and stained with 2% uranyl formate. Micrographs were imaged on a Talos 120C microscope with a Ceta camera.

Characterization of L9 complexes by mass photometry (MP)

MP measurements were taken on a TwoMP (Refeyn) mass photometer. Briefly, 20 nM of L9 immunogens were combined in a 1:2 ratio with L9 Fabs, and 5 µL of this sample was added to

one well of a 12-well gasket. The instrument was calibrated beforehand with standards of known molecular weights and oligomeric states. Measurements were collected using AcquireMP software and analyzed with DiscoverMP to determine populations of multimeric states in solution.

Mouse experiments, flow cytometry, and BCR sequencing

Mouse experiments, flow cytometry, and BCR sequencing were carried out as previously described in Kratochvil et al.[42].

Statistical Analysis

Statistical differences between mouse groups were determined by parametric and non-parametric one-way ANOVA analysis with multiple comparisons test using GraphPad Prism (GraphPad Software).

Supplementary Figures

a

Diffusion input	Sequence	Backbones diffused	Backbones passing <0.3 epitope RMSD & 0 Calpha antibody clashes	Success rate
Native	NPDPNANPNVDPN	3750	837	22.3
Hphobic1	NPLPLANPNVLPN	3746	1732	46.2
Hphobic2	NPDPLANPNVDPN	3739	1106	29.6

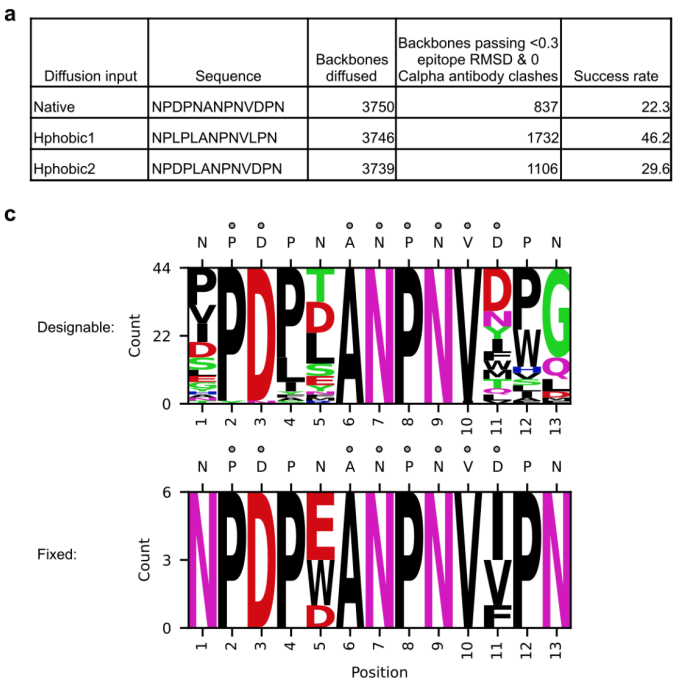

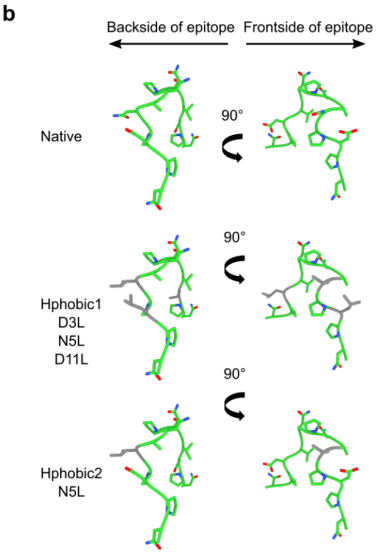

Supplementary Figure 1. RFdiffusion parameters for CIS43 immunogen backbone generation. **a** Table of diffusion inputs, their sequences, total number of backbones diffused, backbones passing filters, and the percent success rate of each parameter. **b** Structure models of inputs used for RFdiffusion. Input residues mutated are listed and are colored in gray. **c** Sequence logo plots for AF2 passing designs (pLDDT immunogen < 80, pAE of interaction with CIS43 < 10) from sets where epitope was fully designable and fixed at several sequence positions. Gray circles over positions represent residues with significant side chain contacts with CIS43 antibody.

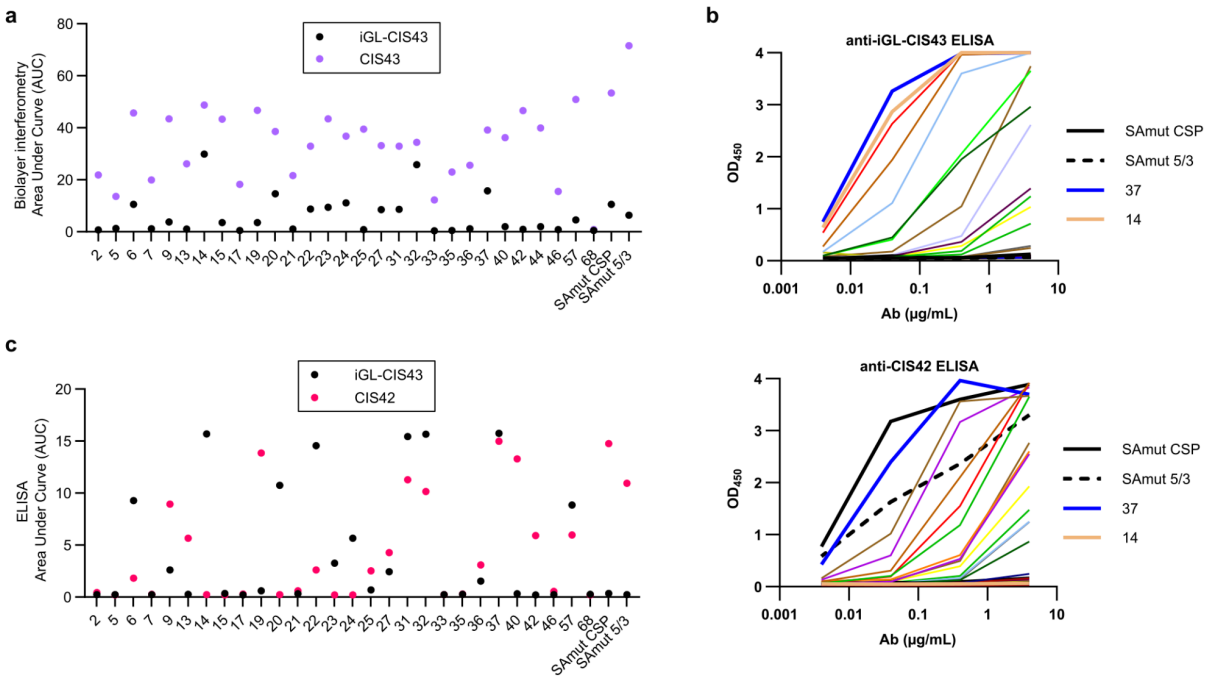

Supplementary Figure 2. BLI and ELISA screening. a Biolayer interferometry with ProA tips loaded with iGL-CIS43 or CIS43. Loaded sensors were tested against 100 nM of immunogen. **b** ELISA curves for designs plated and tested against iGL-CIS43 (top) or CIS42 (bottom) IgG titrated from 4 to 0.004 µg/mL. **c** ELISA AUC plotted for all designs.

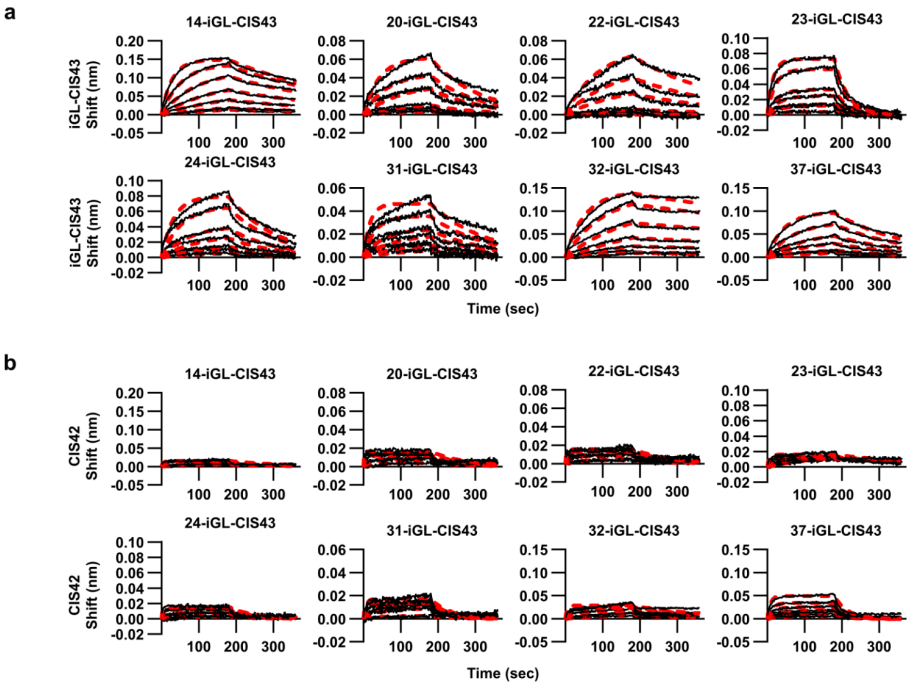

Supplementary Figure 3. Affinity determination of down-selected designs. a BLI curves to determine affinity of down-selected designs against iGL-CIS43 or, **b** CIS42 immobilized on ProA BLI tips (Sartorius).**Supplementary Figure 2. BLI and ELISA screening. a** Biolayer interferometry with ProA tips loaded with iGL-CIS43 or CIS43. Loaded sensors were tested against 100 nM of immunogen. **b** ELISA curves for designs plated and tested against iGL-CIS43 (top) or CIS42 (bottom) IgG titrated from 4 to 0.004 μg/mL. **c** ELISA AUC plotted for all designs.

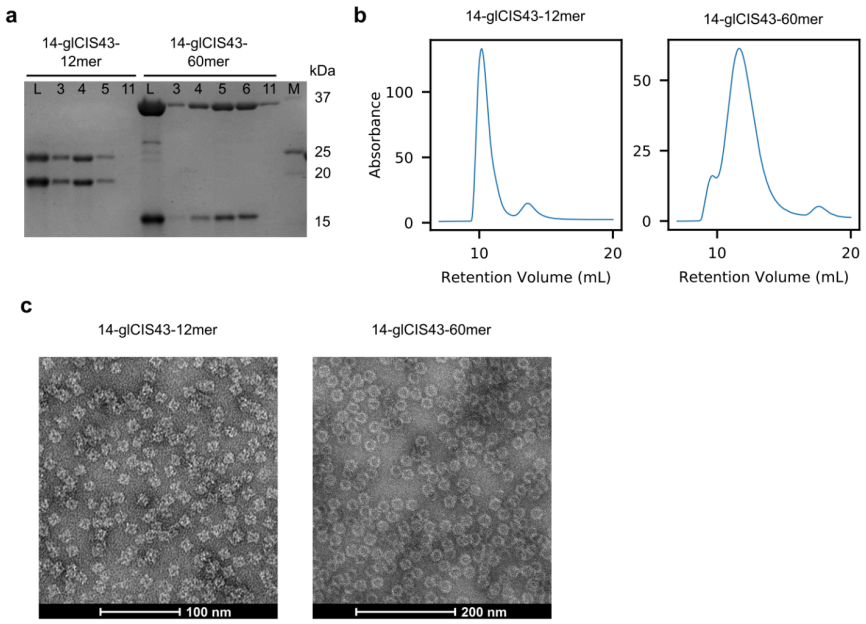

Supplementary Figure 4. Characterization of 14-glCIS43 nanoparticle immunogens. a SDS-PAGE of SEC purified nanoparticle immunogens. **b** SEC chromatograms for 14-glCIS43-12mer and 14-glCIS43-60mer. **c** Negative-stain electron micrographs for 14-glCIS43-12mer (92k magnification) and 14-glCIS43-60mer (57k magnification).

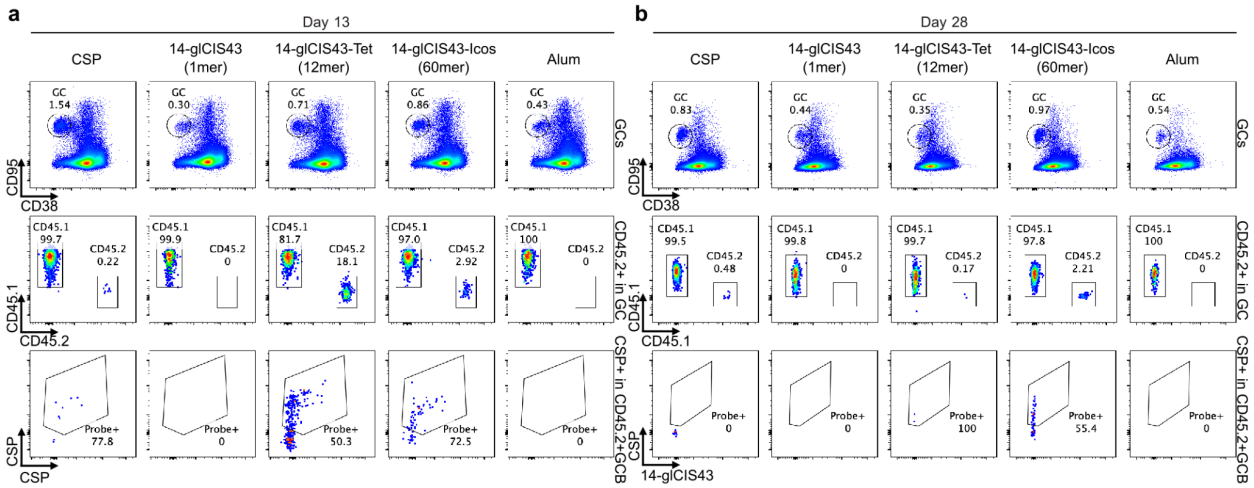

Supplementary Figure 5. Flow cytometry plots for iGL-CIS43 mouse immunizations. a Day 13 and **b** Day 28 flow cytometry graphs for splenocytes from immunized mice. These graphs indicate total GC B cells (top row), CD45.1 or CD45.2 GC B cells (middle row), and PfCSP reactive CD45.2 GC B cells (bottom row).

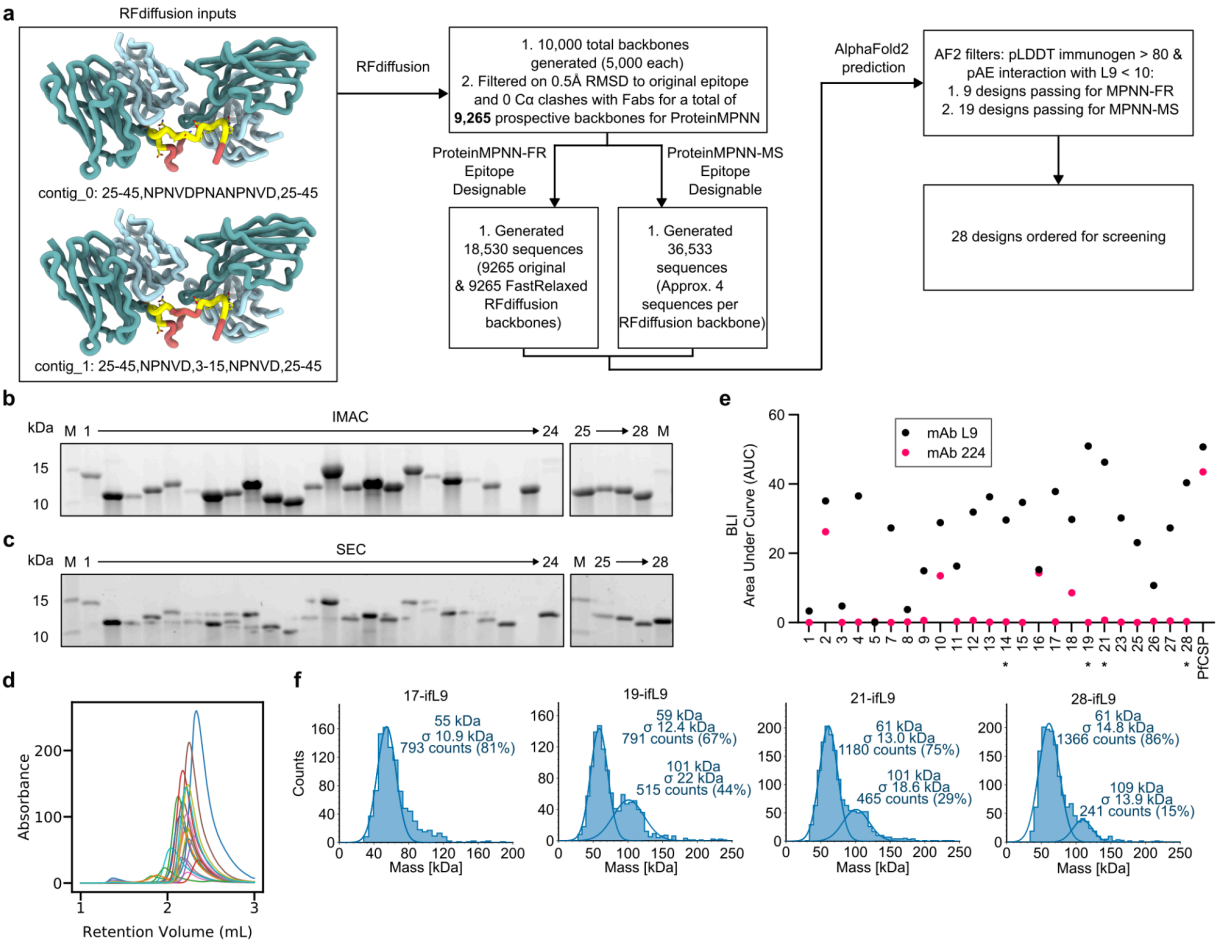

Supplementary Figure 6. Design pipeline and screening characterization for ifL9 immunogens. a Design pipeline overview for interfab L9 (ifL9) immunogens. Designs were scaffolded as two continuous L9 epitopes as found in the native sequence or as discontinuous epitopes. Supporting backbones were generated using RFdiffusion, sequence designed with ProteinMPNN, and filtered with AlphaFold2. **b** SDS-PAGE of IMAC eluates for ifL9 designs 1-28. **c** SDS-PAGE of Superdex 75 Increase 5/150 size exclusion chromatography (SEC) fractions for designs 1-28. **d** SEC chromatograms of all 28 designs. **e** SEC-purified designs at 100 nM tested for their binding against mAb L9 and mAb 224 on ProA BLI tips. mAb224 can cross-react to the L9 epitope sequence. **f** Mass photometry of down-selected ifL9 immunogens in the presence of L9 Fabs. The peak around 100 kDa corresponds to two Fabs bound to one immunogen.

>14-glCIS43
SERRDKIRKLRIELGEAIEEVQEKYADDPRLKDYPDLNANPNVDPGIETLIDIAKDLVKFLKEAGAPKELIER
AEKIKKELEEIK
>19-ifL9
KKEEEEKEKLAKEVAEKLRKRGIKINPNVSPTINPNVDASLYDDLTLEQTVLAWEEGKVSKEDAYRAALELK
KRE
>21-ifL9
EKSFGQISNEINNLIQQAIAEGKSHYFNPNVNPLSVNPNVDPLLQKDVIESNILALSKGDPELAKKLQELLDK
AEELKKK
>28-ifL9
EEKLKELEEKLKEYKKKIEELGGTLEINPNVNPNGLNPNVSESEQGVDVVVNHYALQAKKLEEEIKKLKEE
K

Supplementary Figure 7. Sequences for 14-glCIS43 and ifL9 immunogens used in animal studies.

References

1. *World Malaria Report 2023*. https://www.who.int/teams/global-malaria-programme/reports/world-malaria-report-2023 (2023).
2. Ménard, R. *et al.* Circumsporozoite protein is required for development of malaria sporozoites in mosquitoes. *Nature* **385**, 336–340 (1997).
3. Stewart, M. J., Nawrot, R. J., Schulman, S. & Vanderberg, J. P. Plasmodium berghei sporozoite invasion is blocked in vitro by sporozoite-immobilizing antibodies. *Infect. Immun.* **51**, 859–864 (1986).
4. Cerami, C. *et al.* The basolateral domain of the hepatocyte plasma membrane bears receptors for the circumsporozoite protein of Plasmodium falciparum sporozoites. *Cell* **70**, 1021–1033 (1992).
5. Doud, M. B. *et al.* Unexpected fold in the circumsporozoite protein target of malaria vaccines. *Proc. Natl. Acad. Sci. U. S. A.* **109**, 7817–7822 (2012).
6. The RTS,S Clinical Trials Partnership. First Results of Phase 3 Trial of RTS,S/AS01 Malaria Vaccine in African Children. *N. Engl. J. Med.* **365**, 1863–1875 (2011).
7. Datoo, M. S. *et al.* Safety and efficacy of malaria vaccine candidate R21/Matrix-M in African children: a multicentre, double-blind, randomised, phase 3 trial. *Lancet* **403**, 533–544 (2024).
8. Oyen, D. *et al.* Structural basis for antibody recognition of the NANP repeats in Plasmodium falciparum circumsporozoite protein. *Proc. Natl. Acad. Sci. U. S. A.* **114**, E10438–E10445 (2017).
9. Kisalu, N. K. *et al.* A human monoclonal antibody prevents malaria infection by targeting a new site of vulnerability on the parasite. *Nat. Med.* **24**, 408–416 (2018).
10. Tan, J. *et al.* A public antibody lineage that potently inhibits malaria infection through dual binding to the circumsporozoite protein. *Nat. Med.* **24**, 401–407 (2018).
11. Imkeller, K. *et al.* Antihomotypic affinity maturation improves human B cell responses against a repetitive epitope. *Science* **360**, 1358–1362 (2018).
12. Wang, L. T. *et al.* A Potent Anti-Malarial Human Monoclonal Antibody Targets Circumsporozoite Protein Minor Repeats and Neutralizes Sporozoites in the Liver. *Immunity* **53**, 733–744.e8 (2020).
13. Kayentao, K. *et al.* Safety and Efficacy of a Monoclonal Antibody against Malaria in Mali. *N. Engl. J. Med.* **387**, 1833–1842 (2022).
14. Gaudinski, M. R. *et al.* A Monoclonal Antibody for Malaria Prevention. *N. Engl. J. Med.* **385**,

803–814 (2021).
15. Kayentao Kassoum *et al.* Subcutaneous Administration of a Monoclonal Antibody to Prevent Malaria. *N. Engl. J. Med.* **390**, 1549–1559 (2024).
16. Wu, R. L. *et al.* Low-Dose Subcutaneous or Intravenous Monoclonal Antibody to Prevent Malaria. *N. Engl. J. Med.* **387**, 397–407 (2022).
17. Jelínková, L. *et al.* An epitope-based malaria vaccine targeting the junctional region of circumsporozoite protein. *npj Vaccines* **6**, 1–10 (2021).
18. Atcheson, E., Hill, A. V. S. & Reyes-Sandoval, A. A VLP for validation of the Plasmodium falciparum circumsporozoite protein junctional epitope for vaccine development. *NPJ Vaccines* **6**, 46 (2021).
19. Kurtovic, L. *et al.* Novel Virus-Like Particle Vaccine Encoding the Circumsporozoite Protein of Plasmodium falciparum Is Immunogenic and Induces Functional Antibody Responses in Mice. *Front. Immunol.* **12**, 641421 (2021).
20. Francica, J. R. *et al.* Design of Alphavirus Virus-Like Particles Presenting Circumsporozoite Junctional Epitopes That Elicit Protection against Malaria. *Vaccines (Basel)* **9**, 272 (2021).
21. Langowski, M. D. *et al.* Restricted valency (NPNA)n repeats and junctional epitope-based circumsporozoite protein vaccines against Plasmodium falciparum. *npj Vaccines* **7**, 1–11 (2022).
22. Ludwig, J. *et al.* Glycosylated nanoparticle-based PfCSP vaccine confers long-lasting antibody responses and sterile protection in mouse malaria model. *npj Vaccines* **8**, 1–14 (2023).
23. Calvo-Calle, J. M., Mitchell, R., Altszuler, R., Othoro, C. & Nardin, E. Identification of a neutralizing epitope within minor repeat region of Plasmodium falciparum CS protein. *NPJ Vaccines* **6**, 10 (2021).
24. Dyson, H. J., Satterthwait, A. C., Lerner, R. A. & Wright, P. E. Conformational preferences of synthetic peptides derived from the immunodominant site of the circumsporozoite protein of Plasmodium falciparum by 1H NMR. *Biochemistry* **29**, 7828–7837 (1990).
25. Kucharska, I. *et al.* Structural ordering of the Plasmodium berghei circumsporozoite protein repeats by inhibitory antibody 3D11. *Elife* **9**, e59018 (2020).
26. Martin, G. M. *et al.* Structural basis of epitope selectivity and potent protection from malaria by PfCSP antibody L9. *Nat. Commun.* **14**, 2815 (2023).
27. Tripathi, P. *et al.* Cryo-EM structures of anti-malarial antibody L9 with circumsporozoite protein reveal trimeric L9 association and complete 27-residue epitope. *Structure* **31**, 480–491.e4 (2023).

28. Martin, G. M. *et al.* Affinity-matured homotypic interactions induce spectrum of PfCSP structures that influence protection from malaria infection. *Nat. Commun.* **14**, 4546 (2023).
29. Pholcharee, T. *et al.* Structural and biophysical correlation of anti-NANP antibodies with in vivo protection against P. falciparum. *Nat. Commun.* **12**, 1063 (2021).
30. Oyen, D. *et al.* Cryo-EM structure of P. falciparum circumsporozoite protein with a vaccine-elicited antibody is stabilized by somatically mutated inter-Fab contacts. *Sci Adv* **4**, eaau8529 (10 2018).
31. Kucharska, I. *et al.* High-density binding to Plasmodium falciparum circumsporozoite protein repeats by inhibitory antibody elicited in mouse with human immunoglobulin repertoire. *PLoS Pathog.* **18**, e1010999 (2022).
32. Correia, B. E. *et al.* Computational design of epitope-scaffolds allows induction of antibodies specific for a poorly immunogenic HIV vaccine epitope. *Structure* **18**, 1116–1126 (2010).
33. Correia, B. E. *et al.* Proof of principle for epitope-focused vaccine design. *Nature* **507**, 201–206 (2014).
34. Jardine, J. *et al.* Rational HIV immunogen design to target specific germline B cell receptors. *Science* **340**, 711–716 (2013).
35. Schiffner, T. *et al.* Vaccination induces broadly neutralizing antibody precursors to HIV gp41. *Nat. Immunol.* **25**, 1073–1082 (2024).
36. Sesterhenn, F. *et al.* Boosting subdominant neutralizing antibody responses with a computationally designed epitope-focused immunogen. *PLoS Biol.* **17**, e3000164 (2019).
37. Sesterhenn, F. *et al.* De novo protein design enables the precise induction of RSV-neutralizing antibodies. *Science* **368**, eaay5051 (2020).
38. Ofek, G. *et al.* Elicitation of structure-specific antibodies by epitope scaffolds. *Proc. Natl. Acad. Sci. U. S. A.* **107**, 17880–17887 (2010).
39. Harrison, T. E. *et al.* Rational structure-guided design of a blood stage malaria vaccine immunogen presenting a single epitope from PfRH5. *EMBO Mol. Med.* **16**, 2539–2559 (2024).
40. Watson, J. L. *et al.* De novo design of protein structure and function with RFdiffusion. *Nature* **620**, 1089–1100 (2023).
41. Dauparas, J. *et al.* Robust deep learning–based protein sequence design using ProteinMPNN. *Science* **378**, 49–56 (2022).
42. Kratochvil, S. *et al.* Vaccination in a humanized mouse model elicits highly protective PfCSP-targeting anti-malarial antibodies. *Immunity* (2021)

doi:10.1016/j.immuni.2021.10.017.

43. Bennett, N. R. *et al.* Improving de novo protein binder design with deep learning. *Nat. Commun.* **14**, 2625 (2023).
44. Jumper, J. *et al.* Highly accurate protein structure prediction with AlphaFold. *Nature* **596**, 583–589 (2021).
45. Bachmann, M. F. & Jennings, G. T. Vaccine delivery: a matter of size, geometry, kinetics and molecular patterns. *Nat. Rev. Immunol.* **10**, 787–796 (2010).
46. Marcandalli, J. *et al.* Induction of Potent Neutralizing Antibody Responses by a Designed Protein Nanoparticle Vaccine for Respiratory Syncytial Virus. *Cell* **176**, 1420–1431.e17 (2019).
47. Walls, A. C. *et al.* Elicitation of Potent Neutralizing Antibody Responses by Designed Protein Nanoparticle Vaccines for SARS-CoV-2. *Cell* **183**, 1367–1382.e17 (2020).
48. Brouwer, P. J. M. *et al.* Enhancing and shaping the immunogenicity of native-like HIV-1 envelope trimers with a two-component protein nanoparticle. *Nat. Commun.* **10**, 4272 (2019).
49. Ueda, G. *et al.* Tailored design of protein nanoparticle scaffolds for multivalent presentation of viral glycoprotein antigens. *Elife* **9**, e57659 (2020).
50. Bale, J. B. *et al.* Accurate design of megadalton-scale two-component icosahedral protein complexes. *Science* **353**, 389–394 (2016).
51. Wargacki, A. J. *et al.* Complete and cooperative in vitro assembly of computationally designed self-assembling protein nanomaterials. *Nat. Commun.* **12**, 883 (2021).
52. McLellan, J. S. *et al.* Design and characterization of epitope-scaffold immunogens that present the motavizumab epitope from respiratory syncytial virus. *J. Mol. Biol.* **409**, 853–866 (2011).
53. Azoitei, M. L. *et al.* Computation-guided backbone grafting of a discontinuous motif onto a protein scaffold. *Science* **334**, 373–376 (2011).
54. Azoitei, M. L. *et al.* Computational design of high-affinity epitope scaffolds by backbone grafting of a linear epitope. *J. Mol. Biol.* **415**, 175–192 (2012).
55. Azoitei, M. L. *et al.* Computational design of protein antigens that interact with the CDR H3 loop of HIV broadly neutralizing antibody 2F5: CDR H3-Loop Interacting 2F5 Epitope-Scaffolds. *Proteins* **82**, 2770–2782 (2014).
56. Wang, J. *et al.* Scaffolding protein functional sites using deep learning. *Science* **377**, 387–394 (2022).
57. Castro, K. M. *et al.* Accurate single domain scaffolding of three non-overlapping protein

epitopes using deep learning. *bioRxiv* 2024.05.07.592871 (2024) doi:10.1101/2024.05.07.592871.

58. Ghasparian, A., Moehle, K., Linden, A. & Robinson, J. A. Crystal structure of an NPNA-repeat motif from the circumsporozoite protein of the malaria parasite Plasmodium falciparum. *Chem. Commun.* 174–176 (2006) doi:10.1039/b510812h.
59. Satterthwait, A. C. *et al.* The conformational restriction of synthetic vaccines for malaria. *Bull. World Health Organ.* **68 Suppl**, 17–25 (1990).
60. Lyke, K. E. *et al.* Low-dose intravenous and subcutaneous CIS43LS monoclonal antibody for protection against malaria (VRC 612 Part C): a phase 1, adaptive trial. *Lancet Infect. Dis.* **23**, 578–588 (2023).
61. Kester, K. E. *et al.* Randomized, Double-Blind, Phase 2a Trial of Falciparum Malaria Vaccines RTS,S/AS01B and RTS,S/AS02A in Malaria-Naive Adults: Safety, Efficacy, and Immunologic Associates of Protection. *J. Infect. Dis.* **200**, 337–346 (2009).
62. Wang, L. T. *et al.* The light chain of the L9 antibody is critical for binding circumsporozoite protein minor repeats and preventing malaria. *Cell Rep.* **38**, 110367 (2022).
63. Lee, E.-C. *et al.* Complete humanization of the mouse immunoglobulin loci enables efficient therapeutic antibody discovery. *Nat. Biotechnol.* **32**, 356–363 (2014).
64. Dang, B. *et al.* SNAC-tag for sequence-specific chemical protein cleavage. *Nat. Methods* **16**, 319–322 (2019).
65. Wicky, B. I. M. *et al.* Hallucinating symmetric protein assemblies. *Science* **378**, 56–61 (2022).